Stellingen

1. Kreshkov en Karateev sluiten bij het door hun voorgestelde reactieproduct van tetraethylorthosilicaat en fosforpentoxide ten onrechte het bestaan van octaedrisch door zuurstof gecoordineerd silicium uit.

   Kreshkov, A.P.; Karateev, D.A. *J.Appl.Chem.USSR* **1957**, *30*, 1416-1421.

2. Het recept van Bibby en Dale voor de bereiding van een moleculaire zeef van het SOD-type die volledig uit siliciumdioxide bestaat deugt niet.

   Bibby, D.M.; Dale, M.P. *Nature(London)* **1985**, *317*, 157-158.

3. Bij het katalytisch bepalen van de dissociatiegraad van zuurstof in een lage-temperatuur-zuurstofplasma m.b.v. een thermokoppel bedekt met een dunne laag zilveroxide introduceren Bell en Kwong fouten, omdat ze geen rekening houden met de vluchtigheid van hun katalysator

   Bell, A.T., Kwong, K. *AIChE J.* **1972**, *18*, 990-998.

4. Aangezien het verwaarlozen van de quadrupoolinteracties van natriumkernen in Na-Y-zeolieten niet geoorloofd is, is de uitleg die Welsh en Lambert aan hun ^{23}Na-MAS-NMR-spectra geven niet correct.

   Welsh, L.B., Lambert, S.L. *ACS Symp.Ser.* **1988**, *368*, 32-47.

5. De door Mortier, Vaughan en Newsam veronderstelde onderlinge onafhanklijkheid van de kationbezetting van verschillende kooi-types in zeoliet Na-Y vormt geen goede basis voor statistisch-thermodynamische berekeningen.

   Mortier, W.J.; Vaughan, D.E.W., Newsam, J.M. *ACS Symp.Ser.* **1988**, *368*, 194-202.

6. Het verschil in reactiviteit t.o.v. waterige zuren van moleculaire zeven die m.b.v. de huidige fysische karakteriseringstechnieken niet te onderscheiden zijn wijst erop, dat moleculaire zeven nog niet volledig fysisch kunnen worden gekarakteriseerd.

   Van der Gaag, F.J. Thesis, Delft, 1987.
   Kraushaar-Czarnetzki, B. Thesis, Eindhoven, 1989.
   Ferrini, C.; Kouwenhoven, H.W. *Stud.Surf.Sci.Catal.* **1990**, *55*, 53-62.
   Bodart, Ph.; Nagy, B.J.; Debras G.; Gabelica, Z.; Jacobs, P.A. *J.Phys.Chem.* **1986**, *90*, 5183-5190.
   Lee, G.S.; Maj, J.J.; Rocke, S.C.; Garcés, J.M. *Catal.Lett.* **1989**, *2*, 243-248.

7. Het toevoegen van een complexant zoals fosfaat aan fluoride-bevattende synthese-mengsels van nagenoeg neutrale pH leidt tot moleculaire zeven die volledig uit siliciumdioxide bestaan met significant meer fijnstructuur in hun infraroodspectrum dan zeven bereid zonder fosfaat.

8. Wanneer men met ^{23}Na NMR bij laag veld geen signaal meet aan Ca,Na-Y, wil dit nog niet zeggen dat calcium al het natrium dat bijdraagt aan het ^{23}Na NMR spectrum van Na-Y heeft vervangen.

    Basler, W.D. *Colloids and Surfaces* **1984**, *12*, 59-67.

9. Het succesvol verlopen van het calcineren van moleculaire zeven m.b.v. een zgn. lage-temperatuur zuurstofplasma kan worden gebruikt ter ondersteuning van het nog steeds ter discussie staande bestaan van "zuurstof-spillover".

    Dit proefschrift: hoofdstukken 5,6,7.
    Abderrahim, H., Duprez, D. in *Proceedings, 9th International Congress on Catalysis - Catalysis: Theory to Practice* Phillips, M.J., Ternan, M. (Editors), Chem.Inst.Can.: Ottawa, Ont. 1988 Vol.3, pp.1246-1252.

10. Mocht er bij de vereniging van Europa een geschil ontstaan tussen de Nederlandse en de Belgische overheid t.a.v. de manier waarop het bord "splitsing van autowegen" dient te worden gemonteerd, dan verdient het aanbeveling dat de Nederlandse overheid -en niet de Belgische- bijdraait.

11. Als de koopkrachtpariteit geen opgeld doet, loopt een Nederlandse onderneming die per saldo voornamelijk opbrengsten in dollars heeft bij een appreciatie van de gulden ten opzichte van de dollar een wisselkoersrisico dat een negatief effect op de aandelenrendementen van die onderneming tot gevolg zal hebben.

12. De uitspraak van nogal wat Madrilenen dat Spaans na Chinees de tweede wereldtaal is valt moeilijk te rijmen met de stellige overtuiging van vaak dezelfde personen dat er buiten Madrid geen echt Spaans wordt gesproken.

13. Het is niet aan te bevelen valschermzweven met vallen en opstaan te leren.

Theo Maesen
Delft
20 oktober 1990

ACTIVATION AND CHARACTERIZATION OF
SOME MOLECULAR SIEVE CATALYSTS

ACTIVATION AND CHARACTERIZATION OF SOME MOLECULAR SIEVE CATALYSTS

Proefschrift

ter verkrijging van de graad van doctor
aan de Technische Universiteit Delft
op gezag van de Rector Magnificus, prof.drs. P.A. Schenck,
in het openbaar te verdedigen ten overstaan van
een commissie aangewezen door het College van Dekanen
op dinsdag 04 december 1990 te 16.00 uur
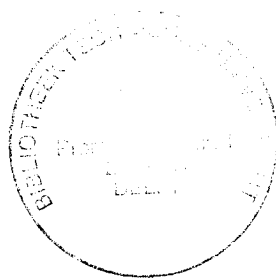
door

Theodorus Ludovicus Michael Maesen

geboren te Stein
scheikundig doctorandus

Dit proefschrift is goedgekeurd door de promotor
Prof. dr. ir. H. van Bekkum
Toegevoegd promotor Dr. H.W. Kouwenhoven

Aan mijn vader en moeder

CONTENTS

Contents

Contents

CHAPTER 1

INTRODUCTION

Molecular Sieves and their Applications: The name "molecular sieve" was coined by McBain in 1932 [1] to denote porous solids with apertures that enable them to reversibly take up molecules up to a certain diameter. At that time only two classes of molecular sieves were known: framework aluminosilicates and some activated carbons [1]. The former were termed "zeolites" (from the Greek ζεειν = to boil and λιθos = stone) by Cronstedt in 1756 referring to the frothy mass that can result when these materials are fused in a blowpipe [2].

Notwithstanding the early taxonomy, elaborate scientific research did not start before the pioneering studies of Barrer et al. in the late 1930's [3]. They provided the impetus for Milton and Breck from the Linde Division of the Union Carbide Corporation to synthesize and completely characterize for the first time an aluminosilicate molecular sieve without natural counterpart: Linde Type A zeolite [4] (which will be referred to as LTA, its mnemonic code [5]).

It appeared that the diameter of the apertures of the uniform pore structure of LTA-type aluminosilicate molecular sieves (see ref. 5 for structural information) could be adjusted from 0.30 up to 0.43 nm [4]. Moreover, LTA-type zeolites appeared to separate molecules like oxygen and nitrogen either according to intracrystalline diffusion rate or according to affinity for the zeolite surface [6]. With the commercial application of the latter property in the Lindox and Unox processes to sieve air and produce pure oxygen [7], the activity in molecular sieve science rapidly increased [8].

LTA still is the zeolite produced on the largest scale [9]. Its commercial success is mainly related to another characteristic of zeolites: their pores contain exchangeable cations to neutralize the negative charge of the aluminosilicate framework. The major use of sodium cation neutralized LTA-type aluminosilicate frameworks is as ion exchanger in low-phosphate and phosphate-free detergents replacing sodium tripoly-

phosphate builders as water softeners [10].

But the main economic incentive for expansion of research on molecular sieves does not come from their application as ion exchangers (see ref.11) or as selective adsorbents in drying and separations. It results from the ability of acidic, proton-neutralized molecular sieve frameworks to shape-selectively catalyze a wide range of reactions such as (hydro-)cracking [12,13,14], (hydro-)isomerisation [15,16], oligomerisation of olefins [17], dewaxing [18,19], alkylation of aromatics [20], and the conversion of methanol into gasoline [21,22] or lower olefins [23,24]. Accordingly, zeolite-based technology has completely altered an impressive number of conventional petrochemical and oil refining processes. Apart from these applications in bulk processes, the use of molecular sieve catalysts in organic fine chemistry is a very promising area for future research and development [25,26]. In this respect the large variety of (metal substituted) (silico-) aluminophosphate molecular sieves recently discovered by Flanigen and co-workers [27,28] is of considerable interest, for phosphate-based molecular sieves have been found to extend the kinetic diameter of molecules that can be shape-selectively processed from 0.74 nm (the largest zeolitic pore diameter [5]) to 1.2 nm [29] or even 1.42 nm [30]. Also the synthesis of (transition metal) substituted crystalline silica molecular sieves [31-35], offers interesting opportunities to extend the use of molecular sieves. Besides allowing shape-selective adsorption or reaction of additional classes of organic compounds, these novel molecular sieves may lead to completely new organic reactions. Molecular sieve-based catalytic conversions and separations are expected to contribute to new less-polluting processes at lower, energy-saving temperatures warranting their continued exploration.

Extensive recent research activities (see ref.36) have not only led to a growth in number and (potential) catalytic applications of molecular sieves, it has also yielded profound knowledge of the more conventional catalysts [12,37,38]. Because of the available detailed information on their regular systems of intracrystalline channels and cavities, these molecular sieves have been extensively used as model compounds for probing modern analytical techniques like high-resolution solid-state nuclear magnetic resonance (NMR) spectroscopy [39,40,41,42], and have contributed substantially to the

maturation of more advanced NMR techniques like quadrupole nutation NMR [43,44,45].

This thesis reports on the preparation of Brønsted acid catalysts from as-synthesized molecular sieves, making ample use of solid-state NMR spectroscopy. Well-known sieves with substantial industrial relevance are studied such as: a FAU-type zeolite (called zeolite Y) used in (fluid) catalytic cracking [12], and applied on the largest scale [22]; (platinum doped) MOR-type zeolite, used in hydroisomerization [38]; and a boron-substituted MFI-type silica polymorph, of potential use in fine chemistry [21].

Turning Molecular Sieves into Catalysts: Invariably, the voids of as-synthesized molecular sieves are filled by templates like sodium or organic cations and water molecules [3,4,37,46,47,48]. In many cases these cations have to be replaced by protons or multivalent cations to obtain catalytically active material. One way (e.g. used for MOR [49]) to accomplish this is simply by washing with mineral acid [50]. In general, however, such a procedure is not satisfactory, because the organic template is too much entangled (as in case of MFI [51]) or sorbed too strongly [52] to be removed, or because the molecular sieve is broken down in the process (as in case of FAU [49]). The former problem is solved by thermal calcination (see e.g. ref. 52), i.e. by decomposing and subsequently desorbing organic compounds by the action of heat [53,54]. The latter difficulty can be circumvented by e.g. ammonium exchanging the sodium-cations neutralizing a zeolite framework and subsequently heating the ammonium-neutralized zeolite to yield the desired proton-neutralized zeolite upon liberation of ammonia [49,55]. In case of e.g. as-synthesized FAU-type zeolites the limited accessibility of sodium cations located in the smaller cages [5,56] requires hydrothermal ammonium exchange [57] or -more conventionally- repeated ammonium-exchange steps combined with intermediate calcination to remove the desired amount of sodium cations [12]. Depending on the geometry of the ammonium-zeolite bed during the heating step two distinct products are obtained: Bed geometry which maximizes rapid diffusion of gaseous products from the sample ("shallow bed" calcination [55]) yields the expected minimally impaired, proton-neutralized FAU framework. Heating conditions which impede removal of gaseous products from the zeolite sample ("deep bed" [55] or

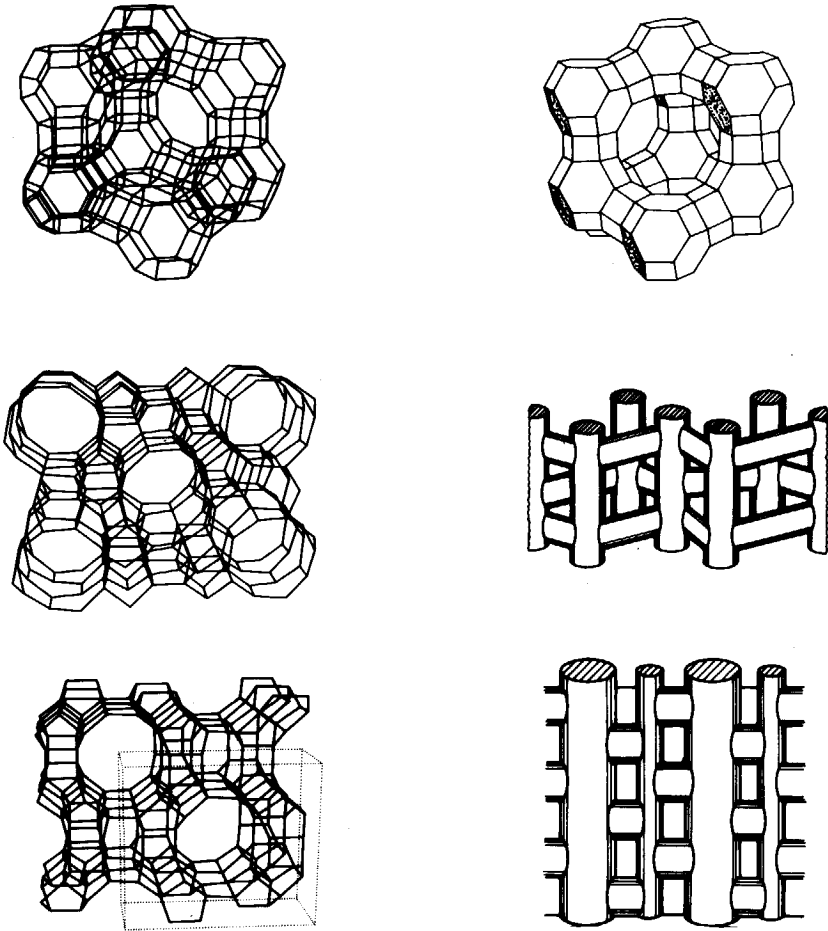*Fig.1: Drawings of FAU- (0.75 nm wide)(a), MFI- (0.55 nm wide)(b), and MOR-type (0.70 nm wide)(c) pore systems:*

At the left: network representation of the zeolite frameworks looking down the main channels; Si and Al atoms are represented by the vertices of the net, the linking oxygen atoms by straight lines

At the right: artist's impressions of the pore systems looking at the main channels from aside.

steam [58] calcination) reduce the number of aluminium atoms in the framework yielding an "ultrastable" [59] zeolite [55,60], with higher acid strength and higher catalytic activity [61].

In chapters 2 to 5 of this thesis the (hydrothermal) ammonium exchange of FAU will be studied in more detail. Moreover, conventional ammonia and organic template removal by thermal calcination procedures are compared with a recently introduced procedure -found in the course of the present study- based on low-temperature plasma technology [62].

Plasma Technology: The plasma state is often considered the fourth, most chaotic state of matter, unique like the solid, liquid and gaseous states [63,64,65]. Nearly all matter in the universe exists in this state, occurring predominantly in this form in the stars and in interstellar space [63,64,65]. Defined as a partially ionized gas [66], fire exemplifies this fourth aggregation state, just like earth, water and air represent the other three states [64]. A plasma is formed when the release of energy, e.g. from combustion, heats a gas to such extremely high temperatures that molecules dissociate and vigorous collisions break the atoms up into electrons and ions [63]. This occurs for instance inside the sun at 10^6 K and in flames at 10^3 K [64]. Alternatively, a plasma can be produced applying a strong electric field [64,66]. Although the preparative application of partially ionized gases generated in flames probably coincides with mankind's first steps in chemistry, the first application of a plasma produced by an electric discharge was not reported before 1796 by the Dutch chemists: Paets van Troostwijk and cowork-ers [67,68]. Investigating low-pressure mercury gas discharges, Langmuir originated the word "plasma" (from the Greek πλασμα = something moulded) in the 1920's [69] to denote the most ionized discharge regions. He was prompted to do so, because the behaviour of the massive, positive ions in the presence of rapidly oscillating electrons reminded him of a jelly [70]. According to modern concepts, a plasma can be defined as a quasi-neutral gas of charged and neutral particles which exhibits collective be-haviour [65]. This notion dates back only to the early 1950's, when space exploration, the growing awareness of the importance of magnetic fields in astrophysical phenome-

na, the quest for nuclear-fusion power reactors and the development of electronic devices increasingly focussed interest on the plasma state [63]. Large scale commercial application of low-temperature plasma technology started in the late 1960's, when it was suggested to use a low-temperature oxygen plasma to combustively remove organic (photoresist) films during the manufacture of microelectronic devices [71]. Since then increasing miniaturization of integrated circuits (IC's), has resulted in a heavy reliance on low-temperature plasma processing [72].

A low-temperature plasma is characterized by a pressure in the range of 5 to 500 Pa, an electron density between 10^{15} and 10^{18} m^{-3} and an average electron temperature of 10^4 to 10^5 K [71]. The ratio of electron to neutral species concentration typically is in the range of 10^{-6} to 10^{-4}, implying fairly low degrees of ionization [71]. When such a plasma is produced by a radio frequency (rf) discharge, the free electrons almost exclusively absorb the energy from the applied large rf field, leaving the ions and neutral species near room temperature [66,71,72]. As electrically insulating samples in contact with a plasma charge negatively [66] and thereby repel the free electrons, the highly energetic, free electrons exert their destructive influence only on the gas molecules. These molecules are ionized, and (more often) dissociated, forming electrically neutral, chemically extremely reactive species like oxygen atoms [73,74]. Considering the reactive species and oxidative properties of a low-temperature oxygen plasma [73,74] used for removal of organic films in microelectronics manufacture, it strikingly resembles a flame [75] at low temperature. In this thesis (chapters 5-7) application of an oxygen plasma is described for burning out (or calcining [53,54]) molecular sieves near 370 K in order to combustively remove ammonia and organic compounds and try to obtain material unaccessible by thermal decomposition (or calcination [53,54]) near 800 K.

Scope of this Thesis: In this thesis (**chapter 2**) conventional ammonium exchange of an as-synthesized sodium-neutralized FAU-type zeolite (referred to as Na-Y [5]) at temperatures well below 373 K is studied by ^{23}Na MAS nutation NMR. Combination of kinetic and NMR data allows to unravel the ammonium-exchange mechanism in three

distinct steps and to unambiguously locate -for the first time- the sodium cations in fully hydrated (partially exchanged) Na-Y zeolite (**chapter 2**). These data are used in a study of the hydrothermal ammonium exchange of Na-Y at 433 K in order to attain 100% ammonium exchange (**chapter 3**). To explore whether a 100% ammonium-exchanged Na-Y zeolite is worth attaining, "deep bed" calcination of this product is compared with ultrastabilization of conventional, around 70% ammonium-exchanged Na-Y (**chapter 4**). Furthermore, "shallow bed" and plasma calcination of ammonium-exchanged Na-Y as well as hydronium exchange at near-neutral pH are employed to try to obtain a fully intact hydronium-neutralized zeolite Y framework (**chapter 5**). Plasma calcination is compared with mild, shallow bed calcination of ammonium-exchanged FAU (**chapter 5**) and (platinum-doped) ammonium-exchanged MOR (**chapter 6**). Finally, applicability of low-temperature oxygen plasma calcination for the oxidative removal of organic templates from as-synthesized zeolites is explored (**chapter 7**).

References:

1. McBain, J.W. *The Sorption of Gases and Vapours by Solids;* Routledge: London, 1932, 167-176.
2. Cronstedt, *A.Fr. Kongl.Svenska Vetenskaps Acad.Handlingar* **1756**, *17*, 120-123.
3. Barrer, R.M. *Hydrothermal Chemistry of Zeolites;* Academic: London, 1982.
4. Breck, D.N. *Zeolite Molecular Sieves: Structure, Chemistry and Use;* Wiley: New York, 1974.
5. Meier, W.M., Olson, D.H. *Atlas of Zeolite stucture types* (Structure Commission of the International Zeolite Association); Butterworths: London, 2nd, 1987.
6. Barrer, R.M. *Zeolites and Clay Minerals as Sorbents and Molecular Sieves;* Academic: London, 1978.
7. Ruthven, D.M. *Principles of Adsorption and Adsorption Processes;* Wiley: New York, 1984.
8. Kerr, G.T. *Sci.Am.* **1989**, *260*, 82-87.

9. Van Bekkum, H.; Kouwenhoven, H.W. *Recl.Trav.Chim.Pays-Bas* **1989**, *108*, 283-294.

10. Schwuger, M.J.; Liphard, M. *Stud.Surf.Sci.Catal.* **1989**, *46*, 673-690

11. Sherman, J.D. *Nato ASI Ser.E* **1984**, *80*, 583-623.

12. Scherzer, J. *Catal.Rev.Sci.Eng.* **1989**, *31*, 215-354.

13. Chen, N.Y.; Maziuk, J.; Schwartz, A.B.; Weisz, P.B. *Oil Gas J.* **1968**, *66*, 154-157.

14. Heineman, H. *Catal.Rev.Sci.Eng.* **1977**, *15*, 53-67.

15. Kouwenhoven, H.W.; Van Zijl Langhout, W.C. *Chem.Eng.Progr.* **1971**, *67*, 65-70.

16. Olson, D.H.; Haag, W.O. *ACS Symp.Ser.* **1984**, *248*, 275-307.

17. Garwood, W.E *ACS Symp.Ser.* **1983**, *218*, 383-396.

18. Smith, K.W.; Starr, W.C.; Chen, N.Y. *Oil Gas J.* **1980**, *78*, 75-78.

19. Chen, N.Y.; Goring, R.L.; Ireland, H.R., Stein, T.R. *Oil Gas J.* **1977**, *75*, 165-170.

20. Chen, N.Y.; Garwood, W.E. *Catal.Rev.Sci.Eng.* **1986**, *28*, 185-264.

21. Chang, C.D.; Silvestri, A.J. *CHEMTECH* **1987**, *17*, 624-631.

22. Chang, C.D. *Catal.Rev.Sci.Eng.* **1983**, *25*, 1-118.

23. Chang, C.D.; Lang, W.H.; Lago, R.M.; Silvestri, A.J. *Ger.Offen.* 2615150, 1976.

24. Kaeding, W.W.; Butter, S.A. *J.Catal.* **1980**, *61*, 155-164.

25. Hölderlich, W.; Hesse, M.; Näumann, F. *Angew.Chem.* **1988**, *100*, 232-251.

26. Van Bekkum, H.; Kouwenhoven, H.W. *Stud.Surf.Sci.Catal.* **1988**, *41*, 4559.

27. Flanigen, E.M.; Lok, B.M.; Lyle Patton, R.; Wilson, S.T. *Stud.Surf.Sci.Catal.* **1986**, *28*, 103-112.

28. Flanigen, E.M.; Lyle Patton, R.; Wilson, S.T. *Stud.Surf.Sci.Catal.* **1987**, *37*, 13-27.

29. Davis, M.E.; Saldarriaga, C.; Montes, C. Garces, J.; Crowder, C. *Nature (London)* **1988**, *331*, 698-699.

30. Moore, P.B.; Shen, J. *Nature(London)* **1983**, *306*, 356-358.

31. Kouwenhoven, H.W.; Stork, W.H.J.; Schaper, L. *Ger.Offen.* 2755770, **1978.**

32. Bell, W.J.; Dwyer, J.; Garforth, A.A.; Smith, W.J. *Stud.Surf.Sci.Catal.* **1986**, *28*, 137-144.

33. Taramasso, M.; Perego, G.; Notari, B. *Proc.Int.Conf.Zeolites 5th;* (Rees, L.V.C. ed.), Heyden: London, **1980;** pp.40-48.

34. Taramasso, M.; Perego, G.; Notari, B. *U.S. Patent* 4410501, 1983.

35. Perego, G.; Bellusi, G.; Corno, C.; Taramsso, M.; Buonomo, F.; Esposito, A. *Stud.Surf.Sci.Catal.* **1986,** *28,* 129-136.

36. *Zeolites: Facts, Figures, Future: Proc.Int.Conf.Zeolites 8th;* (Jacobs, P.A.; Van Santen, R.A. eds.). Published in *Stud.Surf.Sci.Catal.* 1989, *49A* and *49B.*

37. Newsam, J.M. *Science* **1986,** *231,* 1093-1099.

38. Maxwell, I.E. *Catal.Today* **1987,** *1,* 385-413.

39. Klinowski, J. *Progr.NMR Spectrosc.* **1984,** *16,* 237-309.

40. Engelhardt G.; Michel D. *High-Resolution Solid State NMR of Silicates and Zeolites;* Wiley: New York, 1987; pp.218-238.

41. Vega, A.J. *J.Am.Chem.Soc.* **1988,** *110,* 1049-1054.

42. Fyfe, C.A.; Gies, H.; Feng, Y.; Kokotailo, G.T. *Nature(London)* **1989,** *341,* 223-225.

43. Samoson, A.; Lippmaa, E. *Chem.Phys.Lett.* **1983,** *100,* 205-208.

44. Kentgens, A.P.M.; Lemmens, J.J.M.; Geurts, F.M.M.;Veeman, W.S. *J.Magn.Res.* **1987,** *71,* 62-74.

45. Janssen, R. *PhD. Thesis,* Nijmegen, 1990.

46. Flanigen, E.M. *ACS Symp.Ser.* **1973,** *121,* 119-139.

47. Lok, B.M.; Cannan, T.R.; Messina, C.A. *Zeolites* **1983,** *3,* 282-291.

48. Lowe, B.M. *Stud.Surf.Sci.Catal.* **1987,** *37,* 1-12.

49. Scherzer, J. *ACS Symp.Ser.* **1984,** *248,* 157-200.

50. Gelsthorpe, M.R.; Theocharis, Ch.R. *J.Chem.Soc.Chem.Commun.* **1986,** 781-782.

51. Soulard, M; Bilger, S.; Kessler, H.; Guth J.L. *Zeolites* **1987,** *7,* 463-470.

52. Franklin, K.R.; Lowe, B.M. *Zeolites* **1988,** *8,* 508-516.

53. *The Concise Oxford Dictionary of Current English;* Clarendon: Oxford, 6th, 1976, p.138.

54. *Webster's New Twentieth Century Dictionary;* Simon and Schuster: New York, 2nd, 1979, p.255.

55. Kerr, G.T. *ACS Symp.Ser.* **1973,** *121,* 219-229.

56. Sherry, H.S. *Ion Echange, A Series of Advances* **1969,** *2,* 89-133.

57. Alafandi, H.; Stamires, D. *U.S. patent* 4058484, 1977 and *U.S. patent* 4085069, 1978.

58. Hansford, R.C. *U.S. patent* 3354077, 1967.

59. Maher, P.K.; McDaniel, C.V. *U.S. patent* 3293192, 1966.

60. McDaniel, C.V.; Maher, P.K. *ACS Monograph* **1976**, *171*, 285-331.

61. Barthomeuf, D.; Beaumont, R. *J.Catal.* **1973**, *30*, 288-297.

62. Maesen, Th.L.M.; Bruinsma, O.S.L.; Kouwenhoven, H.W.; Van Bekkum, H. *J.Chem. Soc.,Chem.Commun.* **1987**, 1284-1285.

63. Liley, B.S. in *Encyclopaedia Britannica, Macropaedia;* Chicago, 15th, 1985, Vol.23, pp.702-708.

64. Nagel, D.J. in *Kirk-Othmer Ecycl.Chem.Technol.;* Wiley: New York, 3rd, 1984, Suppl.Vol., pp.599-625.

65. Chen, F.F. *Introduction to Plasma Physics and Controlled Fusion; Vol.1: Plasma Physics;* Plenum: New York, 2nd, 1984.

66. Chapman, B.N. *Glow Discharge Processes;* Wiley: New York, 1980, pp.49-76.

67. Bondt, N.; Deiman, J.R.; Paets van Troostwijk, A.; Lauwerenburgh, A. *Ann. Chim.* **1796**, *21*, 58-71.

68. Partington, J.R. *A History of Chemistry;* MacMillan: London, 1970, pp.584-585.

69. Langmuir, I. *Proc.Natl.Acad.Sci.* **1926**, *14*, 627-637.

70. Tonks, L.; Langmuir, I. *Phys.Rev.* **1929**, *33*, 195-210.

71. Mucha, J.A.; Hess, D.W. *ACS Symp.Ser.* **1983**, *219*, 215-285.

72. Graves, D.B. *AIChE J.* **1989**, *35*, 1-29.

73. Cook, J.M.; Benson, B.W. *J.Electrochem.Soc.* **1983**, *130*, 2459-2464.

74. Walkup, R.; Saenger, K.; Selwyn G.S. *Mater.Res.Soc.Symp.Proc.* **1985**, *38*, 67-76.

75. Glassman, I. *Combustion;* Academic: New York, 1977.

CHAPTER 2

CATION POSITIONS IN FULLY HYDRATED Y ZEOLITES MONITORED BY ^{23}Na (MAS) NUTATION NMR[*]

Abstract

^{23}Na MAS nutation NMR is used to investigate cation distributions in a fully hydrated Y-zeolite. Combination of ^{23}Na MAS nutation NMR and kinetic data on ammonium exchange establishes that fully hydrated Na-Y (Si/Al = 2.5±0.1) contains 7±1 sodium cations in the hexagonal prisms, 16±1 in the sodalite cages and 32±1 in the supercages. Ammonium exchange is shown to proceed in three progressively slower steps. In the first step ammonium exchanges with sodium in the supercages; in the second step sodium in the hexagonal prisms is replaced by ammonium in the supercages and only in the last step ammonium exchanges with sodium in the sodalite cages. Sodium exchange kinetics confirm that NH$_4$-Y contains 39±1 ammonium cations per unit cell in the supercages and 16±1 in the sodalite cages. Both the second and the last step of the exchange process are shown to be accelerated by (hydrothermal) heating. Hydrothermal heating as well as ammonium or cesium exchange appear to induce the removal of the sodium cations from the hexagonal prisms. This cation redistribution is explained as the result of a decrease in cation-framework interaction energy inside the hexagonal prisms caused by the observed enhancement of cation-framework interactions in supercages and sodalite cages. Finally, ^{23}Na MAS nutation NMR on fully hydrated H,Na-Y shows that not only the sodium-framework interactions in the sodalite cage and hexagonal prism, but also those in the supercage are sensitive to ion exchange.

---

[*]Maesen, Th.L.M.; Janssen, R.; Van Bekkum, H.; Kouwenhoven, H.W.; Veeman, W.S., *J.Phys.Chem.*, in press.

Introduction

The now well established structure of the faujasite (FAU) framework [1] was elucidated as early as 1958 from a natural mineral specimen [2]. Reflecting the importance of synthetic FAU-type zeolites in petrochemical industry [3], FAU has been subject of numerous structural studies since [4,5,6]. However, the exact locations of sodium cations in hydrated FAU have never been determined unambiguously [6,7,8], even though sodium has a predominant effect on acidity, stability and catalytic properties [9,10]. Reasons include the fact that conventional X-ray and neutron powder diffraction structure determinations are severely hindered by i) motions or disorder of sodium and ii) similar scattering factors of sodium and oxygen ions [4]. Moreover, far-IR spectroscopy has provided only qualitative data on the possible location of the counter ions in partially hydrated FAU because of unknown extinction coefficients [11].

Sodium-FAU containing n absorbed water molecules can be represented as $Na_xAl_xSi_{192-x}O_{384}.nH_2O$ ($n \leq 252$)[1,4,5]. Since FAU is observed to obey Loewenstein's rule [12] of Al-O-Al linkage avoidance [13,14], only compositions $x \leq 96$ ($Si/Al \geq 1$) occur. By convention, synthetic FAU-type zeolites are termed X when $x \geq 77$ ($Si/Al < 1.5$) and Y when $x \leq 76$ ($Si/Al > 1.5$) [5]. As only for compositions $x \leq 56$ ($Si/Al \geq 2.4$) cation exchange has not been reported to be complicated by concomitant hydronium ion exchange [11,15] and as compositions $x \leq 56$ are often used for preparation of commercial catalysts [10,16], zeolite Y with $x = 55$ ($Si/Al = 2.5$) has been chosen for study in the present paper.

FAU-type zeolites consist of TO_4 tetrahedra (T = Si or Al) which are all connected through their corners of shared oxygen atoms to form cubooctahedral structures (sodalite cages) joined together through hexagonal prisms. The tetrahedral arrangement of cubooctahedral cavities gives rise to supercages (see Fig.1) [1]. The unit cell of FAU consists of 192 TO_4 tetrahedra which together form 8 supercages, 8 sodalite cages and 16 hexagonal prisms [4]. For each substitution of Al^{3+} for Si^{4+} in a TO_4 tetrahedron one negative charge is acquired by the oxygen framework. This negative charge may be considered to be distributed fractionally among the four structurally inequivalent

framework oxygens of each AlO_4 tetrahedron and is compensated by exchangeable counter ions such as Na^+. The counter ions are distributed over a limited number of sites: in the hexagonal prism (site I), in the sodalite cage at a six-ring shared with a hexagonal prism (site I') and in the supercage at a six-ring (site II) or four-ring (site III [6,17,18,19]) [6].

Sites in a sodalite cage at the six-ring shared with a supercage (site II') are usually not occupied by cations but rather by small neutral molecules like water [6].
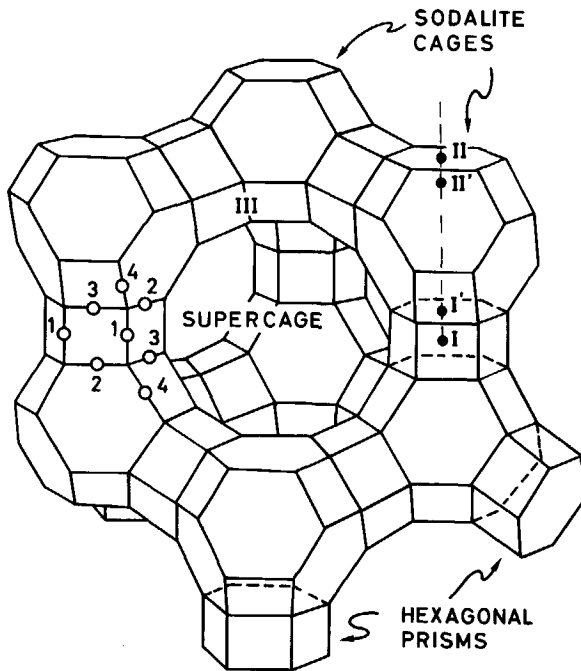

Fig.1: FAU framework showing oxygen type (○) and non-framework (●) locations

Adjacent sites in sodalite cage (I') and hexagonal prism (I) are not occupied by cations simultaneously [4,6]. Since there are less cations required to neutralize the negative framework charge of zeolite Y than there are potential locations, cations can populate the three different cages to various, though interdependent [20] degrees. Accordingly, charges on O2 can be compensated by coordination to cations inside the hexagonal prisms (site I) or to cations inside the supercages (site II). Likewise, charges on O3 can be compensated from within the hexagonal prisms (site I) or from within the sodalite cages (site I'). Charges on O1 and O4 are accessible only to cations in the supercages (site II and III) [17]. The exact cation distribution is known to depend on the relative energy of the respective locations as modified by the interaction strength of a cation at a particular location with anionic framework oxygens, adsorbed water and other cations [18,19,21,22]. In the present paper it is shown (in agreement with ref. 20) that, in addition, the relative energy of a particular location is modified by cation-framework interactions at other sites. These interactions will also give rise to variations in the symmetry of the first coordination sphere of e.g. a sodium cation and therefore are amenable to quadrupole nutation NMR.

A quadrupole nutation NMR spectrum is recorded when a series of free induction decays is acquired during an interval t2 while monotonically increasing the length t1 of the preceding pulse. Double Fourier transformation in t2 and t1 gives a two-dimensional NMR spectrum with information about combined chemical shift and quadrupole interactions along the F2 axis and information exclusively about the quadrupole interactions along the F1 axis. The interactions between nuclei with a quadrupole moment eQ and an electric field gradient, V, are characterized by the asymmetry parameter η (defined as $(V_{xx}-V_{yy})/V_{zz}$ where V_{ii} is the electric field gradient along the i principal axis and $0 \leq \eta \leq 1$) and by the product of eQ and V_{zz} ($=eq$) (the so called quadrupole coupling constant, e^2qQ/h). When the quadrupole interaction is much smaller than the rf field strength, ω_{rf}, a peak appears at $1\omega_{rf}$ in dimension F1; when the quadrupole interaction is much larger than ω_{rf}, sodium resonates at $2\omega_{rf}$ in this dimension. In intermediate cases, when quadrupole interactions and ω_{rf} are of the same order of magnitude, e^2qQ/h and η can be estimated by computer simulation [23].

Magic angle spinning (MAS) is applied to enhance the resolution of quadrupole nutation NMR spectra. This technique removes broadening in the F2 dimension due to chemical shift anisotropy, dipolar and second order quadrupole interactions. MAS will not lead to effects along the F1 axis, provided that the sample spinning frequency is not of the same order of magnitude as the quadrupole interactions and the rf field strength [24].

This chapter will show that ^{23}Na (MAS) nutation NMR is particularly well suited to monitor changes in cation distribution and cation-framework interaction strength i) upon cesium and ammonium ion exchange of Na-Y, ii) upon ("shallow bed" [25]) calcination of partially ammonium-exchanged Y zeolite, and iii) during hydrothermal heating of hydrated Na-Y. Recently it has been shown that ^{23}Na NMR allows determination of the sodium population of the supercages in fully hydrated Na-Y [26]. Claims based on ^{23}Na MAS NMR assuming no quadrupole interactions [27] appear not to be validated. In the present paper it will be demonstrated that ^{23}Na (MAS) nutation NMR data combined with kinetic data on ion exchange allow determination of the cation distribution in Na-Y and NH$_4$-Y, elucidation of the mechanism of ammonium exchange and explanation of the observed cation redistributions.

Experimental

Materials: The parent sample was zeolite Na-Y with Si/Al = 2.5±0.1 as determined by XRF, ICP-AES, XRD and ^{29}Si MAS NMR. According to standard thermogravimetric analysis, it contains 252±5 water molecules per unit cell, when fully hydrated. The average crystal size, Φ, estimated by scanning electron microscopy (SEM) was 1 μm. A fully ammonium-exchanged sample, NH$_4$-Y, was prepared contacting 5.0 g Na-Y first with 200 ml 1.0 mol.l^{-1} aqueous silver nitrate, then with 200 ml 0.3 mol.l^{-1} aqueous silver nitrate, and finally extracting the resulting Ag-Y twice with 200 ml 1.0 mol.l^{-1} aqueous ammonium thiocyanate [28]. The ammonium-to-aluminium ratio of NH$_4$-Y as determined by ICP-AES and Kjeldahl analysis [29] after dissolution (as described by

Von Ballmoos [30]) and suited neutralization was 0.99 and according to ICP-AES NH_4-Y contained less than 0.1 sodium or silver atoms per unit cell. 54.2% cesium-exchanged Na-Y (Cs,Na-Y-54) was made by contacting 5.0 g Na-Y with 200 ml 1.0 mol.l^{-1} aqueous cesium nitrate at 360 K for 3 hours. The amount of sodium exchanged was calculated from the sodium, aluminium and cesium content determined by ICP-AES and flame-AES after dissolution [30] of the zeolite. 53.4%, 70.4% and 86.8% ammonium-exchanged samples (which will be referred to as NH_4,Na-Y-53, NH_4,Na-Y-70 and NH_4,Na-Y-87, respectively) were prepared by ion exchange with aqueous ammonium nitrate at 298 K [15]. The extent of sodium exchange was calculated from the sodium-to-aluminium ratio determined by ICP-AES on the dissolved [30] zeolite. Under optimally dry ("shallow bed" [25]) conditions and at a final calcination temperature of 670 K NH_4,Na-Y-70 was converted into H,Na-Y-70. Upon careful hydration ^{29}Si MAS NMR and ^{27}Al MAS NMR showed that this H,Na-Y-70 contained only a very small amount of extra-framework aluminium (see ref. 31). MAS NMR measurements on samples referred to as "freshly prepared" were performed as quickly as incipient drying of a sample separated from an ion exchange solution and exposed to laboratory air permitted. All other samples were fully hydrated in a desiccator over saturated ammonium nitrate solution (80% relative humidity) before NMR or kinetic measurements. Prior to NMR measurements samples were additionally wetted.

Kinetic Measurements: Cation exchange was followed in time at 298 K stirring 0.1 g Na-Y or NH_4-Y with 25 ml 0.1 mol.l^{-1} ammonium and sodium nitrate, respectively. At selected intervals exchange was stopped by filtration of the suspension with a micropore filter (0.22 μm pores). After thorough washing, the zeolite was analysed for sodium and aluminium as described above.

Characterization: ^{23}Na MAS nutation NMR spectra were recorded using a Bruker AM-600 multinuclear spectrometer at 158.71 MHz. Static ^{23}Na nutation NMR spectra at temperatures up to 460 K were recorded on a Bruker CXP-300 spectrometer with a home-built variable temperature probe (described in ref. 32) at 79.35 MHz on an

aqueous suspension of Na-Y, which was contained in a sealed quartz tube. Following Kundla et al. [33] an aqueous 3.0 mol.l^{-1} NaCl solution was chosen as chemical shift reference. A ^{27}Al MAS NMR spectrum was recorded using a Varian VXR-400 S spectrometer at 104.23 MHz. Nitrogen adsorptions were measured on a Digisorb 2600 (Micromeritics) at 77 K. Samples (0.25 g) were degassed overnight in vacuo at 820 K. Relative pressures were converted [34] into t-values as follows:

$$t = [13.99/(\log(p^0/p) + 0.034)]^{0.5} \qquad (1)$$

Results and Discussion

^{23}Na MAS (nutation) NMR on Na-Y: The ^{23}Na MAS nutation NMR spectrum at 290 K
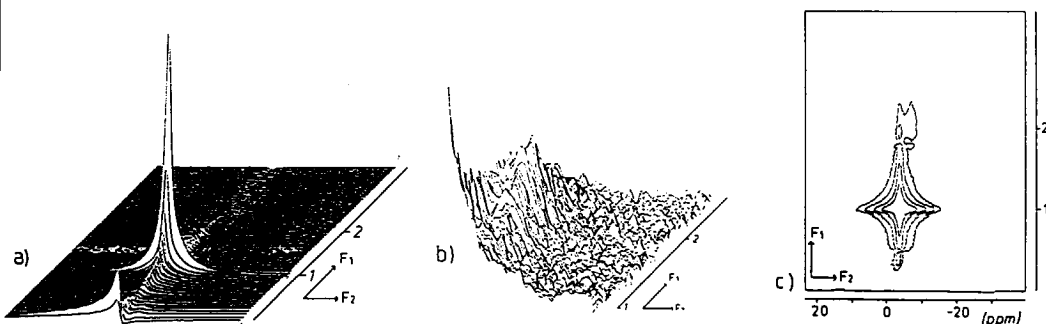

Fig.2: ^{23}Na MAS nutation NMR spectrum of fully hydrated Na-Y. The numbers along the
F1 dimension indicate $1\omega_{rf}$ and $2\omega_{rf}$ (ω_{rf} = 50 kHz).
a) stacked plot
b) blow-up of region around (-5ppm, $2\omega_{rf}$)
c) contour plot

of fully hydrated Na-Y consists of a signal at (-1ppm,$1\omega_{rf}$) and an intermediate quadru-pole pattern with a main absorption at (-5ppm,$2\omega_{rf}$) (Fig.2). As even at ω_{rf} = 5 kHz the former signal resonates at $1\omega_{rf}$, comparison with theoretical spectra [23] reveals that its quadrupole coupling constant, e^2qQ/h, is at most 0.1 MHz. Simulation shows that in case of a quadrupole coupling constant as small as 0.1 MHz characteristic ($\pm3/2 \leftrightarrow \pm1/2$) satellite transitions should be detectable (Fig.3). Since this characteristic
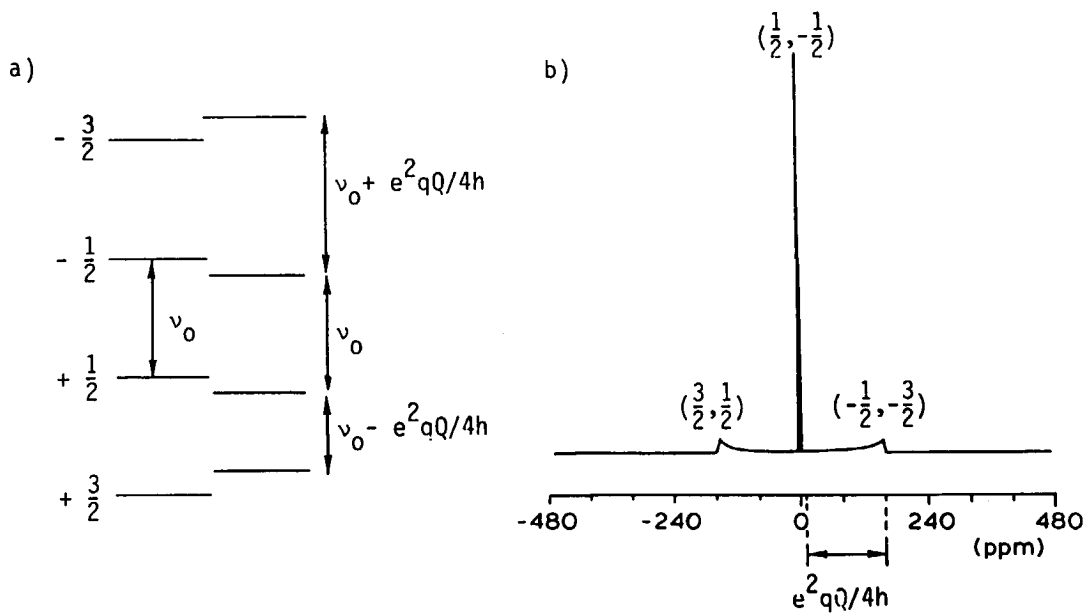

Fig.3: a) *energy level diagram of* ^{23}*Na (I=3/2) upon Zeeman and additional quadrupolar splitting;*

b) *simulated* ^{23}*Na NMR spectrum (no MAS) at 158.71 MHz using* e^2qQ/h *= 0.1 MHz and axial symmetry ($\eta=0$)*

pattern (see Fig.3b) has not been observed in ^{23}Na NMR spectra whether recorded

with or without MAS, the quadrupole coupling constant of the signal at $(-1\text{ppm},1\omega_{rf})$ apparently is so small that both satellite and central transitions resonate around -1 ppm. Accordingly, at $(-1\text{ppm},1\omega_{rf})$ all transitions, i.e. 100% of the absorption, are detected. At $(-5\text{ppm},2\omega_{rf})$, on the contrary, the absorption can be simulated with a quadrupole coupling constant in the order of 0.7 MHz implying that in this case the $(\pm3/2 \leftrightarrow \pm1/2)$ satellite transitions are broadened beyond detection and that only the central $(-1/2 \leftrightarrow \pm1/2)$ transition, i.e. 40% of the total absorption, can be detected [35]. The one dimensional ^{23}Na MAS NMR spectrum of fully hydrated Na-Y (corresponding to the sum projection of the ^{23}Na MAS nutation NMR spectrum on the F2 axis) is shown in
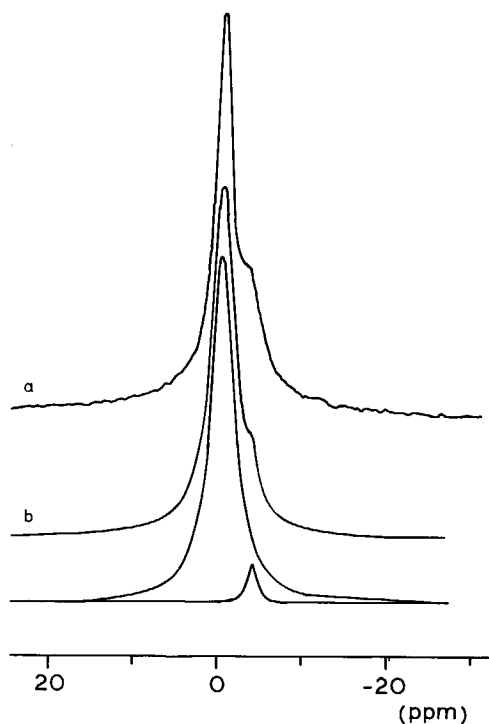

Fig.4: a) ^{23}Na MAS NMR spectrum of fully hydrated Na-Y

   b) deconvolution and simulation of Fig.4a

Fig.4a. Deconvolution (with an estimated absolute error of 1.5%) using Lorentzian lines yields that 95.5% of the signal resonates at -1ppm and 4.5% at -5ppm (see Fig.4b). When these values are corrected for the fact that at -1ppm the absence of quadrupole interactions allows detection of 100% of the absorption, whereas at -5ppm merely 40% of the absorption can be detected due to quadrupolar broadening of the satellite transitions, $89.5 \pm 3.3\%$ or 49 ± 2 sodium cations per unit cell (Si/Al$=2.5 \pm 0.1$) appear to resonate at -1ppm and $10.5 \pm 3.3\%$ or 6 ± 2 sodium cations per unit cell resonate at -5ppm. Although to our knowledge under experimental conditions comparable to ours (high magnetic field, MAS, hydrated system) NMR-invisible sodium due to excessively high quadrupole interactions has never been reported, we made an experimental check on this point with a sample consisting of a physically separated NaCl and hydrated Na-Y. All Na spins were detected.

When a ^{23}Na MAS nutation NMR spectrum is recorded on a Na-Y sample that has been dried overnight at 750 K (not shown), all resonances are found at $2\omega_{rf}$ at the F1 axis and at more negative ppm values at the F2 axis. Thus the absent quadrupole interactions of the 49 ± 2 sodium cations per unit cell resonating at (-1ppm,$1\omega_{rf}$) in the spectrum of fully hydrated Na-Y (Fig.2) have strongly increased upon drying. Apparently the absence of quadrupole interactions is due to the presence of water. Accordingly, it is known that the eight supercages of a unit cell of fully hydrated Na-Y contain some 220 water molecules [4,5,6,7], which should easily provide sodium with an oxygen coordination symmetric enough to induce only small quadrupole interactions. Furthermore, these water molecules can average out residual asymmetry of the electric field gradient at a sodium nucleus in a supercage, for they change position at a frequency in the order of 10^9 Hz [36], i.e. very fast compared to the quadrupole interaction. The 32 water molecules in the eight sodalite cages [37,38] together with the framework oxygens can provide sodium in these cages with a tetrahedral oxygen coordination [4,5,6, 7,8]. Their reorientation frequency [38] in the order of 10^7 Hz [37] is likely to average out a not too large distortion of the symmetry of the electric field gradient at sodium inside these cages as well. Upon drying sodium cations in supercages and sodalite cages are coordinated to oxygen atoms from only one side [4,5,6] and thus will no longer find

themselves in a highly symmetric electric field gradient. Therefore, the 49 ± 2 sodium cations which display no quadrupole interactions in fully hydrated Na-Y, but interact with an asymmetric electric field gradient upon drying, are assigned to sites in the supercages and sodalite cages. Inside the hexagonal prisms, sodium (diameter $\Phi=0.23$ nm [39]) is completely surrounded by asymmetrically spaced negatively charged framework oxygens [4] and has at most 0.08 nm free space [6,7,39]. Water molecules do not fit in the hexagonal prisms and cannot symmetrically surround the sodium ions [6,39]. Therefore the 6 ± 2 sodium cations which reveal quadrupole interactions even in the fully hydrated sample must be located inside the hexagonal prisms.

Finally, the observed differences in chemical shift between sodium in dry and wet environment lead to the conclusion that a larger chemical shift indicates less hydration or stronger interactions with the anionic oxygen framework (cf. references 40,41).

Cation Redistribution upon Cesium Exchange: Since cesium cations are too large to enter any other cage but the supercages [42], cesium exchange of Na-Y can assist in distinguishing sodium cations inside sodalite cages or hexagonal prisms from those inside supercages. From the ^{23}Na MAS nutation NMR of freshly prepared hydrated Cs,Na-Y-54 it can be estimated that when 29.8 ± 0.9 sodium cations per unit cell are
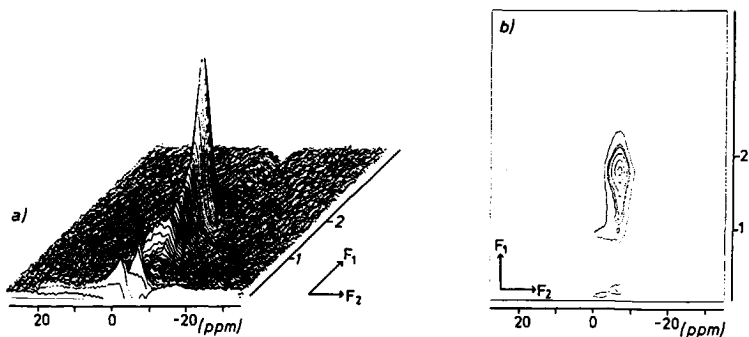

Fig.5: ^{23}*Na MAS nutation spectrum of Cs,Na-Y-54. The numbers along the F1 dimension indicate* $1\omega_{rf}$ *and* $2\omega_{rf}$ *(*ω_{rf} *= 60 kHz).*

replaced by cesium 11±4% of the absorption is found at (-1ppm,1ω_{rf}) and 89±4% at (-5ppm,2ω_{rf}) (Fig.5). Similar to the spectrum of fully hydrated Na-Y (Fig.2), the former resonance reveals no quadrupole interactions, whereas the latter can be simulated with a quadrupole coupling constant in the order of 0.7 MHz. Thus at (-1ppm,1ω_{rf}) 100% of the absorption is detected, whereas at (-5ppm,2ω_{rf}) a mere 40% is detected due to quadrupolar broadening of the satellite transitions. With this correction, 1.2±0.5 sodium cations per unit cell (4.7% of the 25.2±0.5 sodium cations still present) can be calculated to resonate at (-1ppm,1ω_{rf}), whereas the remaining 23.9±0.8 resonate at (-5ppm,2ω_{rf}). Since upon cesium exchange the supercages of fully hydrated zeolite Y remain very aqueous [4,43], it is expected that sodium inside supercages will preserve its weak framework interactions and highly symmetric oxygen coordination. Therefore the 1.2±0.5 sodium cations still resonating at (-1ppm,1ω_{rf}) in the spectrum of Cs,Na-Y-54 are supposed to be located in the supercages, whereas the other 23.9±0.8 sodium cations are to be located inside sodalite cages and hexagonal prisms. Since adjacent sites in the 8 sodalite cages and 16 hexagonal prisms are not occupied simultaneously [4,6], each cation inside a hexagonal prism will inhibit occupation of 2 of the 32 potential sites in the sodalite cages (see Fig.1). Thus of the 23.9±0.8 sodium cations at most 8.1±0.3 can be inside hexagonal prisms and at least 15.8±0.5 are inside the sodalite cages. This implies that the rise in number of cations absorbing at (-5ppm,2ω_{rf}) from 6±2 in Na-Y to 23.9±0.8 in Cs,Na-Y-54 cannot be ascribed to a strongly increased occupation of the hexagonal prisms, but points to enhanced framework interactions and decreased symmetry or decreased mobility of sodium inside the sodalite cages, due to the presence of cesium in the supercages.

When this Cs,Na-Y-54 sample has been at 440 K under saturated water vapor pressure, ^{23}Na MAS nutation NMR shows, that 57±4% of the resonance can be found at (-1ppm,1ω_{rf}) and 43±4% at (-5ppm,2ω_{rf}) (Fig.6), whereas ICP-AES and flame-AES indicate that the sum of sodium and cesium ions is still equal to the number of aluminium atoms. Correcting for the undetected absorption at (-5ppm,2ω_{rf}), it can be calculated that now 8.7±1.0 sodium cations resonate at(-1ppm,1ω_{rf}), whereas 16.4±1.0 sodium cations still resonate at (-5ppm,2ω_{rf}). Since the 29.8±0.9 cesium cations cannot leave the
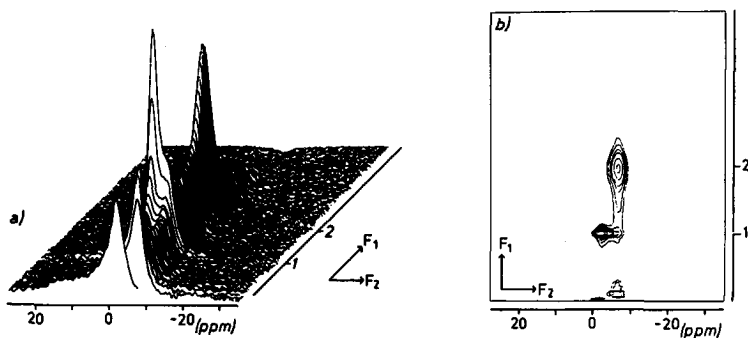
Fig.6: ^{23}Na *MAS nutation NMR spectrum of Cs,Na-Y-54 after heating. The numbers along the F1 dimension indicate $1\omega_{rf}$ and $2\omega_{rf}$ (ω_{rf} = 58 kHz)*

supercages [45], this implies that upon hydrothermal heating 7.0 ± 1.5 additional sodium cations have attained a symmetric first coordination sphere and hence have entered the supercages. To find out were they come from, it can be stated that the cation selectivity series of zeolite Na-Y [44] qualifies the framework as a soft (Lewis) base [45], indicating that (soft) cesium cations in the aqueous supercages interact more strongly with the framework than (hard) sodium cations [45]. From structural considerations [17], it can be deduced that cesium exchange will increase the cation framework interaction energy with anionic O1, O2 and O4 from within the supercages. Moreover, the increased sodium-framework interaction energy from inside the sodalite cages (noted above) implies an increased interaction with anionic O3. Increased interactions with O2 and O3 from outside the hexagonal prisms will reduce the interaction energy inside the hexagonal prisms and is likely to induce their depletion [20,21,22]. Accordingly, the 7.5 ± 0.9 additional sodium cations which are observed to have entered the supercages of Cs,Na-Y-54 upon hydrothermal heating (Fig.5,6) most probably correspond to the 6 ± 2 sodium cations located in the hexagonal prisms of fully hydrated Na-Y (Fig.2).

Mechanism and Kinetics of Ammonium Exchange: At 298 K ammonium exchange of zeolite Na-Y appears to occur in three distinct steps: i) within a few minutes of contact between the small Na-Y crystals (estimated diameter approximately 1μm) and an excess ammonium nitrate solution (total ammonium-to-sodium ratio being 8.3) 32±1 sodium ions per unit cell are replaced by ammonium ions (Fig.7); ii)during the next 24 hours 7±1 more sodium ions are replaced (Fig.7), whereas iii) further ammonium exchange of
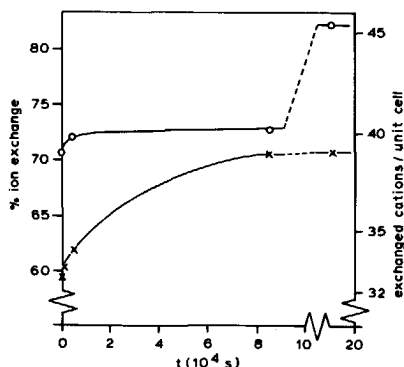

Fig.7: Ammonium exchange of Na-Y (X) and sodium exchange of NH$_4$-Y (o) followed in time

the remaining 16±1 sodium cations requires a larger excess of ammonium ions and even then takes 30 to 50 days [15].

The supercages are accessible through 0.74 nm wide [1] pores. As sodalite cages and hexagonal prisms are accessible to potassium but not to rubidium cations [44], the free diameter of their entrance must be in between 0.30 and 0.34 nm [39]. Therefore, the 32±1 sodium cations quickly replaced during the first ammonium exchange step are most probably located in the more easily accessible supercages. This is confirmed by ^{23}Na MAS nutation NMR. The spectrum of freshly prepared NH$_4$,Na-Y-53 (Fig.8) shows that 24±4% of the absorption is detected at (-1ppm,1ω_{rf}) and 76±4% at (-5ppm,2ω_{rf}) with an estimated e^{2}qQ/h of 0.7 MHz. Thus it can be calculated (applying the correction discussed above) that 2.9±0.2 sodium cations per unit cell are located in the supercages and that 22.7±0.9 sodium cations are located in hexagonal prisms or
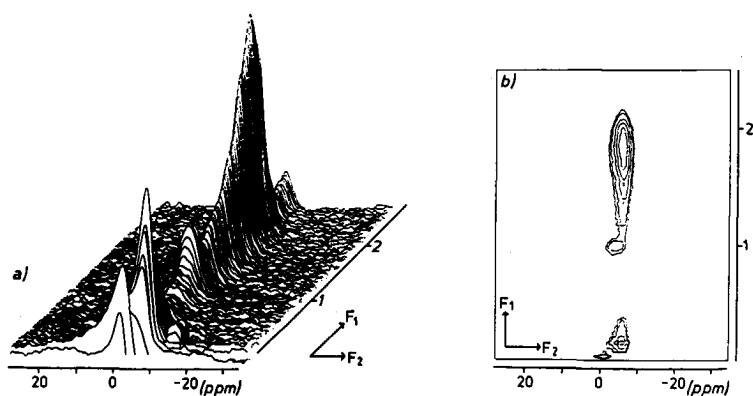
Fig.8: ^{23}Na MAS nutation NMR spectrum of NH$_4$,Na-Y-53. The numbers along the F1 dimension indicate 1ω_{rf} and 2ω_{rf} (ω_{rf} = 54 kHz)

sodalite cages. Since both the ammonium ion [39,46] and the six-membered oxygen window which separates a supercage from a sodalite cage [44] have a diameter somewhere in between 0.30 nm and 0.34 nm, penetration of NH$_4^+$ into the sodalite cages is expected to be extremely slow (cf. ref. 15). Thus all 29.3±0.8 ammonium cations in freshly prepared NH$_4$,Na-Y-53 will still be located in the supercages, together with the 2.9±0.2 sodium cations (see Table I). Accordingly, the supercages of freshly prepared Cs,Na-Y-54 (Table I, Fig.6) and NH$_4$,Na-Y-53 (Table I, Fig.8) appear to contain 31.6±0.6 cations on average, which compares well to the 32±1 sodium cations located in there by ammonium exchange kinetics (Fig.7, see above). Finally, the shift of the 16.7±2.9 sodium cations from (-1ppm,1ω_{rf}) in Na-Y to (-5ppm,2ω_{rf}) in NH$_4$,Na-Y-53 indicates an increase in interaction energy of sodium inside the sodalite cages with anionic O3 as was also observed upon 54.2% cesium exchange.

At the end of the second, slower ammonium exchange step (Fig.7) NH$_4$,Na-Y-70 is formed. ^{23}Na MAS nutation NMR on this sample shows that only the absorption at

Table I: Na counts (atoms per u.c.) and site assignments

sample	total #Na	(-1ppm,$1\omega_{rf}$) #Na sites		(-5ppm,$2\omega_{rf}$)[a] #Na sites	
Na-Y	55	49	super&sodal	6	hex.
Cs,Na-Y	25	1	super	24	sodal&hex.
Cs,Na-Y,heated	25	9	super	16	sodal.
NH_4,Na-Y-53	26	3	super	23	sodal&hex.
NH_4,Na-Y-70	16	0		16	sodal.
NH_4,Na-Y-70,heated	16	3	super	13	sodal.
NH_4,Na-Y-87	7	0		7	sodal.
Na,NH_4-Y-71	39	39	super	0	

a: The estimated e^2qQ/h of all ^{23}Na nuclei resonating at (-5ppm,$2\omega_{rf}$) is 0.7 MHz

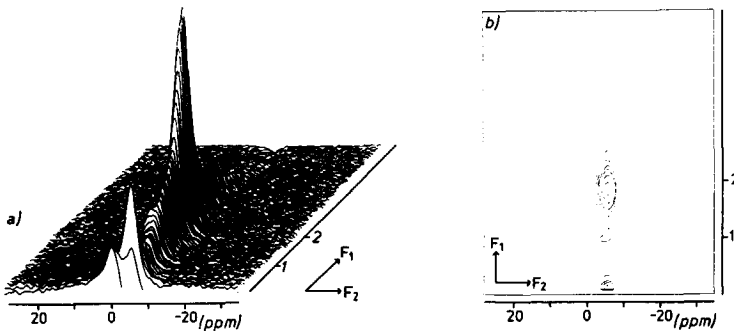*Fig.9: ^{23}Na MAS nutation NMR spectrum of NH_4,Na-Y-70. The numbers along the F   1 dimension indicate $1\omega_{rf}$ and $2\omega_{rf}$ (ω_{rf} = 50 kHz)*

(-5ppm,$2\omega_{rf}$)(Fig.9) has been left, indicating the supercages to contain no sodium anymore. Because of the slow diffusion of ammonium from supercage to sodalite cage (see above, ref. 15,42,47,48), all 38.6±1.1 ammonium ions introduced at the end of the second exchange step (Fig.7) leading to NH_4,Na-Y-70 are assumed to be still located in

the supercages. These 38.6 ± 1.1 will have stronger interactions with the anionic oxygen framework (and hence with O2) than the 31.6 ± 0.6 sodium cations occupying the supercages of Na-Y previously (see table I). As noted above, already upon 53.4% ammonium exchange the interactions with anionic O3 and sodium in the sodalite cages have increased. Analogous to the cesium exchanged sample it thus is tempting to conclude that during the second ammonium exchange step the polarisation of the framework changes so that the interaction energy of sodium inside the hexagonal prisms with O2 and O3 decreases to such an extent that these cages no longer remain occupied. Thus the 7 ± 1 additional cations accommodated by the supercages in the course of the second ammonium exchange step (Fig.7) most likely substitute for the 6 ± 2 sodium cations from the hexagonal prisms of fully hydrated Na-Y (Fig.2,4).

As suggested above, the third and slowest step of the ammonium exchange involves the slow diffusion of NH_4^+ through similarly sized [39,44,46] six-membered oxygen windows to replace the 16.2 ± 0.5 sodium cations still left in the sodalite cages of NH_4,Na-Y-70. Except for a loss in spectral intensity it appears to have no effect discernible by ^{23}Na MAS nutation NMR, for the spectra of NH_4,Na-Y-70 (Fig.9) and NH_4,Na-Y-87 (not shown) look virtually identical. Under exchange conditions the suggested interchange will be difficult to register because sodium will be exchanged fairly quickly after having entered a supercage (see discussion of first step), but some evidence of it can be obtained from ^{23}Na MAS nutation NMR on NH_4,Na-Y-70 that has been heated in an aqueous suspension at 440 K under saturated water vapor pressure. This ^{23}Na MAS nutation NMR spectrum (Fig.10) reveals that upon hydrothermal heating 2.9 ± 0.4 sodium cations have entered the supercages for they now resonate at ($-1ppm, 1\omega_{rf}$) whereas 13.4 ± 0.6 sodium cations have remained in the sodalite cages for they still display the intermediate quadrupole pattern with a major absorption at ($-5ppm, 2\omega_{rf}$). Since it is known that (hydrothermal [49]) heating greatly facilitates the passage of NH_4^+ through the window in between supercages and sodalite cages [50,51], the observed sodium redistribution is interpreted as an intracrystalline ion exchange between ammonium in the supercages and sodium in the sodalite cages. More conclusive evidence for the possibility of replacing the 16.2 ± 0.5 sodium cations located
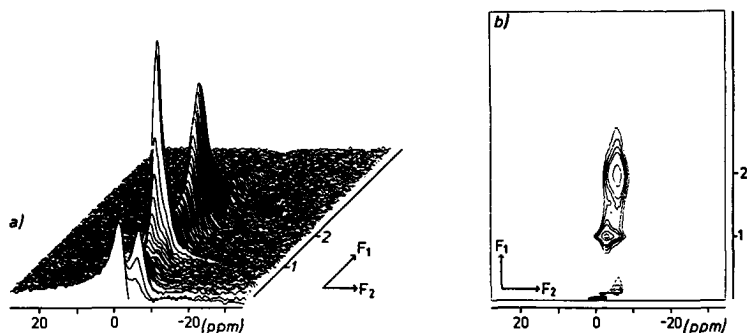
Fig.10: ^{23}Na *MAS nutation NMR spectrum of* NH_4 *,Na-Y-70 after heating. The numbers along the F1 dimension indicate* $1\omega_{rf}$ *and* $2\omega_{rf}$ *(* ω_{rf} *= 54 kHz)*

in the sodalite cages of NH_4,Na-Y-70 by ammonium is obtained from the sodium exchange kinetics of NH_4-Y (Fig.7). It appears that within a few minutes 39 ± 1 ammonium cations are replaced by sodium, whereas ^{23}Na MAS NMR applying short, high-power pulses on the resulting Na,NH_4-Y-71 reveals a peak at -1ppm, but detects no absorption at -5ppm. The absence of the latter absorption indicates that sodium has not yet penetrated into the hexagonal prisms of the freshly prepared Na,NH_4-Y-71. As the supercages are easily accessible through 0.74 nm [1] windows, the 39 ± 1 quickly replaced ammonium cations are located in the supercages, whereas the 16 ± 1 other ammonium cations (±0.32 nm in diameter, see above) remain locked up behind the ±0.32 nm (see above) windows of the sodalite cages. As ammonium is generally agreed to be larger than potassium [39,46,52], the hexagonal prisms of NH_4-Y will contain even fewer cations than those of K-Y (with similar silicon-to-aluminum ratio)(see ref. 17) and most probably will be empty. Consequently the 16 ± 1 ammonium cations outside the supercages of NH_4-Y are all located in the sodalite cages and appear to substitute for the 16.2 ± 0.5 sodium cations located in the sodalite cages of NH_4,Na-Y-70.

Cation redistribution upon calcining NH_4,Na-Y-70: The ^{23}Na nutation NMR spectrum of fully hydrated H,Na-Y-70, prepared by very careful ("shallow bed" [25]) decomposition of NH_4,Na-Y-70, shows 77±4% of the absorption at(-2ppm,1ω_{rf}) and 23±4% at (-5ppm,2ω_{rf}) (Fig.11). Because of its small quadrupole interaction and chemical shift,

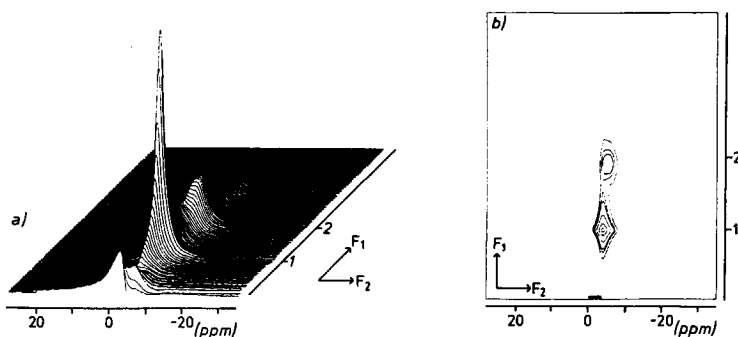*Fig.11:* ^{23}Na *MAS nutation NMR spectrum of H,Na-Y-70. The numbers along the F1 dimension indicate 1ω_{rf} and 2ω_{rf} (ω_{rf} = 60 kHz)*

the former absorption is attributed to well hydrated sodium ions in the supercage. Both the broader nutation line and the larger chemical shift suggest that interactions of the sodium cations with the framework of the supercage of H,Na-Y-70 (Fig.11) are stronger than in Na-Y (Fig.2), Cs,Na-Y (Fig.5,6) or NH_4,Na-Y (Fig.8,10). When it is nevertheless assumed that at (-2ppm,1ω_{rf}) 100% of the absorption is detected, the usual correction (see above) yields that 9.4±0.9 sodium cations are inside the supercages, whereas 6.9±0.9 sodium cations are outside of them. This is in good agreement with the sodium distribution found by powder neutron diffraction in a dry, comparable H,Na-Y [53]. The relatively large quadrupole interactions observed in H,Na-Y (Fig.11), can be explained on the basis of the strong acidity of the protons in dry, freshly prepared H,Na-Y as established by mid-infrared spectroscopy [54]. Most protons in hydrated H,Na-Y will be dissociated from the framework and substitution of ammonium or sodium by hydronium ions will result in a reduced cation-anion association. Apparently,

this enhances cation-framework interactions of the sodium cations remaining in the supercages accordingly. A similar reasoning holds for sodium cations in sodalite cages or hexagonal prisms implying that in both cages sodium cations are expected to interact strongly with the anionic oxygen framework and to be asymmetrically coordinated (see above). Consequently, ^{23}Na MAS nutation NMR can no longer differentiate between them. However, it has been observed, that sodium cations usually prefer water ligands to the anionic framework oxygens of zeolite Y [18,19,22]. As water is present in the sodalite cages but not in the hexagonal prisms [4], the most probable location of sodium resonating at (-5ppm,$2\omega_{rf}$) therefore is inside the sodalite cages [22].

Cation redistribution in hydrated Na-Y upon hydrothermal heating: Cross-sections along the F2 axis at $1\omega_{rf}$ and $2\omega_{rf}$ of a static (i.e. no MAS) ^{23}Na nutation NMR
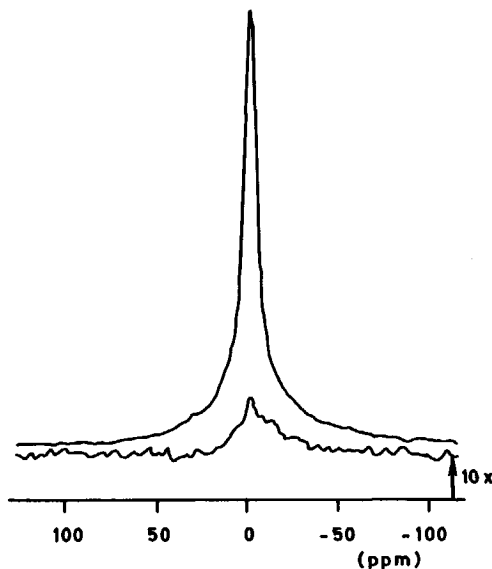
Fig.12:Cross section along F2 axis at $1\omega_{rf}$ (top, gain = 1) and $2\omega_{rf}$ (bottom, gain = 10) of ^{23}Na nutation NMR spectrum of suspension of Na-Y at 290 K
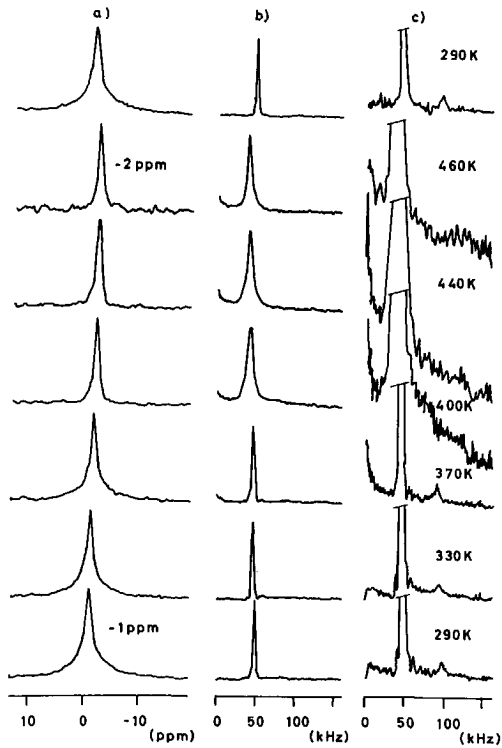
Fig.13: a) static ^{23}Na NMR spectra along F2 axis of hydrothermally heated Na-Y suspensi-
on; the top spectrum shows the spectrum at 290 K recorded again after the
complete heating cycle.

b) Cross-sections along the F1 axis, taken at -1ppm at the F2 axis, of static ^{23}Na
nutation spectra of hydrothermally heated Na-Y suspension; $\omega_{rf} = 50$ kHz; at the
top the 290 K projection after heating. The decrease of the nutation frequency at
temperatures of 400 K and higher is due to a change of the rf efficiency of the
probe.

c) Same as b, but vertical multiplied by 10.

spectrum (recorded at 79.35 MHz instead of 158.71 MHz) of an aqueous suspension of Na-Y at 290 K are shown in Fig.12. They reveal that the static ^{23}Na NMR spectrum of this suspension at 290 K (shown at the bottom of Fig.13a) consists of a 750 Hz broad resonance at $1\omega_{rf}$ on top of an about 1.7 kHz broad resonance at $2\omega_{rf}$. In agreement with the ^{23}Na MAS nutation NMR spectrum of fully hydrated Na-Y the narrow absorption at $1\omega_{rf}$ is attributed to the 49 ± 2 sodium cations inside supercages and sodalite cages, and the broad absorption at $2\omega_{rf}$ to the 6 ± 2 sodium cations inside the hexagonal prisms (see Table I). Static ^{23}Na NMR spectra as well as cross-sections of the static ^{23}Na nutation NMR spectrum along the F1 axis (taken at -1ppm at the F2 axis) of the aqueous Na-Y suspension at progressively higher temperatures are shown in Figures 13a-c. Upon hydrothermal heating to 400 K the large absorption at $1\omega_{rf}$ is seen to broaden in the F1 dimension (Fig. 13b,c) and to shift to more negative ppm-values in the F2 dimension (Fig.13a). The broadening in the F1 dimension can be explained in two ways: i) an interference of the fluctuation rate of the electric field gradient at sodium nuclei inside supercages and sodalite cages with the $5 \cdot 10^4$ Hz nutation frequency [55] or by ii) an increase of the quadrupole interactions at these sites. Contrary to what is suggested by the former explanation, motions of water molecules and sodium nuclei are already more frequent than $5 \cdot 10^4$ Hz at 298 K [26,36,37,38]. In support of the latter explanation it should be noted that, the shift of the ^{23}Na NMR absorption along the F2 axis to more negative ppm-values indicates increased sodium-framework interactions which is usually accompanied by decreased coordination symmetry.

Finally, the disappearance with temperature of the broad part of the ^{23}Na NMR spectrum at the F2 axis and the absorption at $2\omega_{rf}$ at the F1 axis (Fig.13a, 13c) attributed to the 6 ± 2 sodium cations inside the hexagonal prisms can be explained i) by motional averaging of the quadrupole interactions and chemical shift differences, ii) by broadening of the resonance beyond detection or iii) by there being no longer any sodium inside the hexagonal prisms. Considering the first explanation it can be remarked that a sodium cation fits too tight in an hexagonal prism to allow large-amplitude motions to average out the electric field gradient (see above). A disappearance of the

signals of sodium in the hexagonal prisms due to broadening as suggested by the second explanation presupposes an increase in sodium framework interactions in these cages. From structural considerations it follows that at higher temperatures the observed (see above) increased sodium-framework interaction energy inside sodalite and supercages will increase the interaction energy with anionic O2 and O3 from outside the hexagonal prisms (see Fig.1). This again will decrease the sodium-framework interaction energy inside the hexagonal prisms and thus makes excessive broadening of the ^{23}Na NMR absorption due to sharply increased quadrupole interactions unlikely. Moreover, the decreased sodium-framework interaction energy inside the hexagonal prisms will contribute to the depletion of the hexagonal prisms [20,21,22]. Thus a cation redistribution involving the actual depletion of the hexagonal prisms appears to be the most probable explanation for the spectral features observed on the heated suspension of Na-Y.

Reversibility of the hydrothermal treatment is illustrated by the ^{23}Na NMR spectra having not changed after this treatment (cf. top and bottom of Fig.13a,b,c). Moreover, after heating an aqueous suspension of Na-Y to 470 K, the volume of micropores as determined by the t-plot method has remained 0.33 $cm^3 \cdot g^{-1}$, indicating no change in crystallinity [56]. Finally, ^{27}Al MAS NMR detects no dealumination (cf. ref. 13), so that it is concluded that the hydrothermal treatment has no lasting effect on the sample under study.

Conclusions

^{23}Na MAS nutation NMR indicates that the hexagonal prisms of fully hydrated NaY (Si/Al = 2.5) contain 6±2 sodium cations per unit cell. According to high-temperature ^{23}Na nutation NMR these cages appear to be no longer occupied upon hydrothermal heating to 460 K, presumably because increased cation-framework interactions in the supercages and sodalite cages have reduced the cation-framework energy in the hexagonal prisms to such an extent that they no longer offer cations sufficient stabiliza-

tion (cf. references 19,20,50). It is demonstrated that the increased interaction energy inside supercages and sodalite cages upon 54.2% cesium exchange also destabilizes the occupation of the hexagonal prisms. Ammonium exchange of Na-Y is shown to proceed in three stages: i) in the fast first step the 32 ± 1 sodium cations in the supercages are replaced by NH_4^+; in the second slower step 7 ± 1 more ammonium cations enter the supercages replacing sodium originally occupying the hexagonal prisms, whereas iii) the substitution of the 16 ± 1 sodium left inside the sodalite cages is reserved for the third, very slow step. ^{23}Na MAS nutation NMR shows that hydrothermally heating accelerates the cation redistribution in the second exchange step (illustrated on a cesium exchanged sample) as well as the intracrystalline exchange necessary to achieve complete ammonium exchange. The sodium exchange kinetics of NH_4-Y confirm that upon complete ammonium exchange cations have redistributed and that the population of the supercages has risen to 39 ± 1, whereas the sodalite cages have retained their 16 ± 1 cations. Finally, ^{23}Na MAS nutation NMR shows that sodium in the supercages of H,Na-Y has a larger chemical shift and quadrupole interaction than in Na-Y or NH_4,Na-Y which has been hydrothermally heated, indicating that not only the cation-framework interaction strength in sodalite cages and hexagonal prisms but also in the supercages can be affected by ion exchange.

References:

1. Meier, W.M., Olson, D.H. *Atlas of Zeolite stucture types*(Structure Commission of

the International Zeolite Association); Butterworths: London, 2nd, 1987, pp.62-63.

2. Bergerhoff, G.; Bauer, W.H.; Nowacki, W. *Neues Jahrb.Mineral.,Monatsh* **1958**, 193-200.

3. Corma A. *Stud.Surf.Sci.Catal.* **1989**, *49*, 49-67.

4. Smith, J.V. *ACS Symp.Ser.* **1970**, *101*, 171-200.

5. Breck, D.N. *Zeolite Molecular Sieves: Structure, Chemistry and Use;* Wiley: New York, 1974; pp.29-185.

6. Mortier, W.J. *Compilation of Extraframework Sites in Zeolites;* Butterworths: Guildford, 1982; pp.19-31.

7. Mortier, W.J.; Van den Bossche, E.; Uytterhoeven, J.B. *Zeolites* **1984**, *4*, 41-44.

8. Calestani, G.; Bacca G.; Andreetti G.D. *Zeolites* **1987**, *7*, 54-58.

9. Fritz, P.O.; Lunsford, J.H. *J.Catal.* **1989**, *118*, 85-98.

10. Maher, P.K.; McDaniel, C.V. *U.S. Patent* 3293192, 1966.

11. Ozin, G.A.; Baker, M.D.; Godber, J.; Gill, C.J. *J.Phys.Chem.* **1989**, *93*, 2899-2908.

12. Loewenstein, W. *Am.Mineral.* **1954**, *39*, 92-96.

13. Klinowski, J. *Progr.NMR Spectrosc.* **1984**, *16*, 237-309.

14. Engelhardt G.; Michel D. *High-Resolution Solid State NMR of Silicates and Zeolites;* Wiley: New York, 1987; pp.218-238.

15. Franklin, K.R.; Townsend, R.P.; Whelan, S.J.; Adams, C.J. *Stud.Surf.Sci.Catal.* **1986**, *28*, 289-296.

16. Scherzer, J. *Catal.Rev.Sci.Eng.* **1989**, *31*, 215-354.

17. Mortier, W.J.; Bosmans H.J. *J.Phys.Chem.* **1971**, *75*, 3327-3334.

18. Mortier, W.J.; Vaughan, D.E.W.; Newsam, J.M. *ACS.Symp.Ser.* **1988**, *368*, 194-202.

19. Van Dun, J.J.; Dhaeze, K.; Mortier, W.J.;Vaughan, D.E.W. *J.Phys.Chem. Solids* **1989**, *50*, 469-477.

20. Cremers, A. *ACS Symp.Ser.* **1977**, *40*, 179-193.

21. Van Dun, J.J.; Mortier, W.J. *J.Phys.Chem.* **1988**, *92*, 6740-6746.

22. Van Dun, J.J.; Dhaeze, K.; Mortier, W.J. *J.Phys.Chem.* **1988**, *92*, 6747-6754.

23. Kentgens, A.P.M.; Lemmens, J.J.M.; Geurts, F.M.M.; Veeman, W.S. *J.Magn. Res.* **1987**, *71*, 62-74.

24. Samoson, A.; Lippmaa, E. *J.Magn.Reson.* **1988,** *79,* 255-268.

25. Kerr, G.T. *J.Catal.* **1969,** *15,* 200-204.

26. Basler, W.D. *Colloids and Surfaces* **1984,** *12,* 59-67.

27. Welsh, L.B.; Lambert, S.L. *ACS Symp.Ser.* **1988,** *368,* 32-47.

28. Sulikowski, B., private communication.

29. Crowther, J.; Evans, J. *Analyst(London)* **1980,** *105,* 849-854.

30. Von Ballmoos, R. *The ^{18}O-Exchange Method in Zeolite Chemistry;* O. Salle Verlag: Frankfurt-am-Main; Verlag Sauerländer: Aarau, 1981; pp.200-205.

31. Maesen, Th.L.M.; Sulikowski, B.; Van Bekkum, H.; Kouwenhoven, H.W.; Klinowski, J. *Appl.Catal.* **1989,** *48,* 373-383.

32. Janssen, R.; Tijink, G.A.H.; Veeman, W.S.; Maesen, Th.L.M.; Van Lent, J.F. *J.Phys.Chem.* **1989,** *93,* 899-904.

33. Kundla, E.; Samoson, A.; Lippmaa, E. *Chem.Phys.Lett.* **1981,** *83,* 229-232.

34. De Boer, J.H.; Lippens, B.C.; Linsen, B.G.; Broekhoff, J.C.P.; Van den Heuvel, A.; Osinga, Th.J. *J.Colloid Interface Sci.* **1966,** *21,* 405-414.

35. (a)Schmidt, V.H. *Proceedings of the Ampere International Summer School II* 1971, 75-83. (b)Man, P.P.; Klinowski, J.; Trokiner, A.; Zanni H.; Papon, P. *Chem.Phys.Lett.* **1988,** *151,* 143-150.

36. Pfeifer, H.; Gutsze A.; Shdanov S.P. *Z.Phys.Chem(Leipzig)* **1976,** *257,* 721-734.

37. Pfeifer H. *Surface Sci.* **1975,** *52,* 434-436.

38. Basler W.D.; Lechert H.; Kacirek H. *Ber.Bunsenges.Phys.Chem.* **1976,** *80,* 451-456.

39. Shannon, R.D. *Acta Cryst.* **1976,** *A32,* 751-767.

40. Deverell C.; Richards R.E. *Mol.Phys.* **1966,** *10,* 551-564.

41. Templeman G.J.; Van Geet A.L. *J.Am.Chem.Soc.* **1972,** *94,* 5578-5582.

42. Sherry, H.S. *Adv.Chem.Ser* **1971,** *101,* 350-379.

43. Li, C.Y.; Rees, L.V.C. *React.Polym.Ion.Exch.Sorbents* **1988,** *7,* 89-99.

44. Sherry, H.S. *J.Phys.Chem.* **1966,** *60,* 1158-1168.

45. Pearson, R.G. *Inorg.Chem.* **1988,** *27,* 734-740.

46. Aue, D.H.; Webb, H.M.; Bowers, M.T. *J.Am.Chem.Soc.* **1976,** *98,*318-329.

47. Barrer, R.M. *Zeolites and Clay Minerals as Sorbents and molecular Sieves;* Acad-

emic: London, 1978; pp.76-87.

48. Maes, A.; Cremers, A. *J.Chem.Soc.Faraday Trans.I* **1978**, *74,* 136-145.

49. Alafandi, H.; Stamires D. *U.S. patent* 4058484, 1977; *U.S. patent* 4085069, 1978.

50. Chu, P.; Dwyer, F.G. *J.Catal* **1980**, *61,* 454-460.

51. Herman, R.G.; Bulko, J.B. *ACS Symp.Ser.* **1980**, *135,* 177-186.

52. Böhm H.-J., McDonald J.R. *J.Chem.Soc.Faraday Trans.II* **1984**, *80,* 887-998.

53. Jirak, Z.; Vratislav, S.; Bosacek, V. *J.Phys.Chem.Solids* **1980**, *41,* 1897-1095.

54. Ward, J.W. In "Zeolite Chemistry and Catalysis"; Rabo, J.A., Ed.; *ACS Monogr.* **1976** *171,* 118-284.

55. Janssen, R.; Tijink, G.A.H.; Veeman, W.S. *J.Chem.Phys.* **1988**, *88,* 518-523.

56. Hudec, P.; Novansky J.; Silhar, S.; Trung T.N.; Zubek M.; Madar J. *Adsorpt. Sci.Technol.* **1986**, *3,* 159-166.

CHAPTER 3

FAST HYDROTHERMAL AMMONIUM EXCHANGE OF ZEOLITE Na-Y[*]

Abstract

Hydrothermal heating to 433 K is shown to reduce the time needed for attaining 70-100% ammonium exchanged zeolite Na-Y drastically, without impairing the zeolite. Upon approaching complete ammonium exchange the affinity of zeolite Y for ammonium falls sharply. Complete exchange requires a total molar ammonium-to-sodium ratio of more than 200. Extensive ammonium exchange is accompanied by an expansion of the faujasite framework eventually leading to sodalite cages of sufficient size to accommodate two ammonium ions.

Introduction

To produce a Y zeolite that can be used for fluid catalytic cracking, extensive sodium removal is required for maximal catalytic activity, stability and octane-boosting capacity [1]. Normally, this is accomplished by first replacing 70% of the sodium ions present in as-synthesized zeolite Na-Y by ammonium ions at temperatures well below 373 K. Subsequently, this NH_4,Na-Y zeolite is heated to about 900 K. A second ammonium exchange followed by heating yields a commercial catalyst of which about 96% of the sodium ions have been removed [2].

It has been established that when more than 99% instead of the usual 96% of the sodium ions originally present in the Na-Y zeolite are removed, the reactor temperature for hydroisomerisation can be lowered by some 50 K [3]. Moreover, with more

than 99% of the sodium ions removed, the cracking activity of the Y zeolite has been found to increase by a factor of three [4] to five [5].

Recently it has been shown that the 70% ammonium exchange level reached during the first step of the present commercial process to turn Na-Y into a fluid catalytic cracking catalyst [2] is kinetically determined [6,7]. As it was first pointed out by Sherry et al. [8], such kinetic limitations can effectively be circumvented by hydrothermal ion exchange. Indeed, it has been claimed that at a pH of 3.5 at 450 K a 97% ammonium exchanged Na-Y can be prepared within 6 hours [9]. The present paper describes exploration of barriers to complete ammonium exchange of zeolite Na-Y at 433 K and at neutral pH.

Experimental

Materials: The parent sample was zeolite Na-Y with molar silicon-to-aluminum ratio of 2.5 ± 0.1 and average crystal size of 1 μm. At 298 K 70% and 87% ammonium exchanged zeolites were prepared by ion exchange with aqueous solutions of ammonium nitrate [7]. A 100% ammonium exchanged sample, which will be referred to as NH_4-Y, was prepared by contacting 5.0 g Na-Y twice with 200 ml 1.0 mol l^{-1} aqueous silver nitrate solution and subsequently extracting the resulting Ag-Y twice with 200 ml 1.0 mol l^{-1} aqueous ammonium thiocyanate solution [10].

Kinetic Measurements:

The tracer method was used to determine the time course of the sodium depletion resulting from the sodium-ammonium exchange of zeolite Na-Y. To this end Na-Y zeolite was irradiated (for 5 s) with thermal neutrons (flux = 4.5 10^{12} s^{-1} cm^{-2}) in the nuclear reactor of the Interfaculty Reactor Institute in Delft. This gives rise to the formation of radioactive isotopes: ^{24}Na and ^{31}Si with half-lives of 15.03 and 2.62 hours, respectively (activity ratio = 1 : 0.09). Both radioisotopes emit β^--particles of almost the same energy. Typically 1.7 g Na-Y zeolite was irradiated in the reactor, dispersed in 20

ml water, sonicated and divided over 10 Teflon vessels inside stainless steel autoclaves (2 ml / autoclave). To each autoclave insert 18.00 ml of 1.11 mol.l^{-1} aqueous ammonium nitrate solution was added. The molar ammonium-to-sodium ratio was 37. Subsequently, these inserts equipped with Teflon lid and Teflon coated stirring rod were quickly closed and the autoclaves were put into a stainless steel stirring block held at 433 K. During 40 minutes, at selected times an autoclave was removed from the block, cooled in ice and its content was quickly filtered using a vacuum-filtration set-up. Filtrate samples of 0.5 ml were mixed with 10 ml counting solution (Luma Gel, Lumac, Landgraaf, The Netherlands) and the β^{-}-activity was measured in a liquid scintillation counter (Tricarb, Packard). To allow for a 99.9% decay of ^{31}Si the samples were counted about 24 hours after the irradiation. Preliminary experiments have shown that the filtrates contain no other activity but ^{24}Na. To be able to relate the ^{24}Na activity with the amount of sodium, two 10 mg portions of the irradiated Na-Y zeolite were dissolved in 1.00 ml of an aqueous solution containing 3.3 mol.l^{-1} hydrofluoric acid, 3.9 mol.l^{-1} sulphuric acid and the two obtained liquid samples were counted as described above.

The time needed to reach a stable cation partitioning between solution and zeolite phase was checked by a non-radioactive experiment and complete elemental analysis of both phases (see below).

Temperatures of stirred suspensions after a certain time inside the stainless steel stirring block were determined with an inserted thermometer strip (Thermindex). At a selected time an autoclave was cooled and opened to read the strip.

Ion Exchange Isotherm: A sodium-ammonium exchange isotherm was determined by stirring 0.17 g zeolite Y with 20 ml solutions containing sodium nitrate and ammonium nitrate in various proportions with a total concentration of 0.1 mol l^{-1} for six hours at 433 K inside the Teflon autoclave inserts described above. After six hours the autoclaves were cooled in ice and their contents quickly filtrated. Both solution and zeolite (washed with 40 ml water and extracted with 50% nitric acid for 3 days at 360 K [7]) were analyzed for sodium and ammonium with inductively-coupled atomic emission

spectroscopy (ICP-AES) and the Kjeldahl method, respectively. Na-Y, 70% and 87% ammonium exchanged Na-Y were used as starting samples. Reversibility of the exchange was checked starting from NH_4-Y. To check for hydronium exchange, 17 mg of 70%, 87% and 100% ammonium exchanged Na-Y that had been under hydrothermal ion-exchange conditions were dissolved in 6 ml of a solution containing 3.3 mol.l^{-1} hydrofluoric acid and 3.9 mol.l^{-1} sulphuric acid. This solution was analyzed for ammonium after neutralization of 2.00 ml with 20.00 ml 1.11 mol.l^{-1} potassium hydroxide. It was analyzed for Si, Al and Na by ICP-AES after cooling another 2.00 ml in liquid nitrogen and diluting with 20.00 ml 0.4% boric acid [11].

Characterization: ^{27}Al and ^{29}Si Magic Angle Spinning (MAS) Nuclear Magnetic Resonance (NMR) spectra (Varian VXR-400 S spectrometer) were recorded at 104.2 and 79.5 MHz, respectively. Before NMR measurement all samples were hydrated for about two months in a desiccator in the presence of a saturated ammonium nitrate solution (80% relative humidity).

The unit cell constant was calculated from the X-ray powder diffraction (XRD) pattern according to ASTM method D3942.

Results and Discussion

Sodium to Ammonium Exchange Kinetics at 433 K: Fig.1 shows the ammonium exchange of Na-Y at 433 K versus time using a NH_4^+/Na ratio of 37. The Figure also shows the rate of heating of the stirred suspension inside the autoclave. Within a few minutes, the autoclaves still being at about room temperature, 58% of the sodium ions are replaced by ammonium ions. These quickly replaced sodium ions are presumably located in the supercages [10,12,13], have a weak interaction with the anionic oxygen framework [10,14] and are easily accessible [15].

Subsequently, the ammonium exchange level is observed to increase monotonously with time and temperature. Within half an hour the autoclaves have reached 433 K and at this stage the exchange is already close to the final figure of 87%. This was also
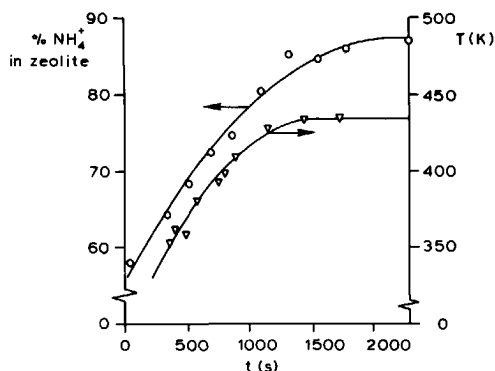
Fig.1: Molar ammonium fraction %NH$_4^+$ (o), and temperature (K) (∇) as a function of time when warming up zeolite Na-Y (0.17 g) in 20 ml 1.00 M aqueous NH$_4$NO$_3$.

found with a non-radioactive sample. It may be noted that at 298 K it takes as many as 50 successive one day exchanges of 1 g sample with fresh 20 ml 1 mol l^{-1} ammonium chloride [7,16] or nitrate (this paper) solutions to reach this value. The slowness of attaining more than 70% ammonium exchange at room temperature has been attributed to the size of the hydrated ammonium ion, which needs to shed its water molecules in order to pass through a six-membered oxygen ring and penetrate into a sodalite cage [6,17]. However, the ammonium-water interaction energy is known [18] to be comparable to and to be probably [19] even smaller than the potassium-water interaction energy and yet complete potassium exchange of zeolite Na-Y is achieved fairly readily [20]. More likely, the stability of the structure constituted by the sodium ions and water molecules inside the sodalite cages [23], the enhancement of the sodium-framework interactions observed upon filling the supercages with ammonium [10], and the approximately equal diameters of the free aperture of a sodalite cage and of a bare ammonium ion (both sized in between 0.30 nm and 0.34 nm [18,20,22], are major factors effecting a slow ammonium-to-sodium interchange into the sodalite cages.

Ammonium Exchange levels upon Heating to 433 K: In Fig.2 the molar ammonium fraction left in the solution after heating to 433 K followed by separation around room temperature is plotted against the molar ammonium fraction in the zeolite phase.
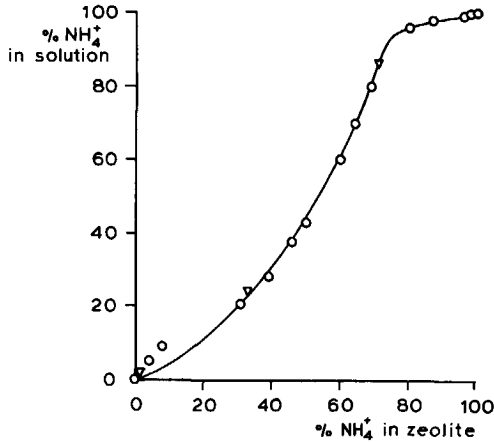

Fig.2: Molar ammonium fraction in solution, %NH$_4^+$, vs. %NH$_4^+$ in zeolite Y separated from it after heating to 433 K.

Sodium exchange of NH$_4$-Y instead of ammonium exchange of Na-Y appears not to affect the cation distribution between solution and zeolite phase reached, indicating that the hydrothermal exchange procedure at 433 K is reversible.

Accordingly, complete elemental analysis of hydrothermally heated 70%, 87% and 100% ammonium exchanged Na-Y shows the amount of sodium plus ammonium ions always to be equal to the number of aluminium atoms confirming that the ion exchange is not complicated by hydronium exchange. Moreover, neither the ^{27}Al MAS NMR nor the ^{29}Si MAS NMR spectrum of 87% or 100% ammonium exchanged Na-Y shows any changes upon hydrothermal treatment (spectra not shown), which proves the absence of dealumination.

The ion distribution between zeolite and solution phase after heating to 433 K (Fig.3), partly resembles the isotherm at 298 K of a similar Na-Y zeolite (Fig.4) [7]. Below 58% ammonium exchange this is as to be expected, for 58% of the ions are
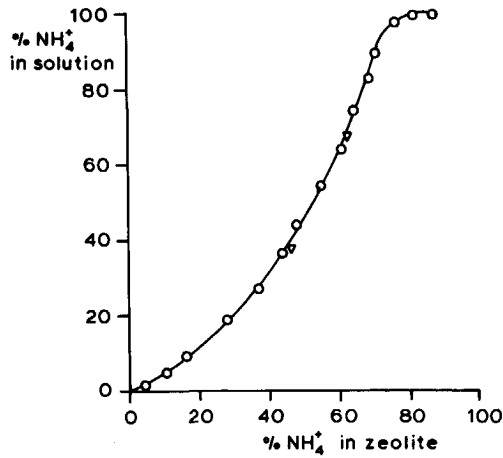
Fig.3: Molar ammonium fraction, %NH$_4$$^+$, in solution vs. molar ammonium fraction, %NH$_4$$^+$, in the NH$_4$,Na-Y zeolite exchanged at 298 K [7].

known to belocated inside the supercages [14,19] and were shown above to exchange within the few minutes needed for separating zeolite and solution phase. At the higher ammonium exchange levels differences do show up; for instance at 298 K preparation of 87% ammonium exchanged Y zeolite with a comparable silicon-to-aluminium ratio needs an ammonium-to-sodium ratio of about 48 [7], whereas at 433 K a ratio of only 37 is sufficient. Moreover, at 298 K no ammonium exchange levels higher than 87% have been reported [7,16], whereas at 433 K a 98% ammonium exchanged Y zeolite can be separated from a solution with an ammonium-to-sodium ratio as high as 188.

Fig.4 shows the total ammonium-to-sodium ratio of this system required to reach a certain ammonium fraction in the Y zeolite. Starting from about 90% ammonium exchange increasingly higher ammonium-to-sodium ratios must be applied to replace ever fewer sodium ions. Thus on top of a barrier related to the hindered diffusion of ions (and water molecules) through six-membered oxygen rings separating supercages from sodalite cages, there apparently is a thermodynamic barrier for attaining 100% ammonium exchanged zeolite Na-Y. This barrier is presumably related to the fact that the unit cell constant of the Na-Y sample is 2.466 nm, whereas that of NH$_4$-Y is 2.474
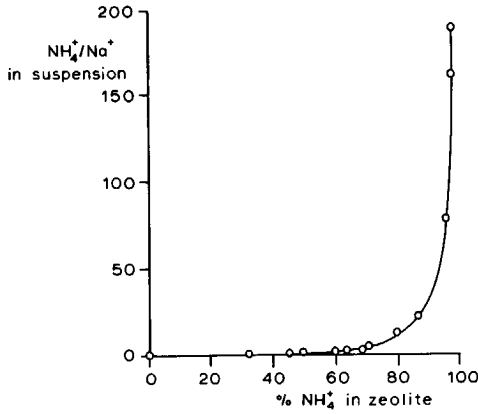
Fig.4: Total NH_4^+/Na^+ ratio of suspension vs. ammonium fraction, $\%NH_4^+$, in the NH_4 ,Na-Y zeolite after exchange at 433 K.

nm. Indeed, the increase in unit cell size reported for a Y zeolite sample of comparable properties to occur at ammonium exchange levels above about 90% (Fig.5) [25]
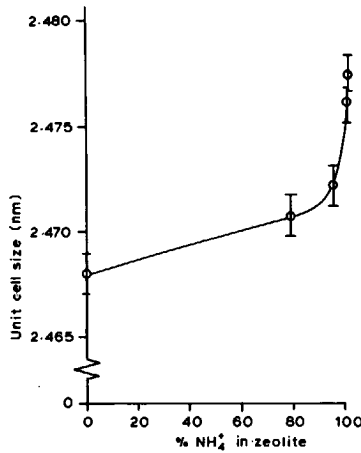

Fig.5: Unit cell size as a function of the ammonium fraction, $\%NH_4^+$ of a NH_4 ,Na-Y zeolite with Si/Al=2.55 [25].

corresponds very well to the increase in ammonium-to-sodium ratio shown in Fig.4. Thus the high NH_4^+/Na^+ required for the substitution of the last few sodium ions per unit cell is probably related to the expansion of the zeolite framework which is required for accommodation of two ammonium ions (each ± 0.33 nm in diameter [18]) in each of the eight sodalite cages (± 0.66 nm in diameter [24]) per unit cell [10,17,23].

Conclusions

It has been shown that hydrothermal heating reduces the time required to attain an 87% ammonium exchanged Na-Y zeolite from 50 days at 298 K [7], to half an hour at 433 K, and therefore allows the attainment of higher ammonium fractions than the 70% encountered in the first step of the commercial preparation of fluid catalytic cracking catalysts nowadays [2]. Without the addition of acid [9] at 433 K, hydrothermal ammonium exchange fractions as high as 98% can be attained. Nevertheless, even at 433 K 100% ammonium exchange proves to be difficult to reach, for it requires ion-exchange systems with high total ammonium-to-sodium ratios. This ultimate barrier to complete ammonium exchange is probably due to the fact that accommodation of 2 ammonium ions per sodalite cage is only possible after expansion of the faujasite framework.

References

1. Scherzer, J. *Catal.Rev.-Sci.Eng.* **1989**, *31*, 215-354.
2. Kouwenhoven, H.W.; De Kroes, B. in *Introduction into Zeolite Science and Practice;* Elsevier: Amsterdam; to be published shortly.
3. Kouwenhoven H.W. *ACS Symp.Ser.* **1973**, *121*, 528-539.
4. Beyerlein, R.A.; McVicker, G.B.; Yacullo, L.N.; Ziemiak, J.J. *Prep.Am.Chem.-Soc.Div.Pet.Chem.* **1986**, *31*, 190-197.
5. Fritz, P.O.; Lunsford, J.H. *J.Catal.* **1989**, *118*, 85-98.
6. Herman, R.G.; Bulko, J.B. *ACS Symp.Ser.* **1980**, *135*, 177-186.
7. Franklin, K.R.; Townsend, R.P.; Whelan, S.J.; Adams, S.J. *Stud.Surf.Sci.Catal.* **1986**, -28, 289-296.
8. Sherry, H.S.; Trenton, N.J., Schwartz A.B. *U.S. patent* 3677698, 1972.
9. Alafandi, H.; Stamires D. *U.S. patent* 4058484, 1977 and *U.S. patent* 4085069, 1978.
10. Sulikowski, B., private communication.
11. Maesen, Th.L.M.; Janssen, R.; Van Bekkum, H.; Kouwenhoven, H.W.; Veeman, W.S. *J.Phys.Chem.*, in press.
12. Methods For Chemical Analysis of Water and Wastes, October 1984 Method 52020
13. Von Ballmoos, R. *The ^{18}O-Exchange Method in Zeolite Chemistry;* O. Salle Verlag: Frankfurt-am-Main; Verlag Sauerländer: Aarau, 1981; pp.200-205.
14. Basler, W.D. *Colloids and Surfaces* **1984**, *12*, 59-67.
15. Welsh, L.B., Lambert, S.L. *ACS Symp.Ser.* **1988**, *368*, 32-47.
16. Sherry, H.S. *Ion Exchange. A Series of Avances* **1969**, *2*, 89-133.
17. Meier, W.M., Olson, D.H. *Atlas of Zeolite structure types* (Structure Commission of the International Zeolite Association); Butterworths: London, 2nd, 1987, pp.62-63.
18. Franklin, K.R.; Townsend, R.P. *J.Chem.Soc,Faraday Trans.I* **1988**, *84*, 2755-2770.
19. Chu, P.; Dwyer, F.G. *J.Catal* **1980**, *61*, 454-460.
20. Aue, D.H.; Webb, H.M.; Bowers, M.T. *J.Am.Chem.Soc.* **1976**, *98*, 318-329.

21. Walker, P.A.M.; Lawrence, D.G.; Neilson, G.W.; Cooper, J. *J.Chem.Soc, Faraday Trans.I* **1989,** *85,* 1365-1372.
22. Shannon, R.D. *Acta Cryst.* **1976,** *A32,* 751-767.
23. Costenoble, M.L.; Mortier, W.J.; Uytterhoeven,J.B. *J.Chem.Soc.,Faraday Trans.* I **1976,** *72,* 1877-1883.
24. Sherry, H.S. *J.Phys.Chem.* **1966,** *60,* 1158-1168.
25. Fritz, P.O.; Lunsford, J.H.; Fu, Ch.-M. *Zeolites* **1988,** *8,* 205-208.
26. Breck, D.W. *Zeolite Molecular Sieves: Structure, Chemistry and Use;* Wiley: New York, 1974; p.84.

CHAPTER 4

DEEP BED CALCINATION OF ZEOLITES NH_4,Na-Y AND NH_4-Y

Abstract

^{23}Na MAS nutation nuclear magnetic resonance (NMR) spectroscopy may be applied to monitor cation redistributions upon ultrastabilization of partially ammonium exchanged Y zeolites. ^{29}Si MAS NMR and ^{27}Al nutation NMR show that ultrastabilization by "deep bed" calcination results in more heterogeneous products than "steam" calcination. According to ammonia TPD and n-hexane cracking activity, deep bed calcination of fully ammonium exchanged Na-Y yields an ultrastable Y zeolite of poor quality.

Introduction:

Faujasite-type zeolites are currently widely employed in fluid catalytic cracking (FCC) for conversion of refinery feedstocks like vacuum gas oil and heavier fractions [1,2]. Of the possible modifications of this zeolite, the most important form is hydrothermally treated ultrastable (US)Y, used in octane enhancing FCC catalysts [2,3]. It is conventionally produced by subjecting a partially ammonium-exchanged Y zeolite, NH_4,Na-Y, to a high-temperature steam treatment [4,5]. During this ultrastabilization hydronium ions attack Si-O-Al bonds and framework aluminium moves to occupy the micropore volume [6]. ^{27}Al quadrupole nutation NMR spectroscopy has revealed that steam treated NH_4,Na-Y zeolites have (distorted) framework tetrahedral aluminium and extra-framework aluminium species [7,8]. Simultaneous with the expulsion of

aluminium from the aluminosilicate framework, portions of the framework collapse. A secondary, mesopore channel system is thereby formed [9] having pore diameters in the range 3-5 nm. Silicon from collapsed framework is transported by steam towards the framework sites vacated by aluminium [5]. These sites are healed by silicon substituting into the framework [10]. The increase in silicon-to-aluminium ratio following ultrastabilization has been determined from ^{29}Si MAS NMR spectroscopy [10,11]. The decrease in the average number of AlO_4 tetrahedra bonded to the same SiO_4 tetrahedron has been calculated from ^{29}Si MAS NMR spectra as well [12,13]. Since AlO_4 tetrahedra with no AlO_4 block bonded to one of their four nearest SiO_4 neighbours are generally held responsible for zeolitic superacidity [14,15,16], the average number of AlO_4 tetrahedra at next-nearest neighbour positions, $\overline{NNN}$, provides valuable information on the expected catalytic activity of a USY zeolite.

Besides strength, number and distribution of acid sites, the residual sodium content of a Y zeolite is a key factor in catalyst preparation and catalytic performance. Sodium cations restrict the degree of dealumination during high-temperature steaming treatment [17,18], and have a detrimental effect on catalyst stability [2] and activity [19,20, 21,22]. Conventionally, sodium is removed by successive ion exchange and ultrastabilization steps. The desired high sodium removal levels can also be attained by a single hydrothermal exchange step [23,24]. In this study completely ammonium exchanged Y zeolite, NH_4-Y, is ultrastabilized by "deep bed" calcination, i.e. by heating whilst impeding removal of the gaseous products from the catalyst bed [4]. The material obtained was characterized by ^{27}Al nutation NMR, ^{29}Si MAS NMR, nitrogen adsorption measurements, ammonia temperature programmed desorption (TPD) and a n-hexane cracking test. As a reference, 64% ammonium exchanged Na-Y zeolite was deep bed calcined. The sodium removal of the latter sample upon successive ammonium exchanges and deep calcinations was studied by ^{23}Na MAS nutation NMR. The deep bed procedure was evaluated by comparison of the products with an ultrastable zeolite prepared from 73% ammonium exchanged Na-Y by calcination in flowing steam [25].

Experimental

Materials: The parent sample was zeolite Na-Y with $Si/Al = 2.5 \pm 0.1$ and an average crystal size of 1 μm. A 64% ammonium exchanged sample was prepared by ion exchange with aqueous ammonium nitrate at 298 K. A fully ammonium exchanged sample, which will be referred to as NH_4-Y, was prepared by extraction of a completely silver exchanged sample with ammonium thiocyanate [26,27].

Ultrastabilization: In a modification of the deep bed procedure [28], ammonium exchanged Na-Y filter cake was arranged in a ± 1 cm deep bed (± 3 cm in diameter) inside a lidded porcelain jar wrapped in aluminium foil. The sample was ultrastabilized by placing it directly into a furnace at 900 K and leaving it there for 15 hours. A sample denoted as USY-A was thus obtained from a 64% ammonium exchanged zeolite, NH_4,Na-Y. Further ammonium exchange of USY-A with 250 ml 1.00 M NH_4NO_3 per gram zeolite followed by ultrastabilization produced USY-B. Repetition of this procedure gave USY-C. USY-Z was obtained from NH_4-Y by deep bed calcination. For comparison a commercial steam calcined sample referred to as USY-α was obtained by calcination in 100% steam. Si, Al and Na contents were determined by ICP-AES after dissolution as described by Von Ballmoos [29].

Characterization:
^{29}Si MAS NMR spectra, static (i.e. no MAS) ^{27}Al nutation NMR spectra and ^{23}Na MAS nutation NMR spectra were recorded using a Varian VXR-400 S spectrometer at 79.5, 104.2 and 105.8 MHz, respectively. A 3.0 M NaCl solution and a 3.0 M $AlCl_3$ solution were used as chemical shift references. Before NMR measurement all samples were hydrated for about two months in a desiccator above a saturated ammonium nitrate solution (80% relative humidity).

Nitrogen adsorptions were measured on a Digisorb 2600 (Micromeritics) at 77 K. Samples (0.25 g) were degassed overnight in vacuo at 820 K. Relative pressures were

converted [30] into t-values as follows:

$$t = [13.99/(\log(p^0/p) + 0.034)]^{0.5} \qquad (1)$$

From the X-ray diffraction (XRD) pattern the unit cell constant (a_0 (nm)) and crystallinity were calculated (according to ASTM methods D3942 and D3906, respectively). Because of the considerable amount of extra-framework aluminium [31], the number of framework aluminium atoms per unit cell (N_{Al}) was calculated from a_0 [32] applying:

$$N_{Al} = 1071 \cdot (a_0 - 2.4238) \qquad (2)$$

Transmission FTIR spectra were obtained on a Bruker IFS66 using the KBr-method. N_{Al} was calculated from the position of the asymmetric O-T-O mode [32] applying:

$$N_{Al} = 0.766 \cdot (1086.7 - \nu_1) \qquad (3)$$

Temperature programmed ammonia desorption profiles were measured with a conventional, laboratory built apparatus. Desorbed molecules were detected by a thermal conductivity detector (TCD). About 100 mg sample was dried in a nitrogen flow (0.17 ml s^{-1}) increasing the temperature from ambient to 470 K at a rate of 2.8 10^{-3} K s^{-1} in case of NH$_4$-Y and to 773 K at a rate of 8.3 10^{-2} K s^{-1} in case of USY-Z. After cooling down to ambient, gaseous NH$_3$ was adsorbed for half an hour, and the reactor was flushed with nitrogen until the TCD signal remained unchanged. Desorbing molecules were measured whilst increasing the temperature from ambient to 1000 K at a rate of 8.3 10^{-2} K s^{-1} at a 0.17 ml s^{-1} nitrogen flow.

The hexane cracking activity was determined at 101 kPa, 733 K in a fixed-bed continuous-flow Pyrex microreactor with an internal diameter of 6 mm. Temperature

was controlled by an external thermocouple (Eurotherm) and registered by a internal thermocouple located close to the catalyst bed. Typically 100 mg ($\pm 7.4\ 10^{-2}$ ml) zeolite powder was placed in the reactor and held in place by quartz wool. Ultrastable Y zeolites were dried under flowing He by heating (0.2 K s^{-1}) the sample to 773 K. Subsequently, the reactor was by-passed and the flow of gas was diverted through a n-hexane saturator and a condensor at 268 K. When a constant signal from a flame ionization detector indicated the partial n-hexane pressure to be stable at 4.5 kPa, the reactant flow was preheated to 773 K and passed through the catalyst bed. The flow rate was determined by a bubble meter and was maintained at 0.133 ml s^{-1}. The product mixture was analyzed by on-line gas chromatography on a Packard model 429 using a 3 m column of 2% diisodecyl phthalate, and 2% Benton on Chromosorb GAW in combination with a flame ionisation detector (FID). Occasionally a sample was analyzed on a 3 m Porapak Q column to check the mass balance.

The apparent first-order rate constant, k^{app} (s^{-1}), was calculated from an expression for an integral plug flow reactor, neglecting volume expansion during reaction:

$$k^{app} = \frac{1}{\tau}\ \ln\left(\frac{1}{1-\xi}\right) \tag{4}$$

where ξ is the conversion and t the residence time, (0.2 s) defined as catalyst volume (ml) divided by gas flow (ml s^{-1}). Initial (k_0^{app} (s^{-1})) and steady state (k_∞^{app} (s^{-1})) rate constants were calculated describing the deactivation rate (k (s^{-1})) [33] as:

$$k^{app} = k_\infty^{app} + (k_0^{app} - k_\infty^{app})\ \exp(-t/\tau_d) \tag{5}$$

where τ_d is the time constant of deactivation.

Results and Discussion:

Deep Bed Calcination of NH_4,Na-Y: The sodium cation redistribution between supercages and the other cages upon deep bed calcination was studied by ^{23}Na MAS nutation NMR spectroscopy. The spectrum of the parent 64% ammonium exchanged Na-Y zeolite (Fig.1a) shows 37% of the absorption at (-1ppm,$1\omega_{rf}$) and 63% at (-6ppm,$2\omega_{rf}$). Upon correction for the 60% undetected absorption at $2\omega_{rf}$, it can be calculated that 4 sodium cations per unit cell in this NH_4,Na-Y sample give the narrow signal at (-1ppm,$1\omega_{rf}$), whereas the other 16 give the broad signal at (-6ppm,$2\omega_{rf}$). The 4 sodium cations thus revealing high mobility and highly symmetric coordination are located in the supercages, whereas the 16 fairly immobile, less symmetrically coordinated cations are located inside the sodalite cages or hexagonal prisms. Based upon
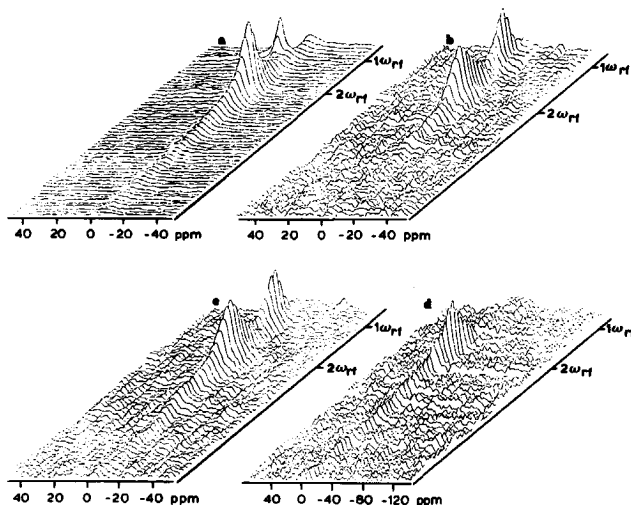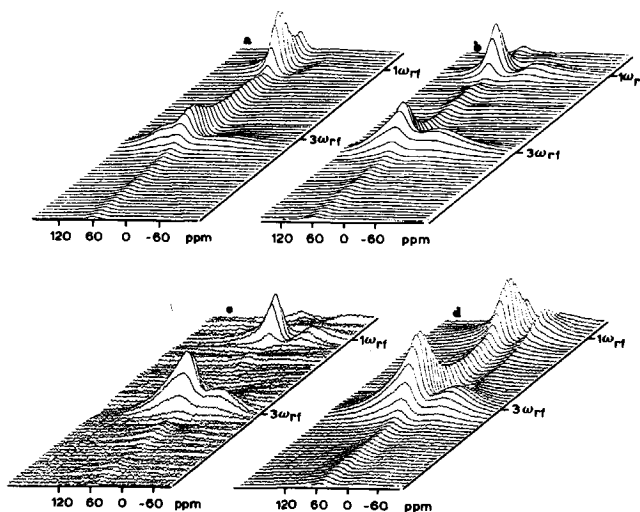

Figs.1a-d: ^{23}Na MAS nutation NMR spectrum of fully hydrated NH_4Na-Y (1a), USY-A (1b), USY-B (1c) and USY-C (1d). The numbers along the F1-dimension indicate $1\omega_{rf}$ and $2\omega_{rf}$ (ω_{rf} = 50 kHz).

previous findings (chapter 2, ref.27) we are inclined to believe that these sodium are only located inside the sodalite cages.

Both the ^{23}Na MAS nutation NMR spectra of USY-A and of USY-B (Figs.1b,1c) show 50% of the absorption at (-1ppm,$1\omega_{rf}$) and 50% of the absorption at (-4ppm,$2\omega_{rf}$). When cesium exchange is used to selectively replace the cations located in the super cages of USY-B, ICP-AES shows that half of the sodium cations are replaced. Thus it appears that ^{23}Na MAS nutation NMR detects at both $1\omega_{rf}$ and $2\omega_{rf}$ an equal percentage of the absorption, indicating that quadrupole interactions at sodium nuclei inside the supercages have increased. This is also indicated by the broadening of the line at (- 1ppm,$1\omega_{rf}$) observed upon ultrastabilization of NH_4,Na-Y (Fig.1) (Chapter 2, reference 27). Moreover, the decrease in chemical shift of asymmetric sodium resonating at $2\omega_{rf}$ from -6 ppm in NH_4,Na-Y (Fig.1a) to -4 ppm in USY-A and -B indicates that the sodium-framework interactions inside the sodalite cages or hexagonal prisms have decreased [27]. Finally, the ^{23}Na MAS nutation NMR spectrum of USY-C (Fig.1d) shows that upon renewed ammonium exchange and deep bed calcination of USY-B, yielding USY-C, all remaining sodium cations resonate at (-4ppm,$2\omega_{rf}$), indicating that at room temperature they are located outside the supercages, are immobile and asymmetrically coordinated. The changes in aluminium coordination upon deep bed calcination were studied by ^{27}Al nutation NMR spectroscopy. The spectra of Na-Y, NH_4,Na-Y and NH_4-Y (spectra not shown) all show the same quadropole pattern along the F1 axis and at the F2 axis at 60 ppm characterizing a slightly distorted tetrahedral oxygen coordination (see ref. 7,8). Upon deep-bed calcination the ^{27}Al nutation NMR spectrum of USY-A (Fig.2a) shows an absorption at 60 ppm at the F2 axis attributed to framework aluminium and non-framework aluminium in tetrahedral coordinations distorted to various degrees [7]; an absorption at 0 ppm attributed to octahedrally coordinated non-framework aluminium and an absorption at (75ppm,$\pm3\omega_{rf}$) attributed to distorted tetrahedral framework aluminium [8]. These spectral features do not change dramatically upon further ammonium exchange and deep bed calcination (Figs.2b,c), although it can be remarked that upon further ultrastabilization the amount of octahedral aluminium steadily decreases and that in USY-C (Fig.2c) the absorption at

(75ppm,$\pm 3\omega_{rf}$) attributed to distortedly tetrahedral framework aluminium [8] has

Figs.2a-d: ^{27}Al MAS nutation NMR spectrum of fully hydrated USY-A (2a), USY-B (2b), USY-C (2c) and USY-Z (2d).

markedly decreased. ^{29}Si MAS NMR spectroscopy was used to follow the changes in framework silicon-to-aluminum ratio and in average number of Al-O-Si-O-Al pairs upon ultrastabilization. ^{29}Si MAS NMR spectra of all samples consist of four lines, at -89.3, -94.8, -100.0 and -105.6 ppm, attributed to framework Si(3Al), Si(2Al), Si(1Al) and Si(0Al) respectively. No signal of Si(4Al) was observed. [Si(nAl) denotes a SiO_4 tetrahedron connected to n AlO_4 tetrahedra and (4-n) other SiO_4 tetrahedra]. The framework Si/Al ratios listed in Table 1 were determined from the ^{29}Si MAS NMR spectra by Gaussian deconvolution using the formula [34]:

$$Si/Al_{NMR} = \frac{I_4+I_3+I_2+I_1+I_0}{I_4+0.75I_3+0.5I_2+0.25I_1}$$

where I_n is the intensity of the peak corresponding to the Si(nAl) building block. The average number of Al-O-Si-O-Al second-nearest neighbour linkages per framework aluminium atom ($\overline{N}\overline{N}\overline{N}$) listed in Table 1 was calculated [12,13] applying:

$$\overline{N}\overline{N}\overline{N} = \frac{36I_4+18I_3+6I_2}{4I_4+3I_3+2I_2+I_1}$$

Table 1:Micropore volume (V_t), mesopore area (S_t), crystallinity according to XRD, unit cell constant (a)), silicon-to-aluminum ratio (Si/Al) as determined by i.r., XRD, 29Si MAS NMR, average number of second-nearest neighbour aluminium atoms per framework aluminium atom ($\overline{N}\overline{N}\overline{N}$), and percentage of sodium atoms removed. The bulk Si/Al of all samples as determined by ICP-AES was 2.5±0.1.

	V_t(ml/g)	S_t(m²/g)	cryst. XRD	a_0(nm)	i.r.[1]	Si/Al XRD[1]	29Si MAS NMR	$\overline{N}\overline{N}\overline{N}$	% Na removed
Na-Y	0.34	14.9	109	2.466	2.5	2.5	2.5	2.5	0
USY-A	0.32	27.2	112	2.462	4.9	3.7	4.2	2.0	64
USY-B	0.29	50.6	98	2.448	7.0	6.4	6.5	1.9	93
USY-C	0.27	58.2	94	2.441	9.7	9.4	9.4	1.5	99
USY-Z	0.30	23.2	70	2.446	12.7	7.1	6.6	2.0	100
USY-α	0.26	50.3	102	2.453	5.2	5.1	5.3	1.2	73

According to ^{29}Si MAS NMR, XRD and i.r. (Table I) the rise in Si/Al ratio upon deep bed calcination yielding USY-A is substantially less than that obtained upon steam calcination yielding USY-α. Concomitantly, the micropore volume, V_t (ml/g), of USY-A has decreased to a lesser extent than that of USY-α, indicating that USY-A contains

less extra-framework material [35]. Also the lower mesopore area, S_t (m^2/g), of USY-A indicates it to be more in tact than USY-α [36,37]. These observations are probably related to the comparatively low partial steam pressure and short steaming time during deep bed calcination applied to prepare USY-A [4,5,18]. Moreover, the average number of second-nearest aluminium neighbour atoms per aluminium atom, $\overline{NNN}$ (Table I), indicates that aluminium in USY-A, -B, and -C is more clustered than in USY-α. Thus our deep bed calcination appears to produce relatively heterogeneous ultrastable Y zeolites, whereas calcination in flowing steam [25], results in a more homogeneous USY-α.

Deep Bed Calcination of NH_4-Y: As shown in Fig.3, the ammonia TPD profile of the parent, completely ammonium exchanged Na-Y zeolite, NH_4-Y, shows maxima near 400 K, 600 K and 700 K, attributed to the desorption of physisorbed ammonia,
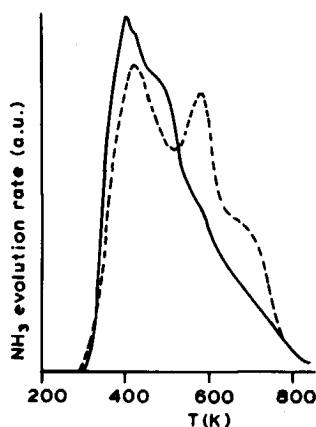

Fig.3: *Temperature programmed NH_3 desorption (TPD) pattern of(---) NH_4-Y and (——) USY-Z.*

ammonia chemisorbed at weakly and at strongly acid sites, respectively [24,25,26]. The TPD of deep bed calcined NH_4-Y, USY-Z, only shows maxima near 400 K and 600 K, indicating that the strongly acid sites have vanished. Accordingly USY-Z shows a high average number of next-nearest aluminium atoms per aluminium atom, $\overline{NNN}$, indicating

that USY-Z contains much less AlO_4 tetrahedra with no AlO_4 tetrahedron as next-nearest neighbour than e.g. the commercial USY-α (Table 1). Since these completely isolated AlO_4 tetrahedra are generally held responsible for the highest zeolitic Brønsted acidity [14,15,16], USY-Z's high $\overline{NNN}$ further illustrates its low acidity. Moreover, when the hexane cracking activity of USY-Z (±24 Al/unit cell) is compared to that of USY-α
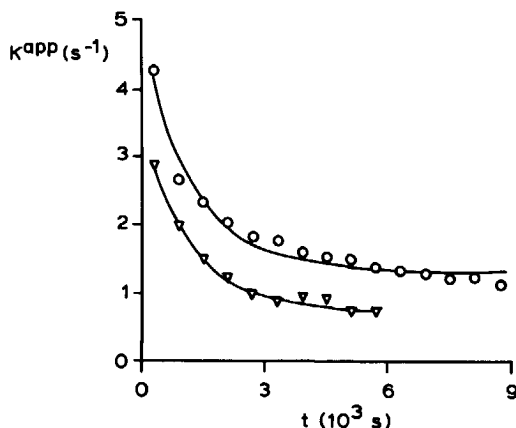

Fig.4a,b: n-Hexane cracking at 773 K over samples USY-Z (o) and USY-α (▽): Activity, k^{app} (s^{-1}) , relative to initial activity, k_0^{app} (s^{-1}), as function of time on stream t (10^3 s)

Table 2: Number of framework aluminium atoms per unit cell not neutralized by sodium (Al_F-Na), average number of next-nearest aluminium sites ($\overline{NNN}$), initial hexane cracking activity, k_0^{app}, and long-term activity, k_∞^{app}, and time constant of deactivation, τ_d

Zeolite	method of calcination	Al_F-Na/unit cell	$\overline{NNN}$	k_0^{app} (s^{-1})	k_∞^{app} (s^{-1})	τ_d (s)
USY-Z	deep-bed	31	2.0	4.8	1.4	1200
USY-α	steam	16	1.2	1.4	0.8	1140

(31 Al/unit cell, 16 Na/unit cell) (Fig.4, Table II) both zeolites display a similar activity per framework aluminium atom not neutralized by sodium. Since it has been observed, that 16 sodium atoms per unit cell are enough to effectively poison all of the strongly acidic, catalytically very active sites in an ultrastable Y zeolite with a framework Si/Al=5.2 [20], the comparable activity of USY-α and USY-Z indicates that USY-Z has no catalytically very active sites. Moreover, the combination of high $\overline{N}\overline{N}\overline{N}$ and high Si/Al determined from the ^{29}Si MAS NMR spectrum of USY-Z when compared with USY-α (see Table I) implies that similar to USY-A, -B and -C aluminium in USY-Z is clustered. The heterogeneity of USY-Z is further illustrated by ^{27}Al nutation NMR. Its spectrum (Fig.2d) shows a sharp peak at (0ppm,1ω_{rf}) in addition to the large variety of aluminium species already observed for USY-A, -B or -C (Figs.2a-c), and attributed to mobile, highly symmetrically octahedrally coordinated non-framework aluminium [10,11]. Finally, the 36% loss of crystallinity which is detected by XRD but not by the changes in micropore volume or mesopore surface area as determined by N_2-adsorption measurements (Table I) again points to the complexity of USY-Z. Thus according to ^{29}Si MAS NMR, TPD and hexane cracking data, USY-Z contains negligible amounts of isolated framework AlO_4 tetrahedra, i.e. superacidic sites associated with superior catalytic activity (cf. ref. 2,3). Nevertheless, highly active catalysts have reportedly been obtained by ultrastabilization of NH_4-Y zeolites with extremely low residual sodium levels [23]. Therefore, the low acidity and catalytic activity of USY-Z proves the inadequateness (too low steam pressure, too short steaming time, non-optimal calcination temperature) of our deep bed calcination rather than the unsuitability of NH_4-Y as starting material for ultrastable Y zeolites. Nevertheless, because of its high porosity, this material might serve in reactions requiring mild acidity

Conclusions

^{23}Na MAS nutation NMR is well suited to follow the sodium cation redistribution between supercages and smaller cages upon successive ammonium exchange and

ultrastabilization steps. The small fraction of sodium cations left after two such steps appears to be located outside the supercages. ^{27}Al nutation NMR shows that the first coordination sphere of aluminium in an ultrastable Y zeolite prepared starting from 100% ammonium exchanged Na-Y is more varied than that prepared from 64% ammonium exchanged Na-Y. The heterogeneity of the former material also shows up in the average number of next-nearest aluminium neighbours as determined by ^{29}Si MAS NMR, and from the loss in crystallinity as determined by XRD but not by nitrogen adsorption. Moreover, ammonia temperature programmed desorption (TPD) and a hexane cracking test show that deep bed calcined NH_4-Y is neither a very acidic nor a highly active catalyst. Comparison with literature data [23] indicates that the procedure applied here for ultrastabilization of NH_4-Y is the most probable cause for the absence of superior catalytic properties in our sample.

Acknowledgements

References:

1. Scherzer, *J. Catal.Rev.-Sci.Eng.* **1989**, *31*, 215-354.
2. Corma, A. *Stud.Surf.Sci.Catal.* **1989**, *49*, 49-67.
3. Groenenboom, C.J. *Stud.Surf.Sci.Catal.* **1988**, *46*, 99-113.
4. Kerr, G.T. *ACS.Symp.Ser.* **1973**, *121*, 219-229.
5. McDaniel, C.V.; Maher, P.K. *ACS Monograph* **1976**, *171*, 285-331.
6. Shannon, R.D.; Gardner, K.H.; Stalely, R.H.; Bergeret, G.; Gallezot, P.; Auroux, A. *J.Phys.Chem.* **1985**, *89*, 4778-4788.

7. Samoson, A.; Lippmaa, E.; Engelhardt, G.; Lohse, U.; Jerschkewitz H.-G.C. *Chem.-Phys.Lett.* **1987**, *134*, 598-592.

8. Hamdan, H.; Klinowski, J. *J.Chem.Soc.,Chem.Commun.* **1989**, 240-242.

9. Lohse, U.; Mildebrath, M. *Z.anorg.allg.Chem.* **1981**, *476*, 126-135.

10. Engelhardt G.; Lohse, U.; Samoson, A.; Mgi, M.; Tarmak, M.; Lippmaa E. *Zeolites* **1982**, *2*, 59-62.

11. Klinowski, J.; Thomas, J.M.; Fyfe, C.A.; Gobbi, G.C. *Nature(London)* **1982**, *296*, 533-536.

12. Vega, A.J. *ACS Symp.Ser.* **1983**, *218*, 217-230.

13. Nieman, J.; De Vos Burchart, E.: to be published.

14. Dempsey, E. *J.Catal.* **1974**, *33*, 497-499; *J.Catal.* **1975**, *39*, 155-157

15. Mikovsky, R.J.; Marshall, J.F. *J.Catal.* **1976**, *44*, 170-173.

16. Pine, L.A.; Maher, P.J.; Wachter, W.A. *J.Catal.* **1984**, *85*, 466-476.

17. Bosacek, V.; Freude, D.; Fröhlich, T.; Pfeifer, H.; Schmiedel, H.J. *Colloid.Interface Sci.* **1982**, *85*, 502-507.

18. Engelhardt, G.; Lohse, U.; Patzelova, V.; Mägi, M.; Lippmaa, E. *Zeolites* **1983**, *3*, 233-238.

19. Kouwenhoven, H.W. *ACS Symp.Ser.* **1973**, *121*, 528-539.

20. Beyerlein, R.A.; McVicker, G.B.; Yacullo, L.N.;Ziemiak, J.J. *Prep.Am.Chem.Soc.-Div.Pet.Chem.* **1986**, *31*, 190-197.

21. Beyerlein, R.A.; McVicker, G.B.; Yacullo, L.N.; Ziemiak, J.J. *J.Phys.Chem.* **1988**, *92*, 1967-1970.

22. Fritz, P.O.; Lunsford J.H. *J.Catal.* **1989**, *118*, 85-98.

23. Alafandi, H.; Stamires, D. *U.S. patent* 4058484, 1977; *U.S. patent* 4085069, 1978.

24. Maesen, Th.L.M. Ph.D. Thesis; Chap. 3, submitted to *J.Chem.Soc., Faraday Trans.*.

25. Van Broekhoven, E.H.; Daamen, S.; Smeink, R.G.; Wijngaards, H.; Nieman, J. *Stud.Surf.Sci.Catal.* **1989**, *49*, 1291-1300.

26. Sulikowski, B., private communication.

27. Maesen, Th.L.M.; Janssen, R.; Kouwenhoven H.W.; Van Bekkum, H.; Veeman, W.S., *J.Phys.Chem.* in press.

28. Kerr, G.T. *J.Catal.* **1969**, *15*, 200-204.

29. Von Ballmoos, R. *The 18O-Exchange Method in Zeolite Chemistry;* O. Salle Verlag: Frankfurt-am-Main; Verlag Sauerländer: Aarau, 1981; pp.200-205.

30. De Boer, J.H.; Lippens, B.C.; Linsen, B.G.; Broekhoff, J.C.P.; Van den Heuvel, A.; Osinga, Th.J. *J.Colloid Interface Sci.* **1966**, *21*, 405-414..

31. Kerr, G.T. *Zeolites* **1989**, *9*, 350-351.

32. Sohn, J.R.; DeCanio, S.J.; Lunsford, J.H.; O'Donnell, D.J. *Zeolites* **1986**, *6*, 225-227.

33. Hammon, U.; Kokotailo, G.T.; Riekert, L.; Zhou, J.Q. *Zeolites* **1988**, *8*, 338-339.

34. Klinowski, J. *Progr.NMR Spectrosc.* **1984**, *16*, 237-309.

35. Hudec, P.; Novansky J.; Silhar, S.; Trung T.N.; Zubek M.; Madar J. *Adsorpt.Sci. Technol.* **1986**, *3*, 159-166.

36. Lohse, U.; Engelhardt, G.; Patzelova, V. *Zeolites* **1983**, *4*, 163-167.

37. Zukal, A.; Patzelova, V.; Lohse, U. *Zeolites* **1986**, *6*, 133-136.

38. Cattanach, J.; Wu, E.L.; Venuto, P.B. *J.Catal.* **1968**, *11*, 342-347.

39. Kerr, G.T.; Chester, A.W. *Thermochim.Acta.* **1971**, *3*, 113-124.

40. Lohse, U.; Parlitz, B.; Patzelova V. *J.Phys.Chem.* **1989**, *93*, 3677-3683.

CHAPTER 5

LOW-TEMPERATURE PLASMA CALCINATION OF ZEOLITE NH$_4$,Na-Y[*]

Abstract

A low temperature oxygen plasma removes all ammonia form 70% ammonium-exchanged zeolite Na-Y causing a comparable degree of dealumination as shallow bed calcination. Hydronium exchange of Na-Y in highly dilute acidic medium also gives partial dealumination. Plasma calcination of 87% ammonium-exchanged Na-Y results in a severe loss of crystallinity, possibly because of mineral acid formation at inaccessible sites. As long as oxidation products can easily leave the crystallite, low-temperature plasma calcination is a mild technique for the oxidative removal of ammonia

Introduction

Low-temperature plasma calcination has been successfully used [1] for the removal of organic templates from as-prepared zeolites without impairing the crystallinity of the aluminosilicate framework. The technique may be particularly useful when the template is resistant to thermal treatment [2]. It can also be used [1] for the efficient preparation of bifunctional zeolitic catalysts (for example by decomposing Pt(NH$_3$)$_4^{2+}$ in mordenite). We report the use of plasma calcination (i) for the decomposition of the ammonium ion in NH$_4^+$-exchanged zeolites to prepare their Brønsted acid forms; (ii) to address the controversial subject of the existence of "pure H-Y zeolite". The latter has been the subject of much discussion ever since Kerr's claim [3] that such material can be generated by shallow bed (SB) decomposition of the ammonium cation in NH$_4$,Na-

Y [4,5]. Engelhardt et al. [6] challenged this on the basis of their ^{29}Si and ^{27}Al NMR work. The weak dealumination observed upon mild (423-573 K) SB treatment was thought to be a result of dehydroxylation and the concomitant removal of aluminium from the framework [7,8]. Since at 350 K no dehydroxylation is expected to take place [9,10], we thought that the use of low-temperature oxygen plasma for oxidative decomposition of NH_4^+ in NH_4,Na-Y might offer a new method for the preparation of pure H,Na-Y. In a separate experiment, we have used acid ion-exchange resin interacting with zeolite Na-Y via an infinitely dilute acidic medium.

A series of samples of zeolite Y was examined using infrared (IR) and magic-angle-spinning (MAS) NMR spectroscopies, X-ray diffraction (XRD) and inductively-coupled plasma atomic emission spectroscopy (ICP-AES) in order to determine the efficiency and applicability of plasma treatment for the preparation of the hydrogen form of the zeolite. We have examined samples of NH_4,Na-Y with different residual sodium contents, SB-treated samples, samples prepared by ion exchange with a hydronium form of a cation-exchange resin and samples exchanged with hydroxylammonium ion.

Low-temperature plasma is a quasi-neutral fluid composed of free electrons, ions and electrically neutral species at low pressure. It is generated by applying a strong alternating electric field to a rarefied gas. Because of their small mass, the field accelerates free electrons to very high kinetic energies, equivalent to temperatures up to 10^4 K. The ions pick up much smaller amounts of energy, and their temperature increases to slightly above room temperature. The neutral species (such as atomic oxygen and highly electronically excited states of molecular oxygen [11]) remain at room temperature [12], because the concentration of ions is too low to warm them by collisional impact. Since these species of different mass and electric charge are not at thermal equilibrium, the temperature of a glow discharge is ill-defined (see also ref.12). Consequently the temperature of zeolite samples within the "low-temperature" plasma can only be estimated [1]. Low-temperature oxygen or air plasma can be used to calcine zeolites, because they contain atomic oxygen [11,13], a very strong oxidant [14].

Experimental

Materials: The parent sample was zeolite Na-Y with Si/Al=2.5 as determined by XRF and ICP-AES. The average crystal size, estimated by scanning electron microscopy (SEM), was 1 μm. 70% and 87% ammonium-exchanged samples (which will be referred to as NH_4,Na-Y-70 and NH_4,Na-Y-87, respectively) were prepared by ion exchange with aqueous ammonium nitrate at 298 K [15]; 79% hydronium-exchanged Na-Y (H,Na-Y-79) was prepared using Dowex 50WX8 resin [16]. 9% Hydroxylammonium-exchanged Na-Y (NH_3OH,Na-Y-9) was made by contacting the parent sample with a freshly prepared mixed solution of 0.5 M NH_3OHCl and 0.5 M NH_2OH[17]. The extent of sodium exchange was calculated from the sodium-to-aluminium ratio measured by ICP-AES after dissolution as described by Von Ballmoos [18].

Characterization: ^{29}Si and ^{27}Al MAS NMR spectra were recorded using a Bruker MSL-400 multinuclear spectrometer at 79.5 MHz and 104.2 MHz, respectively. ^{27}Al spectra were measured with 0.6 μs pulses and 0.2 s repetition time. 4000 Free induction decays (FIDs) were accumulated per spectrum. ^{29}Si NMR spectra were recorded with 5 μs pulses and 20 s repetition time. 400 Scans were accumulated for each spectrum. Further information about the sample was obtained from XRD (Philips PW1710) and transmission FTIR specrtoscopy (Bruker IFS66).

Plasma calcination: A laboratory built barrel asher (see Fig.1) was used for the plasma calcination experiments. Typically 0.3 g of a sample was distributed evenly across the surface of a Pyrex sample holder in a layer less than 1 mm thick. After overnight drying at 350 K in a vacuum oven above zeolite Na-A, the sample was quickly transferred to the plasma reactor, and dried further in a flow of dry oxygen gas (1.3 s mean residence time) at 50 Pa and 300 K for two days. It was subsequently plasma calcined at 10 W rf power. During calcination the temperature of a shielded Pyrex-coated thermocouple at the centre of the oxygen flow was 350 K. The apparatus was switched off after five days and allowed to cool down to ambient temperature. The sample was then slowly
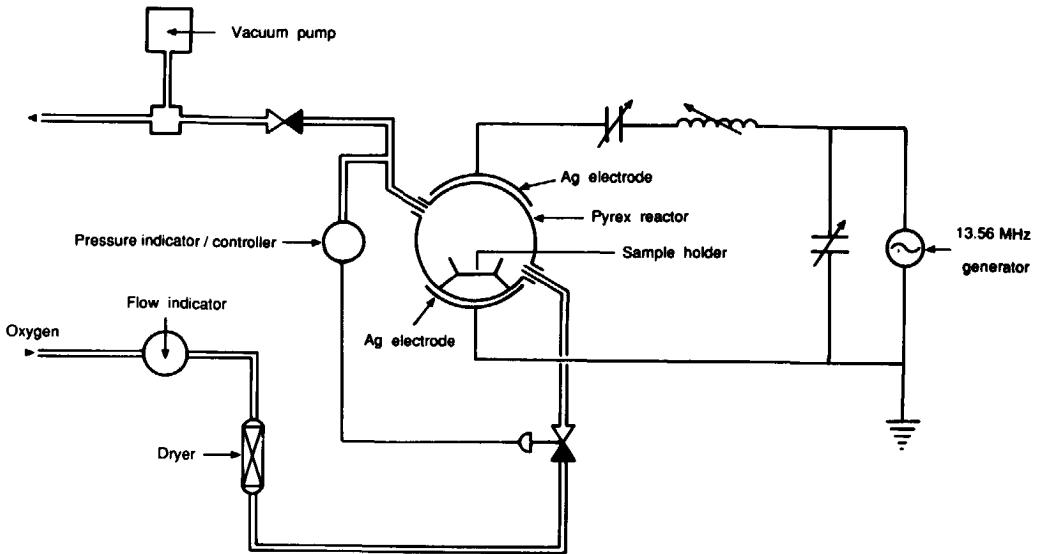
Fig.1: Apparatus used for the plasma calcination experiments

hydrated in order to avoid local heating due to the high hydration enthalpy of the acidic protons by exposing to air for one day at 50 Pa and then at 101 kPa in the reactor. Finally the sample was fully hydrated in a desiccator over saturated ammonium nitrate solution.

SB calcination: In a modification of the SB procedure [3] the samples were thermally decomposed in a flow of dry nitrogen using a bed less than 1 mm thick. The temperature was increased from ambient to 450 K at a rate of 0.2 K s^{-1} and maintained there for 1 h. After cooling, the sample was carefully hydrated by contacting it with laboratory air and finally fully hydrated in the desiccator.

Results and Discussion

IR spectroscopy was used to establish whether plasma calcination resulted in complete deammoniation. The spectra of the parent and plasma calcined $NH_4,Na-Y-70$ are shown in Fig.2. Calcination removes the ammonia absorption bands due to N-H stretching vibrations (at ca. 3200 cm^{-1}) and the bands attributed to N-H bending vibrations (1400 cm^{-1})[19]. In addition, a small sharp peak at 1385 cm^{-1} appears.
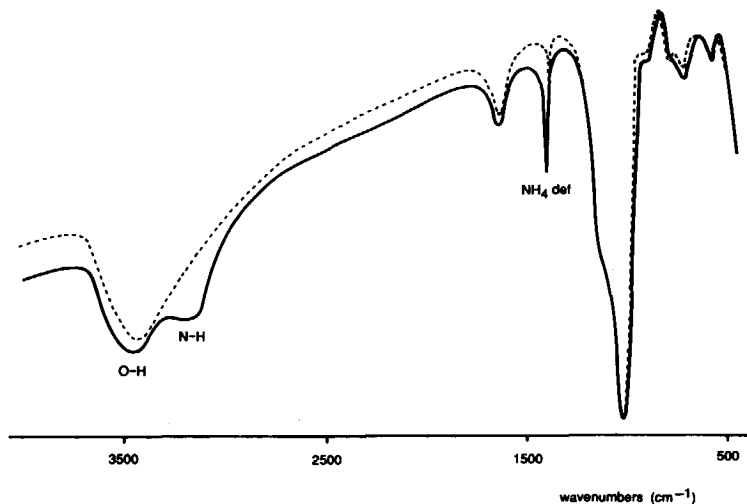

Fig.2: IR spectra of parent and plasma calcined zeolite NH_4 ,Na-Y-70. (——) Parent, (---) plasma calcined.

It disappears upon washing the plasma calcined sample with water. To establish that it is not due to residual ammonia species, IR spectra of ion-exchanged and plasma treated $NH_3OH,Na-Y-9$ were recorded. The region of N-H bending absorptions is shown in Fig.3. One hour plasma treatment of NH_3OH^+, similar to plasma calcination of NH_4^+ , also gives rise to an absorption at 1385 cm^{-1} and to an additional signal at 1260 cm^{-1}. Since the strongly oxidizing oxygen plasma makes regeneration of NH_4^+ from
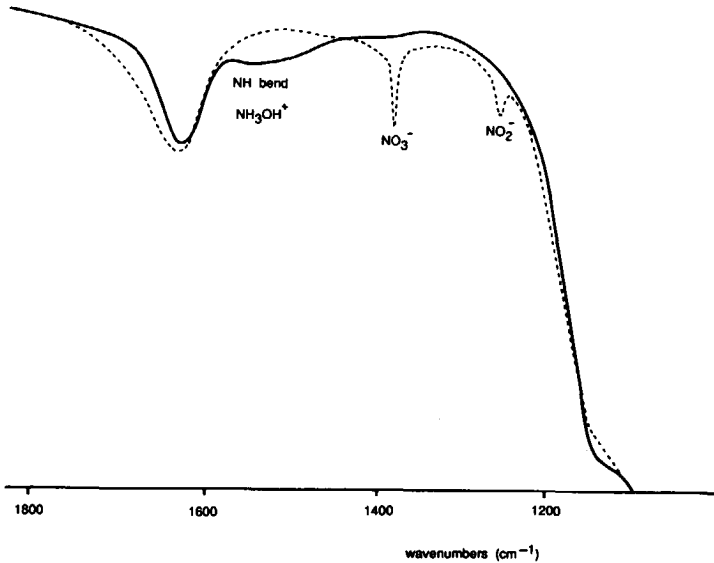
Fig.3:IR spectra of parent (——) and plasma calcined (---) 9% hydroxylammonium-exchanged sample Na,NH₃OH-Y-9.

NH_3OH^+ unlikely, the 1385 cm^{-1} and 1260 cm^{-1} IR absorptions are assigned to oxidation products such as NO_3^- and NO_2^-, respectively [20]. We do not know which cations are associated with such anionic species, but we note that Na^+ and H^+ are present in the intracrystalline environment. Except for the 1385 cm^{-1} absorption the IR spectra of plasma and SB calcined 70% NH_4,Na-Y are virtually indistinguishable.

No change in the IR spectrum was observed upon plasma calcination of H,Na-Y-79, apart from the appearance of a small sharp peak at 1385 cm^{-1}. This is probably caused by NO_3^- created by oxidation of traces of nitrogen from air occluded inside the zeolite prior to calcination [13,21]. In 87% ammonium-exchanged samples ammonia decomposition by plasma calcination appears to be more difficult since a small IR peak at 1400 cm^{-1} shows that deammoniation is incomplete after five days of treatment.

Neither plasma calcination nor SB treatment induce significant changes in XRD

patterns of NH_4,Na-Y-70. Similarly, the crystallinity of H,Na-Y-79 is not affected by the plasma treatment. NH_4,Na-Y-87 tends to be less resistant: the crystallinity of the plasma-treated sample is low. The crystallinity of NH_4,Na-Y-87 deteriorates only slightly under SB treatment.
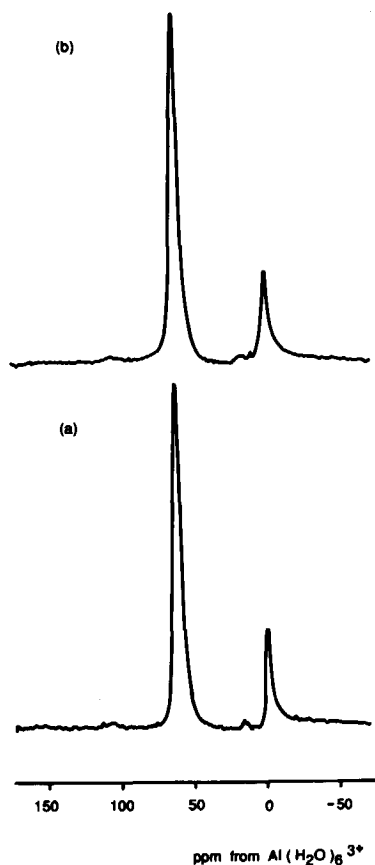

Fig.4: ^{27}Al *MAS NMR spectra of 79% hydronium-exchanged sample H,Na-Y-79, acquired with 0.6 μs pulses and 200 ms repetition time. 4000 Free induction decays were accumulated per each spectrum. (a) Parent sample; (b) plasma calcined sample.*

^{27}Al MAS NMR spectra of the fully hydrated samples contain a signal from tetrahed-
rally coordinated framework aluminium at about 60 ppm and, upon calcination or hy-
dronium ion exchange, also a signal at ca. 0 ppm attributable to octahedrally coordina-
ted non-framework aluminium (see Figs.4 and 5). ^{29}Si MAS NMR spectra of all sam-
ples consist of four lines, at -89.6, -95.0, -100.2, and -105.6 ppm, attributed to framework
Si(3Al), Si(2Al), Si(1Al) and Si(0Al) respectively. [Si(nAl) denotes a SiO_4 tetrahedron
connected to n AlO_4 tetrahedra and (4-n) other SiO_4 tetrahedra]. The framework Si/Al
ratios listed in Table 1 were determined from the ^{29}Si MAS NMR spectra by Gaussian
deconvolution using the formula [7,8]:

$$(Si/Al)_{NMR} = \frac{I_4 + I_3 + I_2 + I_1 + I_0}{I_4 + 0.75 I_3 + 0.5 I_2 + 0.25 I_1}$$

where I_n is the intensity of the peak corresponding to the Si(nAl) building block in the
structure.

TABLE 1:   Framework silicon-to-aluminium ratios of NH_4 ,Na-Y and H,Na-Y samples
before and after different treatment, as calculated from ^{29}Si MAS NMR
spectra

Sample	Degree of exchange		
	70%[a]	87%[a]	79%[b]
Parent	2.5	2.5	2.7
Plasma calcined	2.6	2.8	2.7
Shallow bed (SB) calcined	2.6	2.5	---

[a]Ammonium-exchanged
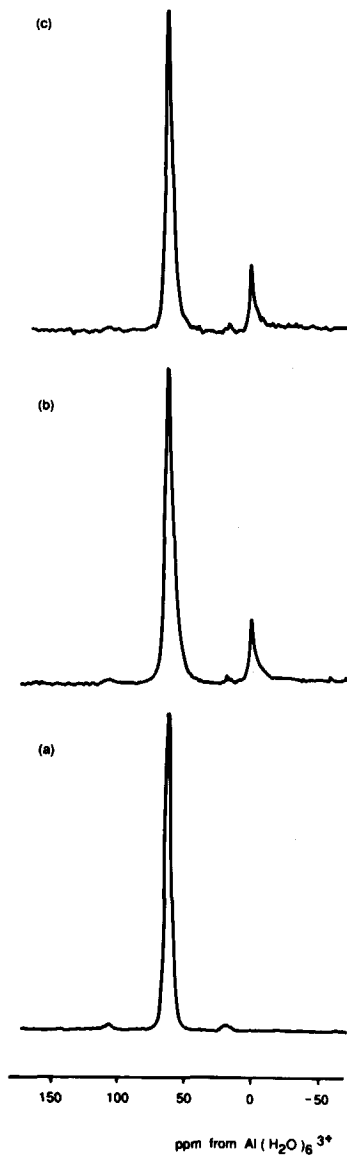[b]Prepared using the hydronium form of Dowex 50WX8 resin

Fig.5: ^{27}*Al MAS NMR spectra of 70% ammonium-exchanged sample NH$_4$,Na-Y-70, recorded as in Fig.4. (a) Parent sample; (b) shallow-bed (SB) calcined; (c) plasma calcined.*

We have ensured that H,Na-Y was stable in a dry oxygen plasma by subjecting H,Na-Y-79 to low-temperature calcination. Although some damage due to radiation [22] or hot spots caused by recombination of oxygen atoms is possible, neither XRD, IR, ^{29}Si nor ^{27}Al NMR (see Table 1 and Fig.4) indicate any deterioration of the zeolite framework. Since NH_4,Na-Y-70 retained full crystallinity upon plasma calcination, the conclusion that our treatment does not affect the crystallinity of H,Na-Y seems to be justified. In agreement with earlier work [6,23], our SB treatment produces a small amount of extra-framework aluminium (Table 1 and Fig.5b). The ^{27}Al and ^{29}Si MAS NMR spectra (Fig.5c and Table 1) of plasma calcined NH_4,Na-Y-70 show a similaramount of extra-framework aluminium. As this low-temperature dealumination cannot be caused by dehydroxylation [9,10], hydrolysis of framework aluminium by protons in Si-OH-Al groupings is a plausible explanation. Hydrolysis might explain the slight dealumination observed in fully hydrated SB calcined samples [4]. Even the use of infinitely dilute acid to prevent the zeolite from direct attack of the acid [16] did not prevent some aluminium being released form the framework, as can be clearly seen from ^{29}Si (Table 1) and ^{27}Al NMR (Fig.4a). It is known that in ammonium exchanged zeolite Y up to about 70% the NH_4 ions are located inside α-cages, and that further exchange must involve sodium cations at less accessible positions (see ref.24, chapter 2 of this thesis). It is thus clear that plasma calcination of NH_4,Na-Y-87 has to remove ammonium from these less accessible sites. Contrary to expectations, crystallinity of the plasma calcined 87% sample was much lower than the SB-treated zeolite. A possible explanation is that the slow removal of oxidation products such as nitrous oxide and water [25,26] from these sites results in further oxidation and formation of mineral acids [21]. A build-up of these species could cause the observed severe deterioration of the crystallinity and incomplete deammoniation. On the other hand, all ammonium sites in NH_4,Na-Y-70 are accessible (see ref.24 and chapter 2 of this thesis), so that the oxidation products can leave the zeolite easily and crystallinity of the aluminosilicate framework is maintained.

Conclusions

A low-temperature oxygen plasma completely deammoniated a 70% ammonium-ex-changed zeolite Na-Y, while the crystallinity of the sample is not impaired. Neither plasma calcined nor shallow bed treated material is "pure H-Y" zeolite, and ^{27}Al MAS NMR indicates a slight dealumination of the zeolitic framework in each case. Hydroni-um ion exchange to produce H,Na-Y from Na-Y using a highly dilute acidic medium also resulted in partial dealumination of the sample. Plasma calcination of 87% ammo-nium-exchanged NH$_4$,Na-Y caused a severe loss of crystallinity, possibly because of mineral acid formation at inaccessible sites. Low-temperature plasma calcination is a mild technique for the oxidative removal of ammonia as long as oxidation products can easily leave the crystallite.

Acknowledgements:

References:

1. Maesen, Th.L.M.; Bruinsma, D.S.L.; Kouwenhoven, H.W.; Van Bekkum, H. *J.Chem. Soc.,Chem.Commun.* 1987, 1284-1285.
2. Bibby, D.M.; Parker, L.M. *Zeolites* 1983, *3*, 11-12.
3. Kerr, G.T. *J.Catal.* 1969, *15*, 200-204.
4. Kerr, G.T. *J.Catal.* 1982, *77*, 307-308.
5. Skeels, G.W. *J.Catal.* 1983, *79*, 246-247.
6. Engelhardt, G.; Lohse, U.; Magi, M.; Lippmaa, E. *Stud.Surf.Sci.Catal.* 1984, *18*,

23-30.

7. Engelhardt G.; Michel D. *High-Resolution Solid State NMR of Silicates and Zeolites;* Wiley: New York, 1987; p.150; pp.272-275.

8. Klinowski, J. *Progr.NMR Spectrosc.* **1984,** *16,* 237-309.

9. Bosacek, V.; Patzelova, V.; Tvaruzkova, Z.; Freude, D.; Lohse, U.; Schirmer, W.; Stach, H.; Thamm, H. *J.Catal.* **1981,** *61,* 435-442.

10. Sulikowski, B. *React.Kinet.Catal.Lett.* **1981,** *16,* 39-42.

11. Capitelli, M.; Molinari, E. *Top.Curr.Chem.* **1980,** *90,* 59-109.

12. Chapman, B.N. *Glow Discharge Processes;* Wiley: New York, 1980; pp.49-76

13. Venugopalan, M.; Rajaei-Rizi, A. *Z.Phys.Chem.(Wiesbaden).* **1984,** *126,* 15-24.

14. Cook, J.M.; Benson, B.W. *J.Electrochem.Soc.* **1983,** *130,* 2459-2464.

15. Franklin, K.R.; Townsend, R.P.; Whelan, S.J.; Adams, C.J. *Stud.Surf.Sci.Catal.* **1986,** *28,* 289-296.

16. Chu, P.; Dwyer, F.G. *Zeolites* **1983,** *3,* 72-76.

17. Schenk, P.W. *Handbook of Preparative Inorganic Chemistry* Vol.I, Braue (Editor), Academic: New York, 3rd, 1975; pp.464-465.

18. Von Ballmoos, R. *The ^{18}O-Exchange Method in Zeolite Chemistry;* O. Salle Verlag: Frankfurt-am-Main; Verlag Sauerländer: Aarau, 1981; pp.200-205.

19. Uytterhoeven, J.B.; Christner, L.G.; Hall, W.K. *J.Phys.Chem.* **1965,** *69,* 2117-2126.

20. Laane, J.; Ohlsen, J.R. *Progr.Inorg.Chem.* **1980,** *27,* 465-513.

21. Jones, K. *The Chemistry of Nitrogen;* Pergamom: Elmsford, New York, 1975.

22. DiMaria, D.J.; Ephrath, L.M.; Young, D.R. *Appl.Phys.* **1979,** *50,* 4015-4021.

23. Freude, D.; Frölich, T.; Pfeifer, H.; Scheler, G. *Zeolites* **1983,** *3,* 171-177.

24. Breck, D.N. *Zeolite Molecular Sieves: Structure, Chemistry and Use;* Wiley: New York, 1974; p.549.

25. Baulch, D.L.; Campbell, J.M.; Hainsworth, R. *J.Chem.Soc.,Faraday Trans.I* **1984,** *80,* 2525-2539.

26. Perry, R.A.; Atkinson, R.; Pitts, Jr., J.N. *J.Chem.Phys.* **1976,** *64,* 3237-3239.

CHAPTER 6

LOW-TEMPERATURE PLASMA CALCINATION OF Pt(NH$_3$)$_4$,NH$_4$-MOR[*]

Introduction

In oil refinery processes like hydrocracking and hydroisomerization bifunctional zeolitic catalysts play a major role [1,2]. The zeolite provides the acidic function needed for cracking and isomerisation. Embedded noble metals like platinum add a powerful hydrogenation function, among others preventing formation of coke and improving catalyst stability [3]. Bifunctional zeolitic catalysts are conveniently prepared by ion exchange of a cationic ammine complex of the noble metal with the hydronium or ammonium zeolite [4]. Optimal dispersion of the noble metal complex in the zeolite crystal is obtained by prolonged ion exchange in the presence of a competing cation such as NH$_4^+$ [5,6,7]. Preservation of this high metal dispersion in the final catalyst requires activation in the presence of oxygen under carefully controlled conditions [5,8]. In case of Pt(NH$_3$)$_4$,NH$_4$-MOR (see Fig.1 and ref. 10 for structural details), a major problem during such a calcination is that around 630 K [5] Pt^{2+} is reduced to Pt metal by its ammonia ligands [5,8,9] and starts to catalyze the strongly exothermic oxidation of evolved NH$_3$ [3,5,11]. This inevitably leads to hot spots causing migration and agglomeration of the Pt metal and damage to the zeolite framework.

Sintering of metal particles on zeolite supports during catalyst activation has been shown previously to be prevented using a low-temperature plasma instead of heat [12-17]. Highly dispersed, very small nickel particles inside a FAU-type framework were prepared by reducing nickel cations with atomic hydrogen from a low-temperature hydrogen plasma [12,13] and highly dispersed cobalt particles were prepared decomposing cobalt carbonyl clusters inside FAU by an argon plasma [14,15,16,17]. Here we
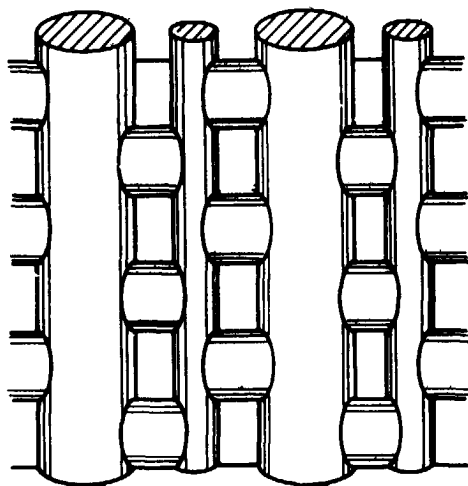

Fig.1:   *artist's impression of MOR structure looking at the main channels from aside.*

report on the de-ammination of Pt(NH$_3$)$_4$,NH$_4$-MOR by atomic oxygen generated in a low-temperature oxygen plasma. Such a low-temperature plasma calcination was shown previously to restrict damage to the zeolite framework to a minimum as long as the products of the ammonia oxidation could freely leave the crystallite [18]. The strongly oxidizing oxygen atoms [19,20] and low temperatures [18] are expected to prevent the destructive, platinum-catalyzed ammonia combustion [5] and to leave the zeolite more in tact than thermal calcination.

Experimental

Materials: The parent Pt(NH$_3$)$_4$,NH$_4$-MOR (0.4 weight-% Pt) was prepared by conventional competitive ion exchange [5]. According to inductively-coupled atomic emission spectroscopy (ICP-AES) it has a silicon-to-aluminium ratio of 10.9. The average crystal size, estimated by scanning electron microscopy (SEM) was less than 1

μm. It was thermally calcined by staged heating in air with a final stage for two hours at 850 K [5].

Plasma calcination: Typically 0.5 g $Pt(NH_3)_4$,NH_4-MOR was spread out evenly (layer less than 1 mm thick) across the surface of a Pyrex sample holder inside the reactor of a home-made barrel asher [18]. The reactor and its contents were heated to 350 K or 470 K for six hours in a He flow at 45 Pa. After cooling down to ambient temperature in an oxygen flow, the sample was exposed to an oxygen plasma at 10 W rf power, 50 Pa in an oxygen flow (1.3s mean residence time). The apparatus was switched off after 14 days in case of the sample previously heated to 350 K and after 21 days for the sample pre-heated to 470 K. The sample was cooled down to ambient temperature and slowly hydrated by exposing to air at 50 Pa for one day and then at 101 kPa inside the reactor. Finally the sample was fully hydrated in a desiccator over saturated ammonium nitrate solution. The temperature of a typical $Pt(NH_3)_4$,NH_4-MOR sample surface during exposure to oxygen plasma was determined with a calibrated microscopic infrared thermometer (Everest Interscience Inc., model 2400) through a temporarily installed CaF_2 window [21].

Characterization: Transmission FTIR spectra were recorded on a Bruker IFS66 using the KBr method. ^{27}Al MAS NMR spectra were recorded on a Varian VXR-400 S at 104.2 MHz with 1.0 μs pulses and 520 ms repetition time. 2000 Free induction decays were accumulated per spectrum. X-ray diffraction (XRD) data were collected on a Philips Compact X-ray Diffractometer System (Model PW 1840). Continuous flow n-hexane cracking rates at 673 K were determined and evaluated as described elsewhere [22]. The oxidation state of platinum after plasma and thermal calcination was determined by reduction with deuterium. After overnight drying at 473 K and reduction at 300 K, the sample was heated to 473 K and the evolved H_2O, D_2O and HDO was monitored by a Varian MAT 44 S Mass spectrometer in multiple ion detection mode. The UV/VIS reflectance spectra were recorded on a Perkin-Elmer 330 spectrometer.

Results and Discussion

IR radiation thermometry showed that the surface temperature of $Pt(NH_3)_4,NH_4$-MOR exposed to oxygen plasma (10 W, 50 Pa) was 370 ± 10 K. This compares well with the 350 K measured by a Pyrex-coated, shielded thermocouple at the centre of the oxygen flow [18]
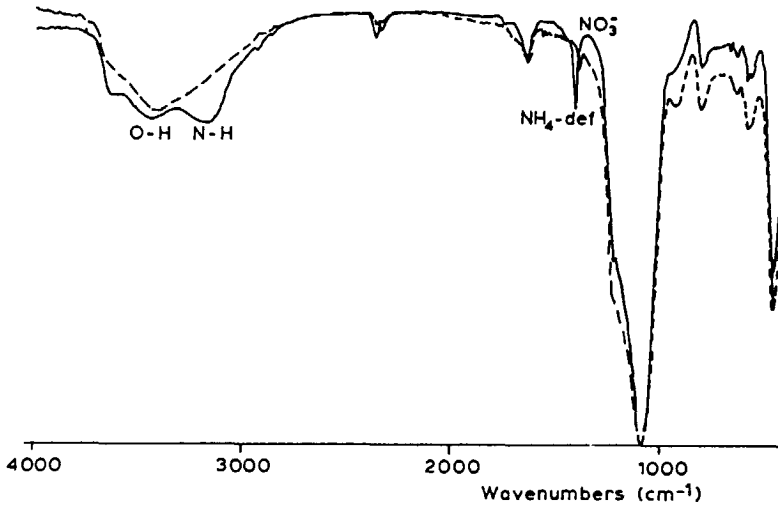

Fig.2: IR spectra of parent (——) and plasma calcined (---) $Pt(NH_3)_4,NH_4$-MOR.

IR spectroscopy was used to establish whether plasma calcination resulted in complete deammoniation. Fig.2 shows the spectrum of the parent $Pt(NH_3)_4,NH_4$-MOR and of a sample heated to 470 K and subsequently plasma calcined. Exposure to an oxygen plasma removes the ammonia absorption bands due to N-H stretching vibrations (3000-3500 cm^{-1}) and due to N-H bending (around 1400 cm^{-1}) [23]. In addition a small peak at 1385 cm^{-1} appears, attributed to nitrate [18]. Complete deammoniation of samples heated to 350 K prior to plasma treatment proved badly reproducible. IR spectra of these samples (not shown) often showed larger nitrate absorptions than those

heated to 470 K prior to plasma calcination. Since heating to 470 K removes water, but virtually no ammonia [24], the channels (0.65 to 0.70 nm in diameter) of $Pt(NH_3)_4$, NH_4-MOR samples dried at 470 K will be blocked by water molecules (0.30 nm in diameter [25]) to a lesser extent than those dried at 350 K. The hindered access of oxygen atoms to intracrystalline ammonium after drying at 350 K could explain the difficulty of successful and reliable plasma calcination. Moreover, the hindered desorption of ammonia oxidation products and the presence of water will enhance the formation of mineral acids [18].

The ^{27}Al MAS NMR spectra of parent $Pt(NH_3)_4,NH_4$-MOR (Fig.3a) shows one absorption at 53 ppm attributed to tetrahedral framework aluminium, Al^{IV}. Upon plasma (Fig.3b) and staged (Fig.3c) calcination an additional peak at 0 ppm appears,
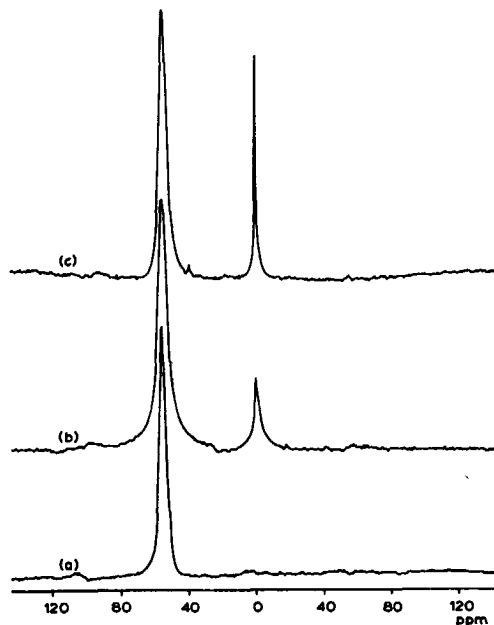

Fig.3: ^{27}Al MAS NMR spectra of $Pt(NH_3)_4,NH_4$-MOR acquired with 1.0 μs pulses and 520 ms repetition time. 2000 Free induction decays were accumulated per each spectrum. (a) Parent sample; (b) plasma calcined; (c) thermally calcined.

attributed to octahedral extra-framework aluminium, Al^{VI}. Spectral integration shows that in both the calcined samples the Al^{IV}/Al^{VI} ratio is 6.2. Since in fully hydrated, carefully calcined MOR all aluminium can be detected by NMR, ^{27}Al MAS NMR can be considered to provide quantitative information on the degree of dealumination [26], and the equal Al^{IV}/Al^{VI} ratio of plasma and thermally calcined $Pt(NH_3)_4$,NH_4-MOR indicates that both samples are dealuminated to the same degree. The strong resemblance of the frameworks of plasma and carefully thermally calcined samples was also observed on partially ammonium-exchanged FAU [18]. Provided that the dealumination is not due to reaction of framework aluminium with mineral acids during plasma calcination, it supports the view that dealumination occcurs by reaction with intracrystalline hydronium ions formed upon hydration [24,27]. By contrast, ^{27}Al MAS NMR on completely plasma deammoniated $Pt(NH_3)_4$,NH_4-MOR samples pre-dried to 350 K instead of 470 K (spectra not shown) results in Al^{IV}/Al^{VI} ratios which can be as low as 4. Thus plasma calcination of ammonium zeolites appears to require zeolites to be as
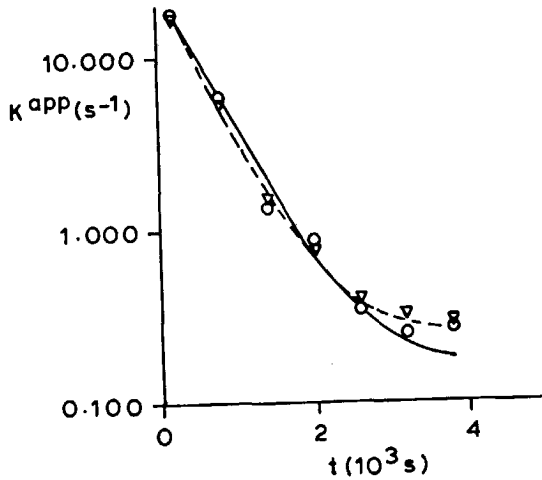

Fig.4: *n-Hexane cracking at 673 K over shallow bed (o) and plasma calcined (▽)
Pt(NH₃)₄ ,NH₄-MOR samples: Activity, k^{app} (s⁻¹) , relative to initial activity, k_0^{app}
(s⁻¹), as function of time on stream t (10³ s)*

dry as possible in order to impede the formation of destructive mineral acids and concomitantly, to minimize the degree of dealumination.

XRD establishes that both plasma calcination and staged thermal calcination leave the crystallinity of the mordenite samples unaffected.

Comparison of the activity in n-hexane cracking at 673 K shows that thermally and plasma calcined Pt(NH$_3$)$_4$,NH$_4$-MOR show a similar initial acivity, rate of decline and final activity (Fig.4). Thus in accordance with the ^{27}Al MAS nutation NMR data both calcined samples are equally acidic. Since ammonium cations very efficiently poison the catalytically active acid sites [28], the equal catalytic activity of these samples also confirms the complete removal of ammonium by plasma calcination indicated by IR spectroscopy (see above).

Information on the platinum phases was obtained from UV/VIS diffuse reflectance spectroscopy. The spectrum of the white parent Pt(NH$_3$)$_4$,NH$_4$-MOR (Fig.5) show the characteristic absorptions of Pt(NH$_3$)$_4^{2+}$ [29]. Upon plasma calcination the sample looks slightly yellow and the UV/VIS absorption above 250 nm has strongly increased
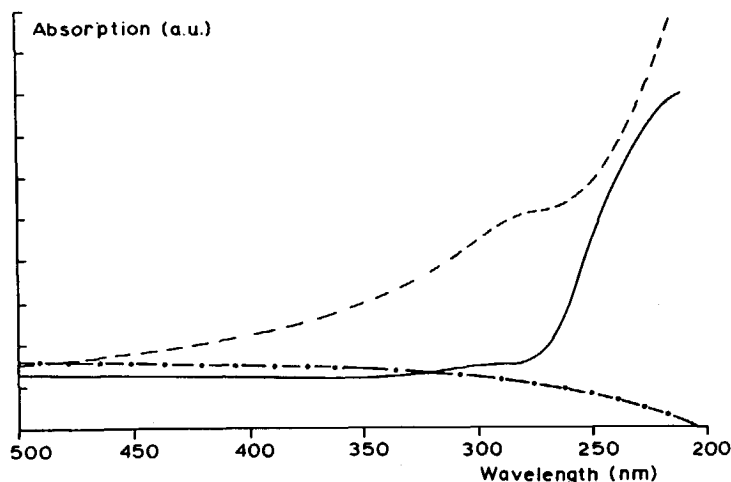

Fig.5: UV/VIS diffuse reflectance spectra of Pt(NH$_3$)$_4$,NH$_4$-MOR; (——) parent; (---) plasma calcined sample; (-.-.-) thermally calcined.

(Fig.5). Since according to IR spectroscopy (and the n-hexane cracking activity) the strongly oxidizing oxygen atoms have removed all ammonia, the increased absorption is attributed to an oxidic platinum phase. Upon thermal calcination the mordenite sample looks greyish and UV/VIS spectroscopy detects no characteristic absorption pattern any more (Fig.5). Since treatment of this sample in D_2 generates substantial amounts of D_2O, the platinum phase upon our thermal calcination is (at least partly) an oxidic state as well. Apparently, the platinum phases obtained upon either calcination are in a different oxidation or hydration state.

Conclusions

Low temperature plasma calcination completely deammoniates $Pt(NH_3)_4,NH_4$-MOR at 370 ± 10 K, whereas thermal deammoniation requires temperatures above 600 K. Provided that the zeolite is thoroughly dried prior to plasma calcination, plasma and thermal calcination result in the same degree of dealumination leaving the crystallinity unaffected. Low temperature plasma calcined $Pt(NH_3)_4,NH_4$-MOR is an equally active and equally stable catalyst for n-hexane cracking as carefully thermally calcined $Pt(NH_3)_4,NH_4$-MOR. Low temperature plasma calcination of $Pt(NH_3)_4NH_4MOR$ yields another platinum phase than thermal calcination. Despite the probable absence of autoreduction of $Pt(NH_3)_4^{++}$ during plasma calcination the MOR framework is damaged to similar degree as upon thermal calcination.

References

1. Weitkamp, J. *Erdöl Kohle Erdgas Petrochem.* **1978**, *31,* 13-22.
2. Maxwell, I.E. *Catal.Today* **1987**, *1,* 385-413.
3. Kouwenhoven, H.W. *ACS Symp.Ser.* **1973**, *121,* 528-539.
4. Gallezot, P. *Catal.Rev.Sci.Eng.* **1979**, *20,* 121-154.
5. Kouwenhoven, H.W.; Van Helden, H.J.A. *Ger.Offen.* 1968.
6. Ribeiro, F.; Marcilly, Ch.; Thomas, G. *C.R. Hebd.Seances Acad.Sci.Ser.C* **1978**, *278,* 431-434.
7. Ribeiro, F.R. *NATO ASI Ser.,Ser.E* **1984**, *80,* 545-569.
8. Reagan, W.J.; Chester, A.W.; Kerr, G.T. *J.Catal.* **1981**, *69,* 89-100.
9. Guerin, M.; Kappenstein, C.; Alvarez, F.; Giannetto, G.; Guisnet, M. *Appl.Catal.* **1988**, *45,* 325-333.
10. Meier, W.M., Olson, D.H. *Atlas of Zeolite Structure Types* (Structure Commission of the International Zeolite Association); Butterworths: London, 2nd, 1987, pp.62-63.
11. Exner, D.; Haeger, N.; Möller, K.; Schulz-Ekloff, G. *J.Chem.Soc.,Faraday Trans.I* **1982,** 78, 3537-3544.
12. Olivier, D.; Richard, M.; Bonneviot, L.; Che, M. *Stud.Surf.Sci.Catal.* **1980**, *4,* 193-199.
13. Che, M.; Richard, M.; Olivier, D. *J.Chem.Soc.,Faraday Trans.I* **1980**, *76,* 1526-15-34.
14. Zerger, R.P.; McMahon, K.C.; Seltzer, M.D.; Michel, .G.; Suib, S.L. *J.Catal.* **1986,** *99,* 498-505.
15. McMahon, K.C.; Suib, S.L.; Johnson, B.G.; Bartholomew Jr., C.H. *J.Catal* **1987,** *106,* 47-53.
16. Zangh, Z.; Suib, S.L.; Zhang, Y.D.; Hines, W.A.; Budnick,J.I. *J.Am.Chem.Soc.* **1988,** *110,* 5569-5571.
17. Nam, S.S.; Iton, L.E.; Suib, S.L.; Zhang, Z. *Chem.Mat.* **1989,** *1,* 529-534.

18.   Maesen, Th.L.M.; Sulikowski, B.; Van Bekkum, H.; Kouwenhoven, H.W.; Klinowski, J. *Appl.Catal.* **1989,** *48,* 373-383.

19.   Cook, J.M.; Benson, B.W. *J.Electrochem.Soc.* **1983,** *130,* 2459-2464.

20.   Selwyn, G. *J.Appl.Phys.* **1986,** *60,* 2771-2774.

21.   Maesen, Th.L.M.; Kouwenhoven, H.W.; Van Bekkum, H.; Sulikowski, B.; Klinowski, J. submitted to *J.Chem.Soc., Faraday Trans.*

22.   Voogd, P.; Van Bekkum, H. *Appl.Catal.* **1990,** *59,* 311-331

23.   Uytterhoeven, J.B.; Christner, L.G.; Hall, W.K. *J.Phys.Chem.* **1965,** *69,* 2117-21-26.

24.   Kühl, G.H. *ACS Symp.Ser.* **1977,** *40,* 96-107.

25.   Bondi, A. *J.Phys.Chem.* **1964,** *68,* 441-451.

26.   Freude, d.; Brunner, E.; Pfeifer, H.; Prager, D.; Jerschkewitz, H.-G.; Lohse, U.; Oehlmann, G. *Chem.Phys.Lett.* **1987,** *139,* 325-330.

27.   Barrer, R.M.; Klinowski, J. *J.Chem.Soc., Faraday Trans. I* **1975,** *71,* 690-698.

28.   Lombardo, E.A.; Sill, G.A.; Hall, K.W. *J.Catal.* **1989,** *119,* 426-440.

29.   Mason, W.R. *Inorg.Chem.* **1986,** *25,* 2925-2929.

30.   Tzou, M.S; Teo, B.K.; Sachtler W.M.H. *J.Catal.* **1988,** *113,* 220-235.

CHAPTER 7

LOW-TEMPERATURE PLASMA CALCINATION FOR TEMPLATE REMOVAL FROM MOLECULAR SIEVES [*]

Abstract

The oxidative removal of templates from the crystals of MFI- and TON-type zeolites using a low-temperature oxygen plasma at 370 K has been investigated. This treatment removes tetrapropylammonium inside 5 μm lengths of channels in the completely siliceous MFI structure (silicalite) and diethylamine to a depth of at least 70 μm in the channels of the completely siliceous TON structure. Substitution of B, Al or Fe into the framework of silicalite significantly obstructs the removal of tetrapropylammonium, but complete decomposition of the template can be accomplished in small samples of [Si,B]-MFI. A comparison of plasma calcination and thermal calcination in air indicates that the release of boron into extra-framework positions upon either treatment is caused by the slow desorption of water at the calcination temperature.

Introduction

It has been suggested that, in order to avoid thermal degradation of heterogeneous zeolitic catalysts during activation at ca. 800 K, the calcination temperature should be reduced, and a more strongly oxidizing atmosphere than air be used, such as ozone in an oxygen flow [1]. Although ozone is able to remove aromatic and olefinic hydrocarbons from zeolites at 420-450 K [2], saturated compounds, particularly aliphatic hydrocarbons, are resistant to ozone [3]. Since template molecules in as-synthesized

---

zeolites are usually aliphatic [4], reduction of the calcination temperature requires the use of a stronger oxidizing species. Atomic oxygen at 390-420 K, known to attack not only adsorbed aliphatics [5,6] but also inert organic materials such as Teflon [7,8], appears suitable for the purpose. It was once believed that atomic oxygen is able to remove only those hydrocarbons which are directly exposed to an oxygen plasma, i.e. which are adsorbed at the surface of zeolite crystallites [9]. However, oxygen atoms generated in an air plasma [10] have since been reported to remove quaternary ammonium compounds occluded in purely siliceous MFI sieve (see Figure 1) and in a MAZ zeolite (structure described in ref. 11) without causing damage to the framework [12].

We report low-temperature plasma removal of tetrapropylammonium cations occluded as templates inside completely siliceous and boron-substituted MFI frame-works (which will be referred to as silicalite and [Si,B]-ZSM-5, respectively) and of
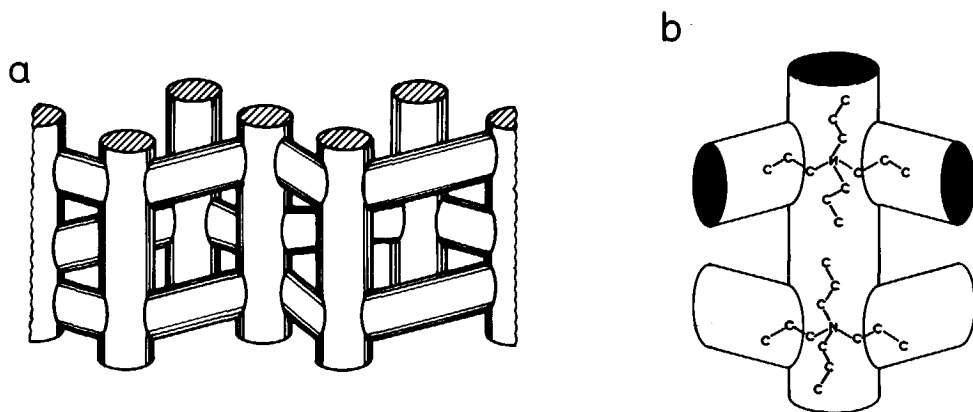

Fig.1:   a)   *Artist's impression of the 0.56*0.53 nm straight and the 0.51*0.55 nm sinusoidal MFI-type channel system*

   b)   *Schematic representation of tetrapropylammonium cations as occluded in MFI-type framework.*

diethylamine occluded inside the completely siliceous TON framework (stucture descri-bed in ref. 11). Although sometimes known as Theta-1 and ZSM-22 [11], the latter will be referred to as Nu-10. Oxygen plasma instead of air plasma was used in order to impede the formation of corrosive mineral acids [13].

Low-temperature oxygen plasma is a quasi-neutral fluid consisting of molecular and atomic oxygen at near room temperature [14], as well as slightly warmer oxygen ions and free electrons with kinetic energies equivalent to temperatures as high as 10^{14} K [15]. A zeolite sample brought into contact with such a plasma acquires a negative electric charge until the comparatively large flux of hot, light electrons is sufficiently reduced by electrostatic repulsion to offset the much smaller flux of massive, relatively cool, positive ions. Conversely, the plasma is positively charged with respect to the sample surface. Because of the high mobility and diffusivity of the electrons, the potential of the plasma potential is essentially uniform. The transition from plasma potential to the potential of the sample surface occurs in the dark narrow region between glow and sample, known as the sheath [15]. The surface temperature of the sample surface is determined by the number of positive oxygen ions which diffuse to the sheath-plasma interface and by the kinetic energy they attain when accelerated into the negatively charged sample [16]. This energy is determined by the voltage across the sheath and modified by the number of collisions (related to the gas pressure) which the ions undergo in traversing the sheath and by the applied radio frequency [17]. In addition, the sample is heated by the surface-mediated [18,19] recombination of oxygen atoms [15]. Consequently, the crystals at the sample-sheath interface are the hottest part of the sample. Their surface temperature can be determined using a microscopic infrared thermometer [20], which probably provides a better estimate of the tempera-ture of the bulk sample than could be obtained with earlier methods [12,13].

Experimental

Materials: Platelet-like silicalite crystals containing tetrapropylammonium (TPA) and [Si,B]-ZSM-5 crystals were synthesized under non-alkaline conditions using F⁻ instead of

OH[21,22]. The average thickness of the silicalite crystals estimated by scanning electron microscopy (SEM, Jeol JXA 50A Electron Microanalyzer) was 5 μm. [Si,B]-ZSM-5 crystals were estimated to be 35 μm thick, but were crushed to 5 μm size. A few prismatic single crystals of [Si,B]-ZSM-5 with 3 B per unit cell as determined by XRD and IR [23] and estimated by optical microscopy to be about 10 μm thick were selected form a batch synthesized starting from the gel composition 9.0SiO_2·7.3Na_2O·7.6 $(TPA)_2O$·7.8B_2O_3·4000.H_2O. Synthesis was carried out at 453 K for 5 days without stirring in a 25 ml Teflon lined autoclave [24]. Purely siliceous zeolite Nu-10 containing diethylamine (DEA) was prepared at 440 K for 86 days without stirring starting from the composition 20SiO_2.100DEA·1000·H_2O using a 250 ml Teflon lined autoclave [25]. Prior to further treatment the Nu-10 crystals were washed three times with water while stirring under reflux for three hours. The average length of the washed lath-shaped crystals, estimated by SEM, was 400 μm. XRD was used to identify the products and to check for crystalline impurities.

Plasma calcination: A home-made barrel asher was used for the calcination experiments, as previously described [13]. The sample was distributed evenly across the surface of a Pyrex sample holder in a very thin (less than 1 mm) layer. Because of the deleterious effect of water on the reactivity of an oxygen plasma [26] and the possibly beneficial effect of helium [27], the reactor of the barrel asher and its contents were dried in a helium flow for various times and at various temperatures (see Table I). The sample was subsequently exposed to an oxygen plasma at 10 W rf power, 50 Pa in an oxygen flow (1.3 s mean residence time) for various periods as indicated in Table I. After treatment the sample was allowed to cool down to ambient temperature. It was then slowly hydrated by exposure to air for 1 day at 50 Pa and then at 101 kPa, inside the reactor. To measure the temperature of a typical sample surface exposed to an oxygen plasma in situ, the reactor was equipped with a CaF_2 window, through which the infrared radiation in the range of 5 to 20 μm wavelength was measured with a microscopic infrared thermometer (Everest Interscience Inc., model 2400). Calibration established that, around 370 K, an emissivity of 0.50 provided a good correction for the

IR absorption of the CaF_2 window and radiation losses due to scattering.

Characterization: The products were analyzed for boron and silicon by ICP-AES after dissolving 10 mg sample in 3 ml 40% HF, cooling in liquid nitrogen and adding 30 ml water. Transmission FTIR spectra were obtained on a Bruker IFS66 using its instrument microscope or the KBr method. Nitrogen adsorption was measured at 77 K on 0.25 g sample after overnight degassing at 820 K using Digisorb 2600 (Micromeritics). Relative pressures were converted [28] into t-values as follows:

$$t = [13.99/(\log(p^0/p) + 0.034)]^{0.5} \qquad (1)$$

A home-built apparatus was used for thermographic analyses. Samples were heated at a rate of 0.2 K s^{-1} in an air flow. The carbon, hydrogen and nitrogen contents were determined after drying overnight at 380 K, 13 Pa by a Heraeus CHN-O-Rapid Elemental Analyzer (Model PEW-F1.1) using Pregl's and Dumas' procedures, respectively. The analysis is based on a quantitative explosion-like combustion of organic material in a stream of pure oxygen at temperatures near 2000 K with $Li_2B_4O_7$ added as a melting agent. The oxidation products are converted into carbon dioxide, water and nitrogen and after separation these three gases are quantified using a thermal conductivity detector [29].

Results and Discussion

The surface temperature of a typical zeolite sample exposed to an oxygen plasma (10 W, 50 Pa, see ref. 13 for further details) as recorded by the IR radiation thermometer was 370 ± 10 K. The reading did not change significantly when the plasma was extinguished, indicating no interference by radiation not emitted by the sample. The recorded temperature of 370 ± 10 K compares well with the 350 K measured by a Pyrex coated, shielded thermocouple at the center of the oxygen flow [13].

The spectra of the parent and the low-temperature plasma calcined silicalite are shown in Fig.2. Calcination removes all the TPA absorption bands due to C-H stretching vibrations (at 3000-2900 cm^{-1}) and all the bands attributed to C-H bending vibrations (1473, 1458, and 1385 cm^{-1})[30]. Thus the TPA$^+$ cations appear to be completely destroyed by the plasma treatment. Indeed, TGA detects no further weight
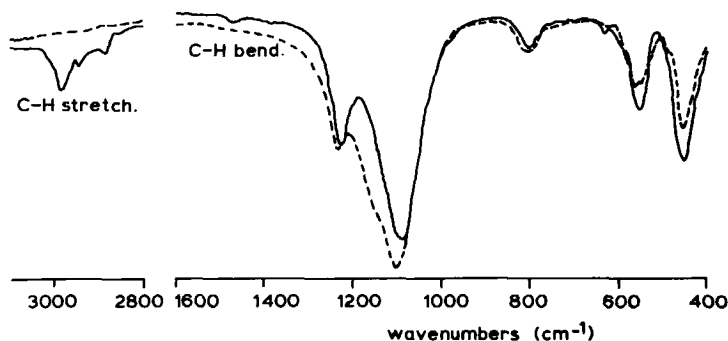

Fig.2: IR spectra of as-synthesized (——) and plasma calcined (---) completely siliceous MFI

loss above 405 K. The fine structure of the bands in the Si-OH and Si-F vibration region observed upon calcination with an air plasma [12] was not found with an oxygen plasma. It follows that complete template removal at 370 K is possible with both air and oxygen plasma, and in the latter case yields a silicalite which is very similar to that obtained by conventional thermal template decomposition above 800 K [31]. Since the dominant diffusion path in a MFI framework is through the straight channels [32], this implies that adsorbed oxygen atoms generated in the plasma are able to penetrate at least 2.5 μm (i.e. half the estimated thickness of the crystal) into the two-dimensional channel system of silicalite crystals (see Figure 1) without losing their strongly oxidizing power.

Purely siliceous zeolite Nu-10 was used to investigate how far reactive oxygen species can penetrate into the channels of silicalite (0.51 to 0.56 nm in diameter [11]). The size

of the channels in this zeolite (0.44 to 0.55 nm in diameter [11]) is comparable to that of silicalite, but here the channels run only in one direction: along the length of the lath-shaped crystals [33]. As a result, heating above 1000 K to remove the DEA template from the ±400 μm long crystals invariably leads to coke formation and the blackening of the crystals [25]. Nevertheless, we were able to remove the carbon completely by heating the carbonized crystals for 8 days at 1070 K in a flow of pure oxygen and obtain a completely white product. The micropore volume 0.09 cm^3 g^{-1} (by nitrogen adsorption), in agreement with the volume measured in small, easily calcined Nu-10 crystals [34] and indicating that all channels were freely accessible to nitrogen. Elemental analysis (see Table I) confirms that upon our thermal calcination carbon corresponding to 0.45 DEA molecules per unit cell. This compares well with the 0.5 DEA molecules reported on washed and more readily calcined completely siliceous TON crystals [25]. The IR spectrum of completely siliceous Nu-10 remains virtually unchanged upon plasma calcination (Figure 3), indicating that crystallinity has been preserved and that the template has not been completely removed (the carbon content
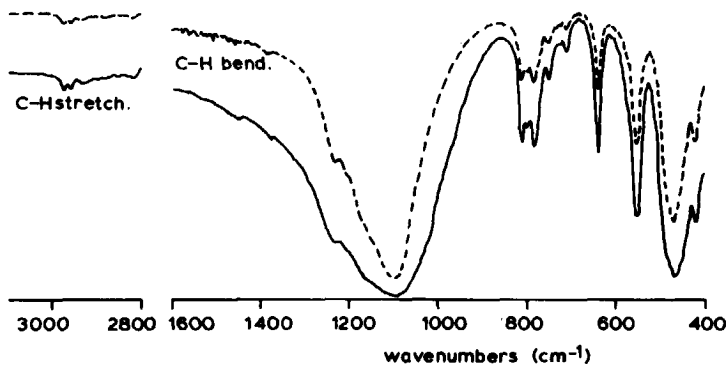

Fig.3: IR spectra of as-synthesized (——) and plasma calcined (---) completely siliceous TON

decreased by only 35%). At the same time, the carbon-to-nitrogen ratio has decreased from 3.9 to 3.2 indicating that occluded DEA has been affected by the treatment.

Assuming a statistical distribution of DEA along the ±400 μm long channels, this implies that oxygen atoms have penetrated ±70 μm into the crystals. DEA is not expected to be distributed statistically, but because of washing there will be more DEA deep inside the crystals than near the surface [25]. The reactive oxygen species are likely to have penetrated even further into the channels without recombining to form O_2.

Since completely siliceous MFI or TON molecular sieves are known to be chemical inert, they are the not suitable for the study of the difference between oxidative plasma removal of a template at 370 K and thermal decomposition at 870 K. [Si,B]-ZSM-5 appears more appropriate, since boron is invariably released from the MFI-type framework as a result of thermal calcination at ca. 870 K [35]. However, when ca. 0.5 g of crushed [Si,B]-ZSM-5 crystals were plasma calcined, carbon analysis (Table I) showed that after 14 days only 46% and after 28 days only 47% of the occluded tetrapropyl-ammonium cations had been removed. Moreover, after the latter sample has been thoroughly washed, ICP-AES indicated that the amount of framework boron has been reduced from 3.4 to 2.7 B atoms per unit cell, although XRD detected no loss of

Table I: Template removal from zeolites by plasma calcination: pretreatment conditions and weight percentage carbon removed.

sample	batch size (g)	T(K) drying	calc. time (days)	penetration depth (μm)	weight-%C before	after
silicalite	0.20	298	7	3	8.6[a]	<0.1[a]
Nu-10	0.50	417	15	>70	1.42	0.92
[Si,B]-ZSM-5[b]	0.43	393	14	3	8.61	4.66
	0.50	390	28	3	8.61	4.58
[Si,B]-ZSM-5[c]	<0.01	385	21	5	n.d.	n.d.

[a] according to thermogravimetric analysis.

[b] Synthesized under non-alkaline conditions using F⁻ instead of OH⁻ [22] and crushed.

[c] Synthesized under alkaline conditions (cf. ref. 24).

crystallinity. Thus complete template removal from [Si,B]-ZSM-5 appears much more difficult than from its completely siliceous structural analogue. Incomplete template removal was also encountered upon plasma treating 0.5 g batches of [Fe]-ZSM-5, [Al]-ZSM-5 and MgAPSO-36 (see ref. 36 for the details on the latter). On the other hand, much fewer experiments were performed to optimize the plasma conditions with these materials.

The main difference between the completely siliceous MFI-type framework and B-, Al- and Fe-substituted MFI is that the completely siliceous framework contains virtually no structural defects [37] making it extremely hydrophobic, while the framework containing isomorphously substituted three-valent elements requires charge-compensating extra-framework cations which render the zeolite hydrophilic [38]. Therefore, water produced at 370 K during oxidation of TPA cations will linger for a longer period of time inside [Si,B]-, [Si,Al]- or [Si,Fe]-ZSM-5 and MgAPSO-36 than inside silicalite. Since the molecules of both water and oxygen are nearly 0.3 nm in diameter [39], water associated with extra-framework cations inside the 0.51 to 0.56 nm channels [11] will block the channel system, hindering the access of the oxygen atoms to the occluded template molecules. Since oxygen atoms are known to oxidize virtually any organic substance near room temperature [6], the slowness of the release of water from [Si,Al]-ZSM-5 at room temperature and the resulting channel blockage might also explain the limited coke removal by oxygen plasma observed by Bibby et al. [9].

Since oxygen atoms start oxidizing occluded TPA near the outer crystal surface, combustion will be most fierce when the plasma has just been ignited and when all channels are still completely filled with template (cf. ref. 9). This is when most water will be evolved. When ventilation is insufficient, water will be re-adsorbed by the zeolite and will inhibit further oxidation (see above) [26].

To minimize this initial rise in water vapour pressure and to maximize the number of oxygen atoms available per crystal, the plasma treated batch was limited to a few ca. 10 μm thick prismatic single [Si,B]-ZSM-5 crystals containing 3 B atoms per unit cell, prepared without F$^-$. Since this batch was too small for carbon analysis, TPA removal was only investigated by transmission IR spectroscopy using a microscope. The spectra

of parent and a low-temperature plasma calcined [Si,B]-ZSM-5 single crystal are shown in Figure 4. Exposure to an oxygen plasma for 21 days at 370 K appears to have removed the bands due to C-H stretching vibrations (in the 3000-2900 cm^{-1} region) as well as the C-H bending vibrations (at 1474, 1458, and 1385 cm^{-1})[30] indicating
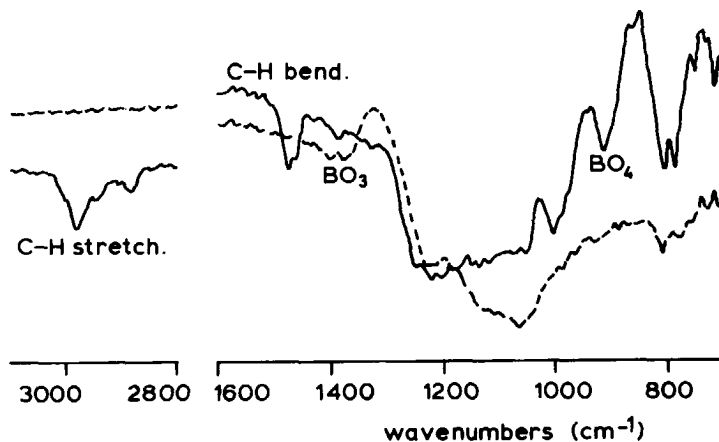

Fig.4: IR spectra of as-synthesized (——) and plasma calcined (---) completely siliceous [Si,B]-ZSM-5

complete TPA removal. Unfortunately, the disappearance of the absorption at 905 cm^{-1} attributed to tetrahedral framework boron [23] and the appearance of bands at 1396 and 1373 cm^{-1} from trigonal boron [40], indicate that most boron has been released from the framework. Since very careful, dry thermal calcination in air results in a similar loss of boron from the framework of this material [41], plasma and thermalcalcination appear to yield a similar template-free [Si,B]-ZSM-5. This implies that the release of framework boron is not necessarily the result of thermal treatment. As extra-framework boron species are likely to block the channels and inhibit oxidation of the template, extended boron release during plasma treatment hinders the complete removal of the template. The hydrolysis of framework boron upon contact with water vapour when the sample is exposed to laboratory air after the plasma treatment, is a more plausible explanation. Hydrolysis can also explain the loss of framework boron

observed in hydrated, carefully calcined [Si,B]-ZSM-5 [35,41]. We conclude that, while [Si,B]-ZSM-5 might be thermally stable, it is not resistant to hydration.

Conclusions

Exposure to a low-temperature oxygen plasma allows complete removal of the tetrapropylammonium template occluded in MFI-type frameworks. IR surface thermometry indicates that sample temperature during plasma calcination does not exceed 370 K. The strongly oxidizing species originating in the low-temperature oxygen plasma can penetrate at least 70 μm into the ± 0.5 nm wide MFI-like channels of a purely siliceous TON framework. Upon B-, Al- or Fe-substitution into MFI-type frameworks, complete template removal is seriously impeded, possibly due to slow desorption of water at 370 K. Nevertheless, plasmacalcination of very small amounts of boron-substituted MFI proves able to remove all occluded template. As upon plasma calcination and thermal calcination a comparably high amount of boron is released from the framework, it is tempting to conclude that boron remains substituted into the MFI-type framework during calcination, but is released upon hydration.

Acknowledgements

References

1. Copperthwaite, R.G.; Hutchings, G.J.; Johnston, P.; Orchard, S.W. *J.Chem. Soc.,Chem. Commun.* **1985,** 644-645.

2. Hutchings, T.G.; Copperthwaite, R.G.; Themistocleus, T.; Foulds, G.A.; Bielovitch, A.S.; Loots, B.J.; Nowitz, G.; Van Eck, P. *Appl.Catal.* **1987,** *34,* 153-161.

3. Hutchings, G.J.; Comninos, H.; Copperthwaite, R.G.; Jansen van Rensburg, L.; Hunter, R.; Themistocleous, Th. *J.Chem.Soc.,Faraday Trans. I* **1989,** *85,* 633-644.

4. Moretti, E.; Contessa, S.; Padovan, M. *Chim.Ind.(Milan)* **1985,** *67,* 21-34.

5. Zadok, E.; Aronovitch, Ch.; Mazur, Y. *Nouv.J.Chim.* **1982,** *6,* 695-698.

6. Taylor, G.N.; Wolf, T.M. *Polym.Eng.Sci.* **1980,** *20,* 1087-1092.

7. Gjerde, H.B.; Chun, T.R.; Low, S.J. in *"Eighteenth International SAMPE Technical Conference",* Vol.18: *"Materials for Space -The Gathering Momentum"*, Hoggattt, J.T.; Hill, S.G. (editors), Seattle, Washington, October 7-9 1986, pp. 262-271.

8. Morra, M.; Occhiello, E.; Garabassi, F. *Langmuir* **1989,** *5,* 872-876.

9. Bibby, D.M.; Milestone, N.B.; Patterson, J.E.; Aldridge, L.P. *J.Catal.* **1986,** *97,* 493-502.

10. Venugopalan, M.; Rajaei-Rizi, A. *Z.Phys.Chem.(Wiesbaden)* **1981,** *126,* 15-24.

11. Meier, W.M., Olson, D.H. *Atlas of Zeolite structure types (Structure Commission of the International Zeolite Association);* Butterworths: London, 2nd, 1987.

12. Maesen, Th.L.M.; Bruinsma, D.S.L.; Kouwenhoven, H.W.; Van Bekkum, H. *J.Chem.Soc.,Chem.Commun.* 1987, 1284-1285.

13. Maesen, Th.L.M.; Sulikowski, B.; Van Bekkum H.; Kouwenhoven, H.W.; Klinowski, J. *Appl.Catal.* **1989,** *48,* 373-383.

14. DiMauro, L.F.; Gottscho, R.A.; Miller, T.A. *J.Appl.Phys.* **1984,** *56,* 2007-2011.

15. Graves, D.B. *AIChE J.* **1989,** *35,* 1-29.

16. Visser, R.J. *J.Vac.Sci.Technol.A* **1989,** *7,* 189-194.

17. Thompson, B.E.; Sawin, H.H.; Fisher, D.A. *J.Appl.Phys.* **1988,** *63,* 2241-2251.

18. Greaves, J.C.; Linnett, J.W. *Trans.Farad.Soc.* **1959,** *55,* 1346-1354.

19. Winters, H.F. *Top.Curr.Chem.* **1980,** *94,* 69-125.

20. Ulrikson, M. *J.Vac.Sci.Technol.A* **1986,** *4,* 1805-1809.

21. Guth, J.L.; Kessler, H.; Wey, R. *Stud.Surf.Sci.Catal.* **1986,** *28,* 121-128.

22. Sulikowski, B.; Klinowski, J. *ACS Symp.Ser.* **1989,** *398,* 393-404.

23. Jansen, J.C.; De Ruiter, R.; Biron, E.; Van Bekkum, H. *Stud.Surf.Sci.Catal.* **1989,** *49,* 679-688.

24. Lermer, H.; Draeger, M.; Steffen, J.; Unger, K.K. *Zeolites* **1983,** *5,* 131-134.

25. Franklin, K.R.; Lowe, B.M. *Zeolites* **1988,** *8,* 508-516.

26. Battey, J.F. *J.Electrochem.Soc.* **1977,** *124,* 147-152

27. Suhr, H.; Schmid, H.; Pfeundschuh, H.; Iacocca, D. *Plasma Chem.Plasma Process.* **1984,** *4,* 285-295.

28. De Boer, J.H.; Lippens, B.C.; Linsen, B.G.; Broekhoff, J.C.P.; Van den   Heuvel, A.; Osinga, Th.J. *J.Colloid Interface Sci.* **1966,** *21,* 405-414.

29. Ma, T.S.; Rittner, R.C. *Modern Organic Elemental Analysis;* Marcel Dekker: New York, 1979, pp.35-69.

30. Silverstein, R.M.; Bassler, G.C.; Morril, T.C. *Spectroscopic Identification of Organic Compounds;* Wiley: New York, 1981, pp.106-107.

31. Soulard, M.; Bilger, S.; Kessler, H.; Guth, J.L. *Zeolites* **1987,** *7,* 463-470.

32. Haag, W.O.; Lago, R.M.; Weisz, P.B. *Faraday Discuss.Chem.Soc.* **1981,** *72,* 317-330.

33. White, D.; Ramdas, S.; Millward, G.R. *Inst.Phys.Conf.Ser.* **1985** (Pub.1986), 79, 501-504.

34. Barri, S.A.I.; Smith, G.W.; White, D.; Young, D. *Nature(London)* **1984,** 312, 533-534

35. Brunner, E.; Freude, D.; Hunger M.; Pfeifer, H; Reschetilowski, W.; Unger B. *Chem.Phys.Lett.* **1988,** *148,* 226-230.

36. Flanigen, E.M.; Lok, B.M.; Lyle Patton, R.; Wilson, S.T. *Stud.Surf.Sci.Catal.* **1986,** *28,* 103-112; Flanigen, E.M.; Lyle Patton, R.; Wilson, S.T. *Stud.Surf.Sci.Catal.* **1987,** *37,* 13-27.

37. Chezeau, J.M.; Delmott, L.; Guth, J.-L.; Soulard, M. *Zeolites* **1989,** *9,* 78-80.

38. Flanigen, E.M.; Bennet, J.M.; Grose, R.W.; Cohen, J.P.; Patton, R.L.; Kirchner, R.M.; Smith, J.V. *Nature(London)* **1978,** *271,* 512-516.

39. Huheey, J.E. *Inorganic Chemistry: Principles of Structure and Reactivity;* Harper: New York, 1983, pp.256-275.

40. Datka, J.; Piwowarska, Z. *J.Chem.Soc.,Faraday Trans.I* **1989,** *85,* 47-53.

41. De Ruiter, R.: personal communication.

SUMMARY

This thesis describes the exploration of new methods to activate molecular sieve catalysts. The (hydrothermal) removal of sodium from a FAU-type zeolite, an outstanding fluid cracking catalyst is studied **(Chapters 2-4)**. Subsequently, scope and limitations of a low temperature oxygen plasma treatment for removing combustibles from some molecular sieves are investigated **(Chapters 5-7)**.

In **Chapter 1** some molecular sieves and their industrial applications are introduced. Attention is focussed on conventional activation of sodium-neutralized as-synthesized FAU-type zeolites by ammonium exchange and subsequent thermal decomposition of the ammonium cation. In addition, activation of MOR- and MFI-type molecular sieves by heat treatment, so called (thermal) calcination, is discussed. Finally, plasma technology is cursorily introduced and its application for calcining molecular sieves at low temperatures is suggested.

    Chapter 2 shows that a ^{23}Na nutation NMR is suited to obtain information on the location and cation-framework interaction energy of sodium upon ammonium and cesium exchange, shallow bed calcination and during hydrothermal heating of a (FAU-type) Na-Y zeolite. Upon ammonium and cesium exchange as well as during hydrothermal heating a cation redistribution is suggested to result in the depletion of the hexagonal prisms. The ammonium exchange mechanism is shown to consist of three distinct step, involving the initial interchange with sodium inside the supercages, subsequent substitution of sodium originating from the hexagonal prisms by ammonium remaining inside the supercages, and a final substitution of the cations inside the sodalite cages. Also upon shallow bed calcination of a partially ammonium exchanged Na-Y zeolite ^{23}Na MAS nutation NMR detects a sodium cation redistribution.

    In **Chapter 3** the ammonium exchange rate of Na-Y is shown to be drastically increased by raising the temperature to 433 K under hydrothermal conditions. Attaining fast complete ammonium exchange in a single steps at 433 K needs high ammonium-

to-sodium ratios, possibly because the FAU framework needs to expand in order to accommodate two ammonium cations per sodalite cage.

Chapter 4 offers a multitechnique characterization of deep bed calcined completely ammonium exchanged Na-Y. The novel Y zeolite thus obtained is compared with more conventionally prepared Y zeolite catalysts. This preliminary investigation indicates that calcination of completely ammonium exchanged Y zeolite with the aim of obtaining a catalyst with high Brønstedt acidity and concomitantly high cracking activity is not straight-forward.

In **Chapter 5** it is shown that a low temperature oxygen plasma can be used to completely oxidatively remove ammonium cations from partially ammonium-exchanged Y zeolites. Such a low temperature plasma calcination is shown to be comparably mild to careful shallow bed calcination as long as oxidation products can easily leave the crystallite.

Similarly, low temperature plasma calcination proves suited to completely deammoniate a thoroughly dried completely ammonium exchanged MOR-type zeolite which has been competitively ion exchanged with a platinum(II) tetraamine complex **(Chapter 6)**. The MOR frameworks obtained upon plasma and upon very carefully thermal calcination appear not significantly different. However, low temperature plasma calcination appears to reuslt in a different platinum phase than thermal calcination.

Finally **(Chapter 7)**, it is shown that at 370 K an oxygen plasma removes not only ammonia from FAU and MOR structures, but also tetrapropylammonium inside 5 μm lengths of channels in the completely siliceous MFI structure, and diethylamine to a depth of at least 70 μm in the channels of the completely siliceous TON structure. Substitution of B, Al or Fe into the siliceous MFI framework significantly obstructs the removal of tetrapropylammonium, but complete decomposition of the template can be accomplished in small samples of the boron-substituted framework. A comparison of plasma calcination with thermal calcination in air indicates that the release of boron into extra-framework positions upon either treatment is caused by the slow desorption of water at the calcination temperature.

SAMENVATTING

Dit proefschrift beschrijft een verkenning van nieuwe technieken om moleculaire zeven te activeren. De (hydrothermale) natriumverwijdering van een zeoliet van het FAU-type, een uitstekende katalysator voor kraken m.b.v. een fluide katalysatorbed, wordt bestudeerd **(Hoofdstukken 2-4)**. Vervolgens worden bereik en beperkingen onderzocht om met een behandeling met een zuurstofplasma moleculaire zeven bij lage temperatuur van brandbare componenten te ontdoen **(Hoofdstukken 5-7)**.

In **Hoofdstuk 1** worden enkele moleculaire zeven en hun industriële toepassingen vermeld. Vervolgens wordt ingegaan op de gebruikelijke activering van zeolieten van het FAU-type. Hieruit wordt eerst het natrium verwijderd door een ammonium wisseling gevolgd door thermische ontleding van het ammonium ion. Verder wordt de activering besproken van moleculaire zeven van het MOR- en MFI-type. Deze worden geactiveerd met behulp van een hitte-behandeling, een zogenaamde (thermische) calcinering. Tot slot wordt kort ingegaan op plasma-technologie en wordt voorgesteld deze techniek te gebruiken om moleculaire zeven bij lage temperatuur te calcineren.

Hoofdstuk 2 laat zien dat ^{23}Na nutatie NMR bij uitstek geschikt is om informatie te verkrijgen over de plaats van natrium en de interactie-energie ervan met het skelet van de zeoliet, zowel na ammonium-, of cesium-wisseling, calcinering in ondiep bed als gedurende hydrothermaal verwarmen van een (FAU-type) Na-Y zeoliet. Er wordt voorgesteld, dat ammonium, cesium wisselen en hydrothermaal verhitten alle tot een kation-herverdeling leiden die erin resulteren dat de hexagonale prisma's worden ontruimt. Er wordt aangetoond, dat het mechanisme van de ammonium-wisseling uit drie verschillende stappen bestaat: eerst wordt natrium in de superkooien gewisseld, vervolgens vervangt ammonium in de superkooien het natrium uit de hexagonale prisma's en tot slot worden de natrium ionen in de sodaliet kooien door ammonium vervangen. Ook na calcineren in een ondiep bed van een Na-Y-zeoliet die gedeeltelijk met ammonium gewisseld is, wordt met behulp van ^{23}Na MAS nutatie NMR een

herverdeling waargenomen van het natrium.

Hoofdstuk 3 laat zien, dat de ammonium-wisseling van Na-Y drastisch wordt versneld door hydrothermaal tot 433 K te verwarmen. Om snel nagenoeg volledige ammonium-wisseling in één stap bij 433 K te bewerkstelligen zijn hoge ammonium over natrium inzet-verhoudingen nodig, mogelijk omdat het hele FAU skelet moet uitzetten om twee ammonium-ionen per sodaliet-kooi te kunnen herbergen.

Hoofdstuk 4 beschrijft de uitgebreide karakterisering van Na-Y waarin eerst alle natrium-ionen voor ammonium-ionen zijn ingewisseld en dat vervolgens in een diep bed is gecalcineerd. Het aldus verkregen nieuwe Y-zeoliet wordt vergeleken met Y-zeolieten die langs meer gebruikelijke weg zijn bereid. Dit eerste verkennende onderzoek duidt erop dat calcineren van volledig ammonium-gewisseld Y-zeoliet met als doel sterk Brønstedt-zuur en hoog-actief materiaal te verkrijgen niet eenvoudig is.

In **Hoofdstuk 5** wordt aangetoond, dat een lage-temperatuur-zuurstofplasma bruikbaar is om alle ammonia oxidatief te verwijderen uit Na-Y zeolieten die gedeeltelijk met ammonium zijn gewisseld. Mits oxidatieprodukten eenvoudig uit de kristallen kunnen desorberen, blijkt deze lage-temperatuur plasma-calcinering even weinig destructief te zijn als een zeer voorzichtige thermische calcinering in een ondiep bed.

Lage-temperatuur plasma-calcineren blijkt eveneens geschikt om alle ammonia te verwijderen uit een goed gedroogde zeoliet van het MOR-type, die naast ammonium alleen nog enkele platina(II)tetra-amine kationen bevat **(Hoofdstuk 6)**. De MOR-geraamtes verkregen na plasma- of voorzichtig thermisch calcineren blijken niet noemenswaardig te verschillen. Het platina is echter na plasma-calcineren in een andere toestand aanwezig dan na thermisch calcineren.

Tot slot wordt in **Hoofdstuk 7** aangetoond, dat een zuurstofplasma niet alleen ammonia bij 370 K uit FAU of MOR verwijdert, maar ook tetrapropylammonium uit 5 μm lange kanalen in een MFI structuur die volledig uit siliciumdioxide bestaat, en bovendien diethylamine op diepte van minstens 70 μm verwijdert uit de kanalen in een TON structuur die eveneens volledig van siliciumdioxide is. Substitutie van B, Al of Fe in een siliciumdioxide MFI geraamte verhindert de volledige verwijdering van tetrapropylammonium in hoge mate, maar het kan volledig worden ontleed in kleine monsters

van het boor-gesubstitueerde geraamte. Uit de vergelijking van plasma-calcineren en thermisch calcineren in lucht blijkt dat de verwijdering van boor uit het geraamte tijdens elk van beide bewerkingen veroorzaakt wordt door de trage desorptie van water bij de calcineringstemperatuur.

DANKWOORD

Aan het werk waarover dit proefschrift gaat hebben velen een bijdrage geleverd. Hiervoor dank ik een ieder hartelijk.

Allereerst wil ik Herman van Bekkum noemen voor de ogenschijnlijk ongebreidelde vrijheid die hij mij geboden heeft om mij uit te leven in wetenschappelijke curiositeiten en voor zijn aanstekelijk optimisme. Niet minder erkentelijk ben ik Herman Kouwenhoven voor de deskundige wijze waarop hij het onderzoek heeft begeleid.

Wiebren Veeman en Tina Weeding (Katholieke Universiteit Nijmegen) verzorgden mijn eerste kennismaking met vaste stof NMR. Van de warme gastvrijheid en de vakkundige experimentele ondersteuning van Ron Janssen en Henny Douma heb ik graag uitgebreid gebruik gemaakt. It was a great pleasure and privilege to cooperate with Jacek Klinowski, Bogdan Sulikowski and Stuart Carr at the University of Cambridge. Also I would like to mention Frans van Buchem and Sean Axon for making my stay most enjoyable.

Joop Peters en Anton Sinnema hebben vaste-stof-(nutatie-)NMR spectroscopie ook in Delft mogelijk gemaakt.

Tony Verburg en Z.I. Kolar (Interfacultair Reactor Instituut) waren bereid mij de basisbeginselen van radiochemisch werken te leren.

Dolf Bruinsma (Universiteit van Amsterdam), Paul van der Put, E.W.J.M. van der Drift en L.C. Agatz (centrum voor submicrontechnologie) introduceerden mij in de plasma-technologie. Ernst Wurtz was niet alleen altijd bereid acute problemen met de gewenste snelheid te verhelpen, ook trotseerde hij verbeten vonken-regens om een plasma-verasser te bouwen. Het technisch vernuft en de bereidwillige ondersteuning van J. Zandijk, J.H.J. Weber en H. van der Vegt (Centrale Electronische Dienst) was bij de bouw van dit apparaat onmisbaar. De snelle service van de instrumentmakerij en van Piet Molenkamp, Frans Horsten en Cor Bezemer uit de glasinstrumentmakerij heeft menige desastreuze vertraging voorkomen.

Johan Tiggelman, J. Padmos en J.P. Koot droegen zeer veel ICP AES data aan.

CURRICULUM VITAE

Theo Maesen werd 27 september 1963 te Stein (Limburg) geboren. Na het behalen van het diploma gymnasium β aan de Scholengemeenschap Sint Michiel te Geleen in 1981, begon hij de studie scheikunde aan de Rijksuniversiteit Leiden. Het kandidaatsexamen organische chemie legde hij op 27 januari 1984 af. Het doctoraalexamen behaalde hij op 25 april 1986 met als hoofdvak heterogene katalyse onder leiding van prof. dr. V. Ponec, en de bijvakken chemische technologie o.l.v. prof. dr. J.A. Moulijn (Universiteit van Amsterdam) en informatica o.l.v. dr. D. van Albada. Het in dit proefschrift beschreven onderzoek werd verricht van juni 1986 tot september 1990. Sinds oktober 1990 werkt de auteur bij Koninklijke/Shell te Amsterdam.